UNIVERSITA' DEGLI STUDI DI PADOVA

Sede Amministrativa: Università degli Studi di Padova

Dipartimento di Ingegneria Idraulica, Marittima, Ambientale e Geotecnica

SCUOLA DI DOTTORATO DI RICERCA IN: SCIENZE DELL'INGEGNERIA CIVILE ED AMBIENTALE
INDIRIZZO: IDRODINAMICA E MODELLISTICA AMBIENTALE
CICLO XX

SIMPLIFIED MODELS FOR MORPHOLOGICAL EVOLUTION OF RIVER AND LAGOON SYSTEMS

Direttore della Scuola: Ch.mo Prof. Andrea Rinaldo
Supervisore: Ch.mo Prof. Giampaolo Di SIlvio

Dottorando: Giacomo Fasolato

DATA CONSEGNA TESI
31 gennaio 2008

A Elena

Le scienze non tentano di spiegare e difficilmente anche tentano di interpretare, ma si occupano principalmente di costruire modelli. Per modello si intende un costrutto matematico che, con l'aggiunta di certe interpretazioni verbali, descrive fenomeni osservati. Quel che ci si attende che funzioni è esclusivamente e precisamente la giustificazione di un tale costrutto matematico.

John von Neumann

I fiumi sono strade che camminano e che portano dove si vuol andare.

Blaise Pascal

Non c'è un solo uomo che non sia uno scopritore. Inizia scoprendo l'amaro, il salato, il concavo, il liscio […]; conclude col dubbio o con la fede e con la certezza quasi totale della propria ignoranza.

Jorge Luis Borges

Scopo del presente lavoro e breve guida per il lettore

Lo studio morfodinamico dei sistemi sedimentari è al giorno d'oggi una parte fondamentale della scienza dell'ingegneria civile ed ambientale, in particolar modo nelle applicazioni fluviali e lagunari.

Se da un lato la morfodinamica è in principio una disciplina estremamente complessa, alcuni fondamentali risultati possono essere ottenuti con modelli matematici e numerici relativamente semplici.

Scopo del seguente lavoro è l'analisi di alcuni di questi modelli semplificati, che ci consenta di investigare la validità e i limiti del loro impiego.

L'intero studio è in particolar modo rivolto all'analisi analitica e numerica dei modelli di formulazione unidimensionale per le applicazioni alla morfodinamica fluviale e di formulazione bidimensionale per le applicazioni alla morfodinamica lagunare.

Capitolo 1 *In questo primo capitolo introduttivo viene presentata una descrizione ed una revisione generale della letteratura recente in merito ai processi sedimentari e ai modelli morfologici che li riproducono.*

Capitolo 2 *Sono introdotte alcune procedure numeriche per la risoluzione di modelli matematici semplificati che descrivono l'idraulica e la morfologia dei sistemi fluviali (Peviani, 2002, Fasolato et al., 2006a).*

Capitolo 3 *Scopo dell' analisi analitica dei modelli fluviali è lo studio degli effetti della variabilità delle condizioni al contorno (idrologiche e di apporto di sedimenti) ed allo stesso tempo della non-uniformità geometriche e spaziali. Vengono individuati, in particolare, alcuni parametri caratteristici che controllano la*

propagazione e l'attenuazione lungo il fiume di questi disturbi (Fasolato et al., 2008a).

Capitolo 4 *La validità e le limitazioni dell'ipotesi di "local uniform water flow" cioè di moto localmente quasi-uniforme (Fasolato et al., 2008b) sono qui analizzate. Questa ipotesi semplificata risulta particolarmente utile nelle applicazioni a scale temporali a lungo termine e grandi scale spaziali, come ad esempio nei "large unsurveyed rivers" e cioè in quei fiumi di grandi dimensioni per cui non sono disponibili sufficienti dati morfologici e granulometrici (Ronco et al., 2008a).*

Capitolo 5 *Nel presente studio morfodinamico viene simulata la generazione di canali a marea in a bacino lagunare con un modello morfologico a lungo termine. Sono riprodotte, in una laguna schematica, l'iniziale rapida ontogenesi della rete di canali e la conseguente graduale evoluzione morfologica del fondo. Sono quindi analizzate le caratteristiche planimetriche e altimetriche del nuovo assetto morfologico e confrontate con lo stato energetico del sistema (Fasolato et al., 2008c).*

Discussione e futuri sviluppi *Infine, vengono discussi i risultati generali ed introdotti i possibili sviluppi futuri, sottolineando come comunque tutti i modelli semplificati analizzati in questo lavoro necessitino di ulteriori verifiche e validazioni attraverso dati sperimentali e misure di campo.*

Purpose of the present study and a guide for the reader

Morphodynamics of sedimentary systems is nowadays a fundamental piece of knowledge for civil and environmental engineers involved in fluvial and lagoonal interventions.
While morphodynamics is in principle an extremely complex discipline, some fundamental results may be achieved with relatively simple models.
Purpose of the present dissertation is providing an analysis of a number of simplified models, discussing the usefulness of their approach and the limits of their applications.
The entire study is especially on the analytical and numerical analysis of simplified one-dimensional formulations of fluvial morphodynamics and two-dimensional formulations of lagoon morphodynamics.

Chapter 1 *A general description and literature review of the sedimentation processes and morphological models are introduced.*

Chapter 2 *Numerical procedures are applied to solve mathematical models that represents hydraulic and morphological aspects of simplified river (Peviani, 2002, Fasolato et al., 2006a).*

Chapter 3 *The objective of the river model analytical analysis is to study the effects of geometry, hydrology and sediment input unsteadiness and non-uniformities, by explicitly indicating the most important parameters that control their propagation and attenuation along the river (Fasolato et al., 2008a).*

Chapter 4 *Are analyzed here the validity and limitations of the local uniform water flow hypothesis (Chapter 4; Fasolato et al., 2008b), an extremely useful*

simplification for large time- and space-scale computations and the only one which permits to cope with large unsurveyed watersheds (Ronco et al., 2008a).

Chapter 5 *Scope of the study, for the lagoon morphodynamics, is to reproduce and valuate the branching channel generation in a short tidal basin with a long term morphological model. In a schematic lagoon, the network ontogeny and the subsequent morphological bottom evolution are reproduced; consequently the planimetric and altimetrical features are analyzed and compared to the state of the system energy (Fasolato et al., 2008c).*

Discussion and further developments *Finally, general results and further developments are discussed, underlining, however, that all simplified the models analyzed in this dissertation require further verifications against experimental or field measurements.*

CONTENTS

Chapter 1 INTRODUCTION AND LITERATURE REVIEW

Chapter 2 ONE-DIMENSIONAL NUMERICAL MODEL OF RIVERS

Chapter 3 ONE-DIMENSIONAL ANALYTICAL MODEL OF RIVERS

Chapter 4 RIVER MORPHODYNAMIC EQUILIBRIUM AND UNIFORM-FLOW HYPOTHESIS

Chapter 5 EVOLUTION OF A RIVER DUE TO SEDIMENT FLUSHING FROM A RESERVOIR

Chapter 6 GENERATION AND EVOLUTION OF A TIDAL NETWORK

Chapter 1

INTRODUCTION AND LITERATURE REVIEW

SUMMARY

The basic forms of sediment motion and the time- and space-scales of sedimentary systems are considered, pointing out the ample variety of features encountered moving along the river from the divide to coastal areas. Under the action of water, sediments are removed from the farthest and highest areas of the watershed and conveyed downstream. Depending on the water action, sediment motion assumes three basic forms: linear, surface and mass movement; moreover a particular attention is dedicated to the linear transport, mainly responsible for river processes.

A large number of morphological models (one-, two- and three-dimensional) developed at different time- and space scales and with various degrees of detail and approximation consent to describes these processes. However a detail and careful analysis is necessary to understand the validity and limitations of models hypothesis, the behavior of solutions with different formulations, type of boundary conditions, possibilities for simple and numerical solutions procedures.

1. SEDIMENTATION PROCESSES

Civilization and economic development of a society are closely related to the ability to maximize the benefits and minimize the damage caused by rivers. A river frequently adjusts its cross-section, longitudinal profile, course of flow and pattern through the processes of sediment transport, scour and deposition. These principles and generally sediment transport, has been studied for centuries by engineers and river morphologists. Different approaches have been used to solve engineering problems and results obtained often differ drastically from each other and from observations in field. Some of the basic concepts, their limits and applications, and the interrelationships among them have become clear to us only in recent years. Many of the complex aspects of sediment transport are yet to be understood, and remain among the challenging subjects for future studies.

In order to provide a picture of these processes, in Fig. 1.1 (Di Silvio, 2006) a middle size watershed of temperate zones (but in fact extendible to other climates) is schematically depicted with total disregard to perspective rules and proportions, as in primitive painting. However, to give an idea of what usually takes place at different elevations and distances along the water course, these quantities are respectively indicated by a linear and logarithmic scale in the foreground cross section.

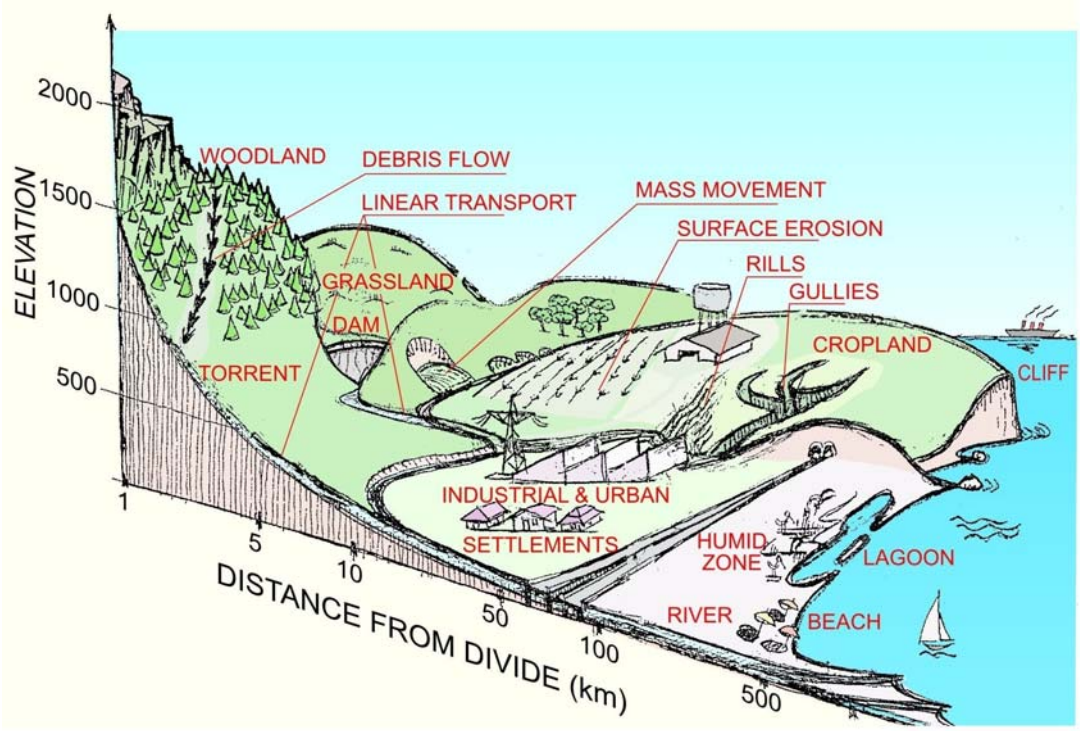

Fig. 1.1 Sketch of a watershed in temperate zones: Basic forms of sediment motion (Di Silvio, 2006)

Under the action of water (rainfall, overland flow, channeled flow, freezing and melting, infiltration, etc.), sediments are removed from the farthest and highest areas of the watershed and conveyed downstream. Depending on the water action, sediment motion assumes three basic forms (*linear, surface and mass movement*), more or less corresponding, respectively, to (i) bedload and suspended transport in the stream network; (ii) distributed soil erosion mainly occurring in undulated, scarcely vegetated surfaces; and (iii) landslides, occasionally produced in the steepest slopes of the watershed even if nicely protected by vegetation; but also to a number of (iv) intermediate forms as, for example, debris flow, rills erosion, gully development, etc. Where rainfall is scarce, as in the desert or in a arid zone, wind is often the most effective cause of surface erosion.
Physical mechanisms driving sediment motion and relevant problems connected with solid transport (but mostly arising, in fact, during the erosion or deposition phases) are therefore extremely numerous and present peculiarities connected with the morphoclimatic conditions of the ones under consideration.

Mass movement phenomena, characterized by quick and short displacements of large portions of soil, represent sometimes a risk for human settlement and infrastructures, but also a physiological source of sediments to the rivers in several natural watershed (e.g. in alpine and humid tropical regions). Investigation on mass movement is generally carried on by applied geologists and, for the structural aspects, by soil mechanics engineers.

Surface erosion, as well as intermediate forms like *rill* and *gully erosion*, for its strict implications with land use and agricultural practices, usually belongs to the province of agronomists and agricultural engineers. It is also investigated however by various scholars of earth science. These forms of erosion constitute a natural source of sediments in arid tropical and temperate regions where rainfall is generally the dominant mechanism of soil production.

Finally, *linear transport* is traditionally in the competences of hydrologists and rivers engineers. Bedload and suspended sediment transport convey coarse and fine particles over extremely long distances along the river, down to the estuary, the sea and the adjacent beaches, where they usually pass under the jurisdiction of maritime engineers and oceanographs.

1.1 MASS MOVEMENT

Mass movement is an important source of material for many rivers and in same cases the most important one. In *humid tropical forests* as well as in *alpine climates*, for example, the natural thick vegetation cover is such that the direct effect of rainfalls (kinetic energy) on the soil is negligible and the sediment production by surface erosion is practically zero. Yet the sediment transport by mountain rivers may be substantial and even extremely large (up to 10^4 t/km^2/year), due to the contribution of repeated *bank collapses* and occasional big *landslides*. Small and large mass movements from the watershed slopes typically occur during large floods and intense storms and are often associated with *mud-* and *debris flows* in the upper branches of the hydrographic network.

Mud- and debris flows (including ash flow or "lahars", taking place along the steepest channels of volcanoes) are intermediate forms of sediment motion, between mass movement and linear transport, which require a minimum slope to be initiated. While their motion depends on particle- and fluid-dynamics (similarly to linear transport), their triggering is controlled by static forces, basically depending on friction, cohesion, slope and the degree of saturation of permeable material (as for mass movement). For this reason attempts have been made to model the triggering of both shallow landslides and debris flows by simulating the saturation process of the surface layers of watershed slopes and steep channels (Seminara and Tubino, 1993; Tubino and Lanzoni, 1994; Di Silvio and Gregoretti, 1997; Dietrich and Montgomery, 1998; Armanini et al., 2000; Dietrich et al., 2001; Rosso, 2002).

1.2 SURFACE EROSION

Surface erosion is definitely the most important source of sediment production wherever vegetation does not provide a sufficient protection of soil from the rainfall impact, and morphological conditions are such as to foster the removal of particle by overland flow. This means that surface erosion is particularly active in cropland areas, especially where the soil is vulnerable and erosion-control measures and correct cultivation practices are not applied, as in many dry tropical countries.

Also in temperate countries, however, extremely high rate of surface erosion took place in historical times, following the rapid expansion of cultivated areas and before sustainable land management was adopted.

The most active institution in this field was certainly the U.S. Department of Agriculture, where the renowned U.S.L.E. model has been proposed. The U.S.L.E. (Universal Soil Loss

Equation) was developed since several decades (Wishmeyer and Smith, 1978) by using the U.S.D.A. data base containing a very large number of (plot by experiments) results.
Besides the U.S.L.E. equation, more sophisticated models as ASWER, WEPP, SHE-SED, EUROSEM etc. have been recently developed for simulating, at catchment level, the detachment of soil particles by rainfall and their subsequent transport by overland flow and by river flow over the entire catchment (Beasley et al., 1980; Morgan, 1995, Nearing et al., 1999). In contrast with the so-called "empirical" models (like USLE), the last models are usually called "physically based", since they are constituted by theoretical differential equations (expressing the mass balance of water and sediments) and by appropriate algebraic equations (describing each of the physical processes involved).

1.3 LINEAR TRANSPORT

Linear transport is the motion of sediments produced by persistent, canalized water flow. It is mainly responsible for river processes, but also for morphological processes in other permanent water bodies like lakes and estuaries.

1.3.1 Transport's modes

Linear transport assumes various modes (*bedload*, *suspension* and *intermediate forms*), but attempts have been made towards a conceptual unification of these forms, through the notion of *adaptation length*. The adaptation length is proportional to the average distance covered by a sediment particle entrained from the bottom before being deposed on the bottom again. The adaptation length depends on the particle grain size and on the characteristics of the water flow, i.e. more precisely on the ratio between friction velocity u^* and particle settling velocity w_s. When the ratio (u^*/w_s) is very small, the adaptation length has the order of magnitude of 10^2 (*grain diameters*) and the particles move by sliding and rolling as bedload. When this ratio increases, also the adaptation length correspondingly increases passing from saltation to suspension. Adaptation length is practically zero for bedload, while for suspended transport may reach the value of tens of kilometers when very fine material is conveyed by fast flow.
When the adaptation length is much larger than the significant length of the river reach, the sediment transport rate does not depend solely on the hydrodynamic and sedimentological characteristics of the reach itself, but also on the condition upstream. This circumstance explains in part why the suspended transport in a given section is often scarcely correlated with the water flow .The adaptation length can be evaluated by different methods (Gallappatti

and Vreugdenhil, 1985; Armanini and Di Silvio, 1988; Seminara, 1998), and its effect should be taken into account, when necessary, in sediment transport computations (see par. 3.1).

1.3.2 Sorted and cohesive material

Experimental formulae providing sediment transport rate have been usually obtained in laboratory with almost uniform material. In most real rivers, however, particle grain sizes are more or less non-uniformly distributed, with markedly different statistical distributions for bed material and transported material. In general, bed material appears to be coarser than transported material, and the two distributions can be mutually related by considering the transport of each grain size class (see Sect. 3).

When treating different grain size classes, due attention should be paid to the interference of particles of different diameter. In sediment mixtures, in fact, the intrinsic larger mobility of finer particles is somewhat diminished by the presence of the coarser ones (*hiding* effect) while the intrinsic smaller mobility of coarser particles is augmented by their protrusion (*exposure* effect) (Egiazaroff, 1968, Parker and Klingeman, 1982; Wu et al., 2000a). With very strong water flow in flood periods, the hiding-and-exposure effect may even lead to an "almost equal mobility" (Parker et al., 1982). In dry periods, by contrast, the different intrinsic mobility of various diameters strongly prevails on hiding-and-exposure effect (indeed, the coarser particles may even not move at all). In any case, over a long period of time, the transported material (e.g. the material intercepted by a reservoir) appears to be definitely finer than average composition of the river bed. The "hiding-and-exposure" effect may be taken into account by various empirical coefficients to be introduced in the formulae developed for uniform material.

The time evolution of bed and transport composition is usually modelled by resorting to the *active layer* concept, first proposed by Hirano (1971) and subsequently incorporated in many morphodynamic models. More sophisticated approaches have been developed more recently, either by disaggregating the bottom *active layer* into a *mixing*-and an *intrusion layer* (Di Silvio 1991a), or by considering the bottom a continuous, indefinitely deep layer, statistically described in terms of entrainment capacity (Armanini and Di Silvio, 1988; Parker et al., 2000).

In some circumstances (e.g. estuaries, flood plains, deep reservoirs) sediments can hardly be considered as non cohesive. The role of cohesion is quite important both in the deposition phase (flocculation) and in the re-entrainment process (compaction). The pioneering work of

Partheniades (1962), Krone (1962) and subsequently of Metha and Partheniades (1975) and Metha (1986) is still the foundation of may models for cohesive materials. Some of the models developed from their basic concepts, however, do not appear completely satisfactory and are unable to explain a number of phenomena observed in nature. It is therefore very much interesting the attempt by Winterverp (2002) to bring together the behaviour of cohesive and non-cohesive material within a unified physical framework with specific definitions of vertical fluxes for each type of sediment.

1.4 SEDIMENTARY SYSTEMS SCALES

When considering morphological processes, however, it is important to have in mind the time and space scales of the *sedimentary system* under consideration. The repeated succession of erosion, transport and deposition, may concern for example: (i) the sliding, rolling and saltation of sediment particles over bed ripples (space scale: boundary layer); (ii) the propagation of dunes (space scale: river depth); (iii) the formation of bars and meanders (space scale: river width); (iv) the general aggradation or degradation of a river (space scale: watershed). The time scale of each system may be associated to the corresponding space-scale, *via* a typical process velocity.

It is important to note, in any case, that each system at a given scale may be considered a component (or sub-system) of the system at the larger scale, needing to be somehow incorporated in the last one. Incorporation is usually made by assuming that any subsystem at a smaller scale (e.g. dunes) is invariably in equilibrium conditions with the "instantaneous" configuration of the system at a larger scale (e.g. bars and meanders). Conversely any system at a larger scale (e.g. river watershed) is supposed to remain stationary at the time scale of interest (e.g. development of bars and meanders). This assumption is only valid, in principle, when the relevant systems and sub-systems have markedly different scales, but it is implicitly assumed in most morphological models (see par. 2).

The scales of morphological processes extend over several orders of magnitudes ranging from microns to continental sizes (in space) and from seconds to millions of years (in time).

2. MORPHOLOGICAL MODELS

A large number of morphological models developed at different time and space scales and with various degrees of detail and approximation are available in literature. In this section attention will be especially concentrated on linear transport. Models of mass movement and surface erosion are briefly mentioned in par. 1.1 and 1.2 respectively.

2.1 SMALL SCALE MODELS

Detailed small-scale models have especially been developed for research purpose. Many of these models (still in their infancy and needing improvements) have the scope to reproduce the movement of individual particles under the action of other particles and water flow and are usually based on a lagrangian approach. They should be able, in principle, to reproduce the behaviour of small scale systems (from microforms up to the depth-scale) (Strom, 2004 and 2007) and may be extremely useful to explain the hydraulic resistance mechanisms (grain and form roughness), to show the validity and limitations of transport formulae, to investigate the dynamics of movable bottom and to describe the motion of hyper-concentrated liquid-solid mixtures.

2.2 INTERMEDIATE SCALE MODELS

These models are the most commonly used for practical applications. They are typically extended to the size of a river reach and applied for relatively short time duration (from one single flood event to a few years). All the subsystem processes (microforms, hydraulic resistance, sediment transport rates etc.) are incorporated via simple predictors, usually "equilibrium" algebraic equations.

Intermediate scale models are obtained by averaging the Reynolds equations (in their turn obtained by averaging the Navier-Stokes equations over turbulence) over appropriate space dimensions. The most common commercial models are *1-D* (*one-dimensional)*, i.e. averaged over the river cross-section (but possibly disaggregated in a number of sub-sections). One-dimensional models can simulate bottom erosion and deposition along the river (generally the most relevant requested information), somehow "re-distributed" over the cross-section (Cui et al., 1996; Cao et al., 2002; Papanicolaou, 2004; Wu et al., 2004; Cui and Parker, 2005; Curran et al., 2005; Wright and Parker, 2005a and 2005b). 1-D models can easily be applied to relatively large portions of the hydrographic network.

Rather common, however, are nowadays becoming *2-D* (*two-dimensional)* models, i.e. averaged over the river depth (Jia and Wang, 1997 and 1999; Ye and McCorquodate, 1997; Stockstill et al., 1997; Nicholas and Walling, 1998; Kassem and Chaudhry, 2002; Defina, 2003; Cea et al., 2007; Abad et al., 2007). Two dimensional models can in principle simulate all the process at the width-scale (migrating and stationary bars, braiding and bifurcations, sediment exchange with flood plains etc.). Bank collapse and reconstruction can also be incorporated in a 2-D model, which therefore will be able to reproduce meander formation and propagation.

Secondary currents over the cross section are important in meander morphodynamics. Their reproduction require in principle a *3-D* (*three-dimensional)* model (Jia and Wang, 1996; Ouillon and Dartus 1997; Duo et al. 1998, Wu et al., 2000b; Wilson et al., 2003; Olsen, 2003; Jia et al., 2005; Nagata et al., 2005; Zedler and Street, 2006), but their local effect can be approximately accounted for by a 2-D model. Reproduction of density currents, often important in certain reservoirs, also requires a 3-D model (Kassem et al., 2003). In some cases, however, a *vertical 2-D* model (i.e. averaged over the reservoir width) can also be considered (Karpik and Raithby, 1990).

Intermediate scale models, either 1-D, 2D or 3-D, are extremely sensitive to the *boundary conditions* to be prescribed at the upstream and downstream ends of the river reach under investigation. Correct boundary conditions for morphological models (Sieben, 1997) should be given in terms of sediment input of each grainsize fraction (at the upstream end) and in terms of either water-level or bottom-elevation, respectively for sub-critical and super-critical water flows (at the downstream end). Note that boundary conditions depend in principle on what is going on respectively upstream and downstream the reach under consideration. For short-term simulations, sediment input upstream can be evaluated by reasonable hypothesis based on "local" quasi-equilibrium conditions (see par. 3); the same can be made for water level or bottom elevation downstream. For long-term simulations, however, the behaviour of the entire river system should be explicitly accounted for.

2.3 LARGE SCALE MODELS

Although 1-D models have been sometimes applied to relatively large real watersheds for specific flood events, no many examples are available in the literature of morphodynamic modelling at very long (historical or geological) time-scale, except in a few very schematized situations (simple geometry, constant waterflow, uniform grainsize) (Coulthard et al., 2007). The effects of geometrical, hydrological and sedimentological *non-uniformities,* invariably present in real systems, have not been thoroughly investigated for long-term, large-scale simulations of actual river and relevant watersheds. In fact, averaging "non-uniformities" of any type in non-linear equations produces "residual terms" which should be properly assessed and eventually modelled with appropriate sub-models.

It may be interesting, in this respect, exploring the possibilities offered by *long-term morphological models* where averaging is performed only on time (year or number of years). In practice, long-term models filter the morphological fluctuations due to short term components and compute only the long-term evolution (time-averaged values over a year or a

number of years). Long-term models have been especially developed for estuaries (de Vriend et al., 1993; de Vriend, 1996; Dal Monte and Di Silvio, 2004) but can in principle be applied also to river systems.

3. SEDIMENT TRANSPORT IN A RIVER

A fundamental component of any morphological model is the predictor of the sediment transport rate as a function of sediment grainsize and flow characteristics. In principle sediment transport may be modelled in detail, considering all the relevant phenomena, from the particle scale up to the depth scale (ripples, dunes, hiding-and-exposure etc.) In practice, what can be utilized for larger scale modelling (par. 2.2 and 2.3) is a series of formulae (the so-called "transport formulae"), sometimes associated to other formulae providing the size of mesoforms and the relevant hydraulic resistance.

Very often, however, sediment transport is disaggregated in two parts: the so-called "bed-material transport" (typically coarser than than a conventional grain-size limit, say between 20 and 80 microns) and the so-called "washload" (below that limit). While the transport of bed-material is supposed to be a function of riverbed composition and flow characteristics, washload is assumed to be fed to the river from the watershed slopes and conveyed downstream by the river flow, without any interaction with the bottom. The distinction between bedload material and washload is obviously made for sake of simplification, but it does not have a solid physical foundation.

3.1 TRANSPORT FORMULAE

Available transport formulae have been obtained from simple small-scale modelling and, above all, from laboratory flume experiments carried out in uniform conditions (uniform flow and uniform grainsize). Since the early work of Du Boys (1879), tens and tens of transport formulae have been proposed by different authors. As all these formulae have been obtained in quite different experimental ranges of flow and sediment characteristics, there is no wonder that they appear inaccurate when applied to other situations. For example, some experiments have been performed in bedload transport conditions, while in other experiments suspended transport was substantial and even dominant. In any case, as flume experiments were carried out in equilibrium conditions (*uniform flow*), the measured sediment transport rate simply represents the "total transport".

Assessing the prediction capability of different formulae, or even recognizing the validity limits of each one, is not an easy task. At first glance all the formulae seem to be hardly comparable. Yet it may be interesting a dimensional analysis of their structure.

Let us define (see for example Yalin, 1963) the non-dimensional sediment transport rate:

$$T_* = \frac{q_s}{d\sqrt{g\Delta d}} \tag{1.1}$$

where q_s is the solid discharge in volume per unit width; $\Delta = \frac{(\rho_s - \rho)}{\rho}$ is the relative density of sediments; g the gravity and d the (uniform) sediment grainsize. It follows that T_* should be a function of 3 independent non-dimensional morphological parameters; for example :

- the particle Froude number (or mobility index, or Shields parameter):

$$F_* = \frac{u_*^2}{g\Delta d} \tag{1.2}$$

- the particle Reynolds number :

$$\mathrm{Re}_* = \frac{u_* d}{\upsilon} \tag{1.3}$$

- the relative depth :

$$\left(\frac{h}{d}\right) \tag{1.4}$$

The particle's Reynolds number plays an important role for fine particles transported in suspension, as it controls the falling velocity. The relative depth, by contrast, is important for very coarse particles moving as bed load, as they can affect the free surface of shallow flows. Conversely, as for several hydraulic phenomena, the influence of both the Reynolds number and the relative depth tends to disappear when these quantities become very large. This occurs respectively for mountain rivers (high flow velocity and coarse material) and for large plain rivers (high depth and fine material).

In any case, the parameter F_* is invariably the most important one as it represents the ratio between the mobilizing effect of the water drag on the particle and the stabilizing effect of the particle's immersed weight. Most of the available transport formulae, in fact, can be approximately plotted on a graph T_* vs. F_* , either in the form

$$T_* = aF_*^{\beta} \tag{1.5}$$

or in the form :

$$T_* = b\left(F_* - F_{*cr}\right)^{\gamma} \tag{1.6}$$

assuming that the coefficients a and b and the exponents β and γ are not constant, but functions of other quantities besides F_*.

The *monomial structure* of eq. (1.5) is typical of many formulae like Brown (1950), Engelund and Hansen (1967) etc. The *binomial structure* of eq. 6 implies that no movement occurs if the mobility (or Shield's) parameter F_* is smaller than a critical value F_{*cr} (usually function of Re_*). The binomial structure is typical of several popular formulae like Meyer-Peter and Müller (1948), Ackers and White (1973), van Rijn (1984) etc. Note that also other formulae in literature, having an apparently different theoretical background (like the ones based on minimal stream power), can approximately be written as eqs. 1.5 and 1.6.

It is matter of philosophical discussion whether in principle a critical value F_{*cr} for incipient sediment transport should exist. Indeed, due to the stochastic character of turbulence, one may even think that an (occasional) transport would take place even with extremely small (average) values of F_*. In any case, since the transport rate should rapidly decrease for very low values of F_*, the exponent β in monomial formulae needs to be rather large (and in fact it ranges between values 2.5-3), while the exponent γ in binomial formulae is much smaller (it ranges between values 1.2-1.5).

For both types of formulae, however, the numerical value of the exponents (β and γ) and of the coefficients (a and b) should depend, explicitly or implicitly, on the other non-dimensional parameters mentioned before, that is Re_* and (h/d). In fact, many of the experimental formulae contain other quantities besides F_* that affect the non dimensional sediment transport. Although these quantities are not explicit functions of Re_* and (h/d), they are very likely somehow related, depending upon the range of flow and sediment characteristics in which the experiments have been carried out.

At this point, for practical applications, instead of selecting a certain available formula, it is perhaps better resorting to an expression like (1.5) or (1.6). In this case, of course, the values of exponents and coefficients should be properly chosen for the river configuration one is interested in (ranging from steep alpine torrents conveying gravel and boulders, to slow lowland rivers conveying silt and sand). This choice corresponds to the transport formula calibration.

For calibrating the transport formula for a given river configuration, the simpler monomial equation (1.5) is preferable to the binomial equation (1.6), even if one has to expect for the

values of a and β a larger variability than for the values of b and γ. The calibration procedure of the transport formula (Di Silvio, 2006) consists in associating to eq. (1.5) a uniform flow formula, either Chézy or Manning-Gauckler-Strickler, and in introducing the grainsize distribution of the bed material together with an appropriate "hiding-and-exposure" coefficient (par. 1.3.2). The final expression for the total sediment discharge (sums of all grainsize classes, $i=1,2,...N$) is:

$$P = \sum P_k = \alpha \frac{\sum \beta_k d_k^{s-q}}{(\sum \beta_k d_k)^s} \cdot \left(\frac{Q^m I^n}{B^p} \right) \tag{1.7}$$

where Q, I and B are respectively the waterflow discharge, the river slope and the river width, d_k is the diameter of the k-th grainsze class and β_k is the percentage of the k-th grainsize class present in the bottom. The value of the exponents m, n, p and q depend on the exponent β in eq. (1.5) and on the selected uniform flow formula, according to the following expressions :

Chézy

$$\begin{aligned} m &= \frac{2}{3}\beta \\ n &= m \\ p &= m-1 \\ q &= \frac{3}{2}(m-1) \end{aligned} \tag{1.8}$$

Manning-Gauckler-Strickler

$$\begin{aligned} m &= \frac{3}{5}\beta \\ n &= \frac{35}{30}m \\ p &= m-1 \\ q &= \frac{3}{2}(m-1) \end{aligned} \tag{1.9}$$

In general, assuming a constant Chézy coefficient (i.e. a constant *relative* roughness) is more appropriate for lowland rivers (dominant bedform resistance); while a constant Manning coefficient (i.e. a constant *absolute* roughness) is more appropriate for mountain rivers (flat bed and dominant grain resistance). The exponent of the hiding-and-exposure coefficients tends to be equal to q for extremely high values of Q (equal mobility). On the averages may be taken equal to 0.8.

Note that eq. (1.7) is just another form of eq. (1.5), in which the transport of each grainsize class present in the bottom has been considered. Equation (1.7) indicates that, being the other quantities constant, a biunivocal relation should exist between P and Q. This is true, however, only for an experimental flume in *equilibrium conditions* (uniform flow for water and sediments): indeed, for a re-circulating flume with prescribed values of I, B and bottom composition, the transport rate P is a unique function of the water flow Q. For a real river, by contrast, even if waterflow in the relevant river reach is reasonably uniform, different values of P may be measured for the same value of Q. This is basically due to the fact that the local energy slope I and the local bottom composition β_k may vary during the hydrological cycle,

as fluctuating erosions and depositions invariably occur. As seen before, moreover, also the exponent *s* may not be constant.

Finally, if the material is very fine, the material transported in suspension may be not solely controlled by the local conditions, but also by the conditions quite upstream. The last circumstance, however, is not so dramatic if the *adaptation length* is shorter than the river reach under investigation. It should be noted, in this regard, that the transport of fine particles depends on the *local* bottom composition, even if their presence in the bottom is extremely scarce. As it appears from eq. (1.7), in fact, due to their much larger mobility, the particles belonging to a very fine faction (say d_k = 50 microns) may have a very small value of β_k, but a very large value of $\left(P_k / \sum P_k\right)$. In other words, the notion that only the transport of the material abundantly represented in the river bed (the relatively coarse, so-called "bed material") depends on the local conditions, while the fine material should be considered "wash-load", may be misleading.

In conclusion, for relatively large watersheds, the scattering of short-term measurement *P* vs. *Q* is generally due to short-term fluctuation of *I*, β and (probably) exponent *s*, rather than to the time-dependent input of fine sediments from the watershed slopes.

Indeed if one supposes that fluctuations of the above mentioned quantities are mutually independent and assumes an exponential duration curve for *Q(t)*, the integration of (1.7) over one year provides:

$$V_s = \frac{\alpha}{m} \frac{I^n}{B^p} \frac{\sum \beta_k d_k^{\,s-q}}{(\sum \beta_k d_k)^s} \cdot \left[Q_o^{m-1} V_o \right] \qquad (1.10)$$

where V_s is the total annual transport of sediments (all classes), V_o is the annual runoff volume and Q_o the annual flood peak.

Although the hypothesis on the statistical independence of *I* and β may be questionable, eq. (1.10) shows a very good correlation between hydrological parameters Q_o and V_o and the annual sediment yield V_s.

3.2 SOIL PRODUCTION

One of the most difficult problems in establishing a sediment balance at watershed scale is the relation between the sediment removed from the watershed slopes (soil production) and the soil transported by the river (sediment yield). The very same definition of those quantities in fact may present some ambiguities.

Sediment yield is defined as the amount of sediment transported during a prescribed period of time trough a given cross-section of the river. The ratio between the sediment yield though the

closure section of a watershed and the amount of sediment removed from the entire watershed surface during the same period of time is called *delivery ratio*. This quantity incorporates all the complexity of the sediment motion down to the closure cross-section of the watershed and strongly depends, again, upon the space- and the time-scale selected for the computation.

While for an *experimental plot* or even for a regular *cropland field*, ditches clearly show where they initiate and terminate, for a *natural slope* the only apparent boundary is represented by the channels and the divides of the hydrographic network. It seems therefore more reasonable computing the length and steepness of natural slopes from the basin's *drainage density* and *relief*.

A definition of *soil production* is the portion of sediments which reaches the closure of the watershed. In this case, the computation at river scale should be affected by an even smaller reduction coefficient (*overall delivery ratio*), which should take into account also the river processes along the entire hydrographic network.

The concept of overall "delivery ratio" for sediments is somehow analogous to the concept of "runoff coefficient" for water. Yet it is much more elusive to be defined and difficult to be predicted, due to its variability in space and time along the sediment route. From the early data in the literature (Maner, 1958; Roehl, 1962; Williams and Berndt, 1972) it appears that delivery ratio decreases from 1 to a few percents, more or less proportionally to the inverse of the stream length (or square root of the watershed area) but scattering of data appears to be extremely high. Several attempts to have a more accurate prediction of delivery ratio as a function of the watershed and river morphology (see for instance Walling and Webb, 1996) did not provide generally valid results.

Similarly to the "runoff coefficient", the concept of "delivery ratio" is hardly useful when it becomes much smaller than 1 (namely for watersheds larger than 50-100 Km^2). The notion of delivery ratio is in fact probably acceptable exclusively at intermediate scale, namely for an overall description of the "monotone" trapping effect the watershed slopes, where few localized permanent sinks may give rise to (averaged) value of the delivery ratio close to 1.

When river processes become dominant it would probably be better substituting the static concept of "delivery ratio" with a dynamic concept of "response delay", in which the time scale also plays a role. Indeed, if the watershed is large, it is not correct assuming that the very same particles detached from the watershed slopes during a certain storm can reach the closure section of the basin during the corresponding flood. The sediments moving as bedload or as suspended transport along the river (including the very fine ones, usually called "washload"), have continuously phases or deposition and re-entrainment with the river bed,

banks and floodplains. Repeated deposition and re-entrainment may produce relevant altimetric and planimetric changes at different time scale and, in any case, will delay the response of river morphology (and river transport) with respect to the sediment input from the watershed slopes.

A direct evaluation of sediment yield is possible by utilizing regular (daily) measurements of turbidity and water dischange carried on at some stations along the river. This procedure assumes that there is a direct relationship between measured "turbidity" and "transport concentrations" (ratio between total sediment transport and water discharge).

The most precious and reliable information about sediment yield in terms of both quantity and grainsize composition, however, is given by the progressive sedimentation of existing reservoirs. The surveying technology based on the joint use of remote sensing and Global Positioning System (GPS) (e.g. Lee et al., 1999; Agarwal and Idiculla, 2002) has already been applied in similar circumstances. In assessing the sediment volume trapped in a reservoir, the time-depending compaction of the deposited material should be taken into consideration (see for instance Morris and Fan, 1998). The data collected in existing reservoirs, as well as at measuring stations, may be used for calibrating reliable semi-empirical relationships (even if limited to a specific river configuration) which provide long-term sediment transport as a function of hydrological, geometrical and sedimentological characteristics of the river reach (see par. 3.1).

4. SEDIMENT TRANSPORT IN A TIDAL LAGOON

Morphological processes in tidal lagoons are controlled by tides, waves and fluvial currents, and develop at different space- and time-scales. At the *tidal scale* (hours), sediments in suspension move from the sea into the lagoon during the flood phase and from the lagoon towards the sea during the ebb phase. At a *seasonal scale* (months), net sediment fluxes are mainly controlled by the wave climate inside and outside the lagoon. When waves produced by local winds inside the lagoon are persistent, stirred sediments leave the lagoon in larger quantity during the ebb phase; contrastingly, if there is a long period of rough sea, the quantity of sediments entering the lagoon is larger during the flood. At *historical scale* (decades or centuries), however, the fluxes of sediments leaving and entering the lagoon, including the positive sediment input by the river, tend to compensate each other. If the combined effect of eustatism (rising of the mean sea level) and subsidence (lowering of the basin bottom) is also taken into account and if the balance is perfectly closed, the lagoon

maintains a steady-state configuration; otherwise, it keeps evolving at geological or even at historical scale.

A very useful tool that has been applied since many years to the Venice Lagoon (Di Silvio, 1989) and then extended to a number of semi-empirical models (De Vriend, 1996) is the concept of *transport concentration*. Morphological models based on this concept are very flexible and can be applied with different degrees of spatial resolution (two-dimensional, one-dimensional and zero-dimensional approach). Moreover, they can incorporate a variety of complex processes, as grain size sorting, effects of vegetation, collapse of steep banks, compaction of sediment deposits, etc. (Di Silvio, 1999; Di Silvio and Teatini, 1992a,b; Di Silvio and Padovan, 1998; Di Silvio et al., 2001).

4.1 THE TRANSPORT CONCENTRATION

The concept of *transport concentration* is particularly suitable for tidal lagoons but can be extended to other coastal systems, like estuaries and deltas, which can be recognized as limit-cases of lagoons. An interesting extension of the concept incorporates in the model of an estuary system (ASMITA) the ebb delta at the inlet and the adjacent coast (Stive et al., 1998).

Transport concentration is defined as the longterm concentration, prevailing in a certain location, which provides the long-term net sediment transport as proportional to the quantity itself (advection) and/or proportional to its spatial gradient (dispersion), depending upon the characteristics of the water flow in the same location.

In a tidal basin, sediments are conveyed (mostly in suspension) from the shoals to the channels and through the channels out to the sea during the ebb phase, and are generally moved inward during the flood phase. At the *tidal scale* (hours), the sediment transport is predominantly advective. It is given by the product of depth-integrated velocity (discharge per unit width, also called water flux) and depth-averaged concentration, while the local longitudinal dispersion (Taylor or Elder type) is almost negligible.

At the *intertidal scale* (weeks), sediment is mainly transported by the intertidal dispersion (several orders of magnitude larger than Taylor's dispersion), while the advective term (i.e. Eulerian residual water fluxes) is generally rather small. Another long-term component of sediment transport is due to the asymmetry of the tidal wave, i.e. to the different duration of the ebb and the flood phases; this gives rise to an intertidal residual motion of particles in either the ebb or the flood direction and may be quite important in the channels of some estuaries or lagoons. At both tidal and intertidal scales, however, the averaged concentration is determined by the shear stress on the bottom. This shear stress is mainly due to wind waves

in the shallow areas and to fluvial and tidal currents in the channels. The transport concentration can be computed by averaging over a long period of time the instantaneous concentration corresponding to the duration curve of the shear stress for both stirring mechanisms.

Long-term transport can then be expressed in terms of the transport concentration and its spatial gradients as soon as the intertidal residual velocities and the intertidal dispersion coefficients are known.

4.2 EULERIAN WATER FLUXES AND INTERTIDAL DISPERSION

Eulerian residual water fluxes are given by the long-term average of depth-integrated velocities (water fluxes) at tidal scale. When fluvial currents are strong, Eulerian water fluxes are basically due to the river discharges. In general, however, Eulerian residual water fluxes also depend on tidal currents. In many lagoons, for instance, residual water fluxes of tidal origin are determined by the interaction of inertial, gravity and friction forces in the tidal channels network. As a consequence, some branches of the interconnected channels convey a larger volume of water during the ebb phase and others during the flood phase. *Intertidal dispersion* is due to the alternate gradient of concentration, between shallow areas and tidal channels and between tidal channels and the sea, taking place respectively during the ebb and the flood phase. This mechanism has been called ‘‘trapping and pumping’’ (Schijf and Schőnfeld, 1953) and the corresponding dispersion coefficient can be evaluated in terms of exchanged volumes and local morphology (Okubo, 1973; Dronkers, 1978).

While intertidal dispersion is driven by the *spatial deviations* of water flux and concentration from their respective average, the long-term sediment transport in the channels due to the asymmetry of tidal phase depends on the *temporal deviations* of those quantities.

In fact, if the duration of one tidal phase is systematically shorter than the duration of the other, the corresponding tidal velocity is larger and the net intertidal sediment transport is not zero, even if the residual water flux is zero. An analysis of the net sediment transport driven by non-symmetrical tidal flow and of the consequent morphological effects has been made for convergent estuaries (Lanzoni and Seminara, 2002).

In conclusion, the long-term (two-dimensional) sediment transport component along the x- and y-axis can be expressed as (Dal Monte and Di Silvio, 2004):

$$T_x = C \cdot \left(q_{R_x} + q_{A_x} \right) - h \cdot \left(D_{xx} \frac{\partial C}{\partial x} + D_{xy} \frac{\partial C}{\partial y} \right) \tag{1.11}$$

$$T_y = C \cdot \left(q_{R_y} + q_{A_y} \right) - h \cdot \left(D_{yx} \frac{\partial C}{\partial x} + D_{yy} \frac{\partial C}{\partial y} \right) \qquad (1.12)$$

where h is the local tide-averaged water depth, C is the transport concentration, D_{ij} are the intertidal dispersion coefficients, q_{R_j} is the x-(or y-)component of the Eulerian residual water flux and q_{A_j} the x-(or y-)component of the "virtual" water flux along the channel (either in the flood or in the ebb-direction) that accounts for the asymmetry of the tidal flow.

In the Venice Lagoon (Dal Monte, 2004), the dispersion terms at the intertidal scale eqs. (1.11 and 1.12) turn out to be much larger than the advective ones. It is important to note that tidal fluxes in channels are basically controlled by the platform of the channel network (area of the tidal watershed and width of the channel) and hardly by the bathymetric configuration.

Since the horizontal morphology of tidal lagoons tends to remain constant in time, the hydrodynamic parameters D_{ij}, q_R and q_A can reasonably be considered constant for very long periods of time (decades or more), even if the bottom elevation is subject to evolution.

4.3 THE EQUILIBRIUM CONCENTRATION

The *equilibrium concentration* C_{eq} in a certain place is the average sediment concentration over the water column which would yield neither erosion or deposition (equilibrium condition). It depends on the grain size diameter of the particles, on the local hydrodynamics (waves and currents) and on the local depth (Dal Monte, 2004).

Let us consider a monomial transport formula for the sediment transport in suspension (e.g. Engelund and Hansen type) produced by *tidal waves* and let us call q_s the volumetric sediment discharge (eq. 1.13) per unit width produced by the water flow $q=vh$, where v is the water velocity averaged over the depth h:

$$q_s \propto v^n \quad where \quad n \cong 5-6 \qquad (1.13)$$

By assuming that the proportionality (eq. 1.13) still holds if v is the instantaneous orbital velocity produced by waves just outside the boundary layer, one finds for the "equilibrium concentration" the following expression, where a_{tid}, which depends on the grain size distribution, can be assumed constant:

$$C_{eq_{tid}} = \frac{q_s}{q} \propto \frac{v^n}{q} \propto \frac{q^{n-1}}{h^n} = a_{tid} \frac{q^{n-1}}{h^n} \qquad (1.14)$$

This assumption implies that the alternate sediment flux q_s during the passage of a wave is in phase, or constantly delayed, with respect to the corresponding alternate water flow q. Note that waves do not transport sediments but just stir them: long-term sediment transport on the

shoals (as well as in the channels) is produced, via the long-term averaged concentration, by intertidal dispersion and residual flow.

The height of significant wave H_w in shallow water is also due to the effects of wind velocity u_A and the length of the effective fetch F_e, as the formula of Bretschneider (1969) computed. In order to facilitate the long-term averaging, we want to approximate the Bretschneider's formula with a monomial formula (1.15):

$$H_w = k_2 \cdot F_e^{\alpha} \cdot h_s^{\beta} \cdot u_A^{\gamma} \tag{1.15}$$

where h_s is the water depth along the fetch.

Although the exponents α, β, γ and the coefficient k_2 depend in general on the local conditions, they are reasonably constant within a limited range of F_e, h_s and u_A (F_e=1000–5000 m, h_s=0.5–2.0 m, u_A=15–25 m/s).

By a comparison between the Bretschneider formula and the monomial approximation (eq. 1.15), it can be found the following acceptable values:

α=0.32 β=0.50 γ=1.45 k_2=3.2·10^{-3}

By assuming that the average depth along the fetch h_s is proportional to the local depth, h, the concentration is:

$$C_{eq_{wind}} \propto \frac{F_e^{4/3} \cdot u_A^6}{h_t} \tag{1.16}$$

Expression (1.16) indicates that the instantaneous concentration produced by waves depends on the local depth h_t (varying with the tide) and on a combination of fetch length and wind velocity. For sake of simplicity we shall consider tide and wind velocity, both time-dependent quantities, as mutually independent. The duration of tidal elevation is almost linearly distributed, all over the lagoon, around its average value. Wind and fetch both depend on direction; however, as it will be seen later, their statistical distributions are again mutually independent. In conclusion, expression (1.16) can be integrated over the time and over directions to get the averaged value:

$$C_{eq_{wind}} = \frac{f_{wind}}{h} \tag{1.17}$$

of the equilibrium concentration produced by *wind waves*, where h is the local tide-averaged depth. The value of f_{wind} depends on wind velocity and fetch length but also on sediment grain size; it tends to decrease for coarser bottom composition. Moreover, an appropriate value of f_{wind} can also account for the enhanced resistance of the bottom due to vegetation, either sea weeds (e.g. Zostera marina) on the shoals or aerial alophile species on the salt marshes.

The total equilibrium concentration $C_{eq} = C_{eq_{tid}} + C_{eq_{wind}}$ in any location is obtained in principle by summing up expressions (1.14) and (1.17).

The derivation of expressions (1.14) and (1.17) justifies the empirical expressions of transport concentration already used in some of the previous models. With respect to other formulations, expressions (1.14) and (1.17) are simpler, robust and susceptible of a relatively easy calibration of their coefficients against morphological data in quasi-steady conditions.

In formulating the concentration C_{eq}, it is relevant the value of the exponent of v (n=5–6) to be introduced in the monomial transport formula (eq. 1.13), as opposed to smaller exponent (2–3) valid for the binomial transport formulae (Meyer-Peter, Ackers, etc.).

The exponent n reflects in the exponent of h in eqs. (1.14) and (1.17), with important consequences that will be discussed in the following paragraph.

4.4 THE SEDIMENT BALANCE EQUATION

Long-term sediment balance can be expressed in two-dimensional form by the well-known Exner equation:

$$\frac{\partial h}{\partial t} = \frac{\partial Ch}{\partial t} + \frac{\partial T_x}{\partial x} + \frac{\partial T_y}{\partial y} + \alpha \qquad (1.18)$$

where $\alpha = \alpha_e + \alpha_s$ is the combined rate of eustatism (sea level rise) α_e and soil subsidence α_s. Note that balance equation may possibly account for a time- and space-lag of suspended transport.

Eq. (1.18) provides the long-term evolution of the tide-averaged depth, h, in each location of the lagoon. For solving eq. (1.18), the following data should be available: distribution all over the lagoon of the hydrodynamic quantities D_{ij}, q_{R_j} and q_{A_j} in eqs. (1.11) and (1.12), provided by a tidal flow model; distribution all over the lagoon of the stirring coefficients a_{tid} and f_{wind} for currents and waves.

The stirring coefficient f_{wind} in salt marshes can be set right away equal to zero or can be evaluated more precisely by biological considerations based on existing flora. The stirring coefficients in channels and shoals can in principle be evaluated by semi-empirical procedures and/or calibrated against field data. An evaluation of these parameters for different zones of the Venice Lagoon has been made for simulating the evolution of the lagoon since 1800 (Di Silvio, 1991b).

For simulating the evolution of the salt marshes, moreover, one needs the equations describing their geotechnical behaviour (collapse and reconstruction of the edges; consolidation process of the captured material). It should be mentioned, in this regard, that

salt marshes of the Venice Lagoon represent a dynamic component as far as planimetric morphology is concerned. In fact, while the planimetric configuration of the tidal channel network has remained very stable through the centuries, the area covered by salt marshes has been and is still subject to a very fast reduction. The extension of salt marshes, on the other end, controls the fetch distribution in the lagoon and, consequently, the value of f_{wind} in eq. (1.17).

Once the quasi-equilibrium spatial distribution of a_{tid} and and f_w is known, by solving the sediment balance equations one may predict the lagoon's evolution ensuing from any possible perturbation introduced in the system. Perturbations may be produced by natural or anthropogenic changes of the external boundary conditions: strongly increased rate of eustatism and subsidence (e.g. due to the global warming or excessive groundwater withdrawal); variations of fluvial input (e.g. due to the diversion of rivers); decreased concentration at the sea side of the inlets (e.g. due to the construction of jetties and consequent increase of the inlet depth). Perturbations may also be produced by variations of the internal conditions. For instance, the depth of channels and shoals may be locally altered because of dredging and dumping operations.

Any of the above mentioned perturbations produces in the model some variations of the local concentration with respect to the initial quasi-uniform distribution and, consequently, the establishment of concentration gradients. Those gradients, in their turn, activate both advective (residual) and dispersive (intertidal) sediment transport and ultimately aggradation or degradation of the bottom. Aggradation and degradation will proceed till a new bathymetric equilibrium configuration will be attained. Eqs. (1.14) and (1.17) constitute the coupling relation between hydrodynamics (represented by the locally constant stirring coefficient) and morphodynamics (represented by the local variable depth), showing a general tendency to reach a stable condition. In fact, when a channel or a shoal is subject to erosion (deposition), the depth increases (decreases) and transport concentration decreases (increases) in such a way that sediments are transported by dispersion towards (away from) that location. Conversely, if local concentration increases (decreases), deposition (erosion) takes place till the new depth is again in equilibrium with the local conditions.

Let us comment, now, the role of the *exponents* 5 and 1 of the local depth h, respectively, in eqs. (1.14) and (1.17). The two values designate a different sensitivity of channel and shoals in reacting to any change of transport concentration. For a (small) relative change of concentration $r=\Delta C/C$, the relative variation of the shoal depth is again r, while the variation of the channel depth is about five times smaller. This means that while channels tend to

remain relatively stable, shoals may give rise to huge modifications, depending upon the new boundary conditions. It is relevant to emphasize that since the external boundary conditions, as well as the internal ones (residual flow, dispersion coefficients, stirring coefficients), do not depend upon the bathymetric evolution of the lagoon, no external adjustment of these data is necessary during the numerical computation. This represents a crucial advantage of expressions (1.14) and (1.17) with respect to other formulations of the transport concentration, often implicitly dependent on the changes of the basin bottom. It should be noted that, in principle, the quantity h_s in eq. (1.15) (average depth along the fetch) does depend on the bathymetric evolution of the basin, but this dependence has been removed by assuming h_s proportional to the local depth h_e. Also, the quantity F_e (fetch length) may in principle remain not constant, as it depends on the extension of marshes and, indirectly, on the bottom evolution (Dal Monte and Di Silvio, 2004).

4.5 SALT MARSHES

Salt marshes are relatively active components of the lagoon and changes of their planimetric configuration may affect the fetch distribution all over the basin. Although some attempts of modelling the complex behaviour of marshes have been made, a thorough verification of those models is not yet available.

Salt marshes are peculiar features of tidal lagoons, characterized by their elevation above the mean sea level and hence by their submergence time. While shoals are permanently submerged by water, salt marshes are very often dry. Consequently, they are generally covered by a thick aerial vegetation. As aerial vegetation strengthens to a very large extent the bottom resistance, stirring of sediments is virtually impossible and transport concentration results to be extremely low or even zero. In other words, salt marshes act as a very efficient trap, capturing sediments from the shoals and the channels nearby. Sediments trapped by salt marshes, while subject to consolidation, contribute to the raising of the marsh surface. As the surfaces rises, water fluxes in the marshes, as well as the corresponding sediment transport, become smaller and smaller. Sediment transport goes practically to zero when the marsh surface approaches the maximum elevation of the tidal range.

At this point, a salt marsh remains permanently dry and evolves into an island. The elevation of salt marshes, however, is almost invariably limited by the rate of subsidence and eustatism, which compensate the capture of sediments. The overall balance of sediments determines not only the elevation, but also the surface area covered by salt marshes. For predicting the elevation of salt marshes, soil consolidation should be accounted for and appropriate

compaction coefficients should be assumed. Finally, for predicting the salt marshes area, the collapse of their steep edges needs to be described. In this regard, a simple zero-dimensional geotechnical model has been proposed (Di Silvio et al., 2001), but not verified against field data. In any case, the geotechnical analysis requires a careful revision with regard to the role of vegetation is strengthening the marsh edges. Special attention should also be given to the growth process of the pioneer vegetation, when the bottom of the salt marshes reaches a sufficient elevation to permit vegetation to thrive.

The behaviour of salt marshes in non-stationary conditions (that is when the long-term overall sediment balance is in excess or deficit) is quite interesting, as their evolution seemingly presents a strong hysteresis and asymmetry (Di Silvio and Padovan, 1998). In fact, while the "construction" phase is gradual and controlled by the progressive grown of vegetation, the "demolition" phase is generally delayed with respect to the sediment deficit as it depends on the collapse of the steep edges. This particular behaviour can be simulated by the long-term morphological model, provided that the biological and geotechnical processes are correctly incorporated.

Chapter 2

ONE-DIMENSIONAL NUMERICAL MODEL OF RIVERS

SUMMARY

Is presented here a one-dimensional morphodynamic model (mathematical and numerical) for non-uniform grain-size sediments which is intended to be employed for computations at relatively large space scale and for both short and long-term calculations.

The mathematical model is based on the "active layer" concept. It considers two layers (Armanini and Di Silvio, 1988): the mixing layer (Hirano, 1971), also called transport layer, containing the particles transported in suspension and as bedload, and the storage layer (Di Silvio, 1991a) containing particles that are not in movement, but are liable to vertical movements to and from the upper transport layer. The water flow equations are solved together with the sediment equations in a quasi-coupled way by means of a predictor-corrector numerical scheme. The predictor step was carried out with a FTBS (Forward Time Backward Space) scheme while the corrector step was performed with a Four Points scheme. A completely new hydrodynamic module was developed based on the simplified steady and unsteady (Kinematic wave propagation) shallow water equations. The models are applied to verify the analytical solutions (Chapter 4; Fasolato et al., 2008b) and to some study cases (Chapter 5, Fasolato et al., 2007; Ronco et al. 2008a).

1. INTRODUCTION

Modelling erosion and deposition processes in rivers and particularly in mountain streams (where the sediment grainsizes vary over several order of magnitude from boulders to silt) requires in principles a careful reproduction of a number of phenomena related to the non uniformity of a sediment mixture. For this reason and for the easily application to relatively large portions of the hydrographic network, the most common commercial models used for this kind of simulations are *1-D* (*one-dimensional)* (Chapter 1, par. 3.2) i.e. averaged over the river cross-section (but possibly disaggregated in a number of sub-sections). They can simulate bottom erosion and deposition along the river (generally the most relevant requested information), evolution of bottom grainsize composition and sediment transport.

Compared to the more complex *2-D*, 1-D models further present a reduced computational time and make possible its application for long-term simulations at watershed scale. At last, models may also include a (quasi 2-D) component for simulating the planimetric evolution of the channel width (bank collapse and reconstruction).

A one-dimensional morphodynamic model (mathematical and numerical) and its hydraulic modifications (*quasi steady* and *unsteady flow*) are presented here. A numerical code implemented by Di Silvio and Peviani (1989) was used for computation, integrating some modifications during different simulations.

2. MATHEMATICAL MODEL

The one-dimensional morphological models studied here, present some common simplified assumptions both for hydraulic and sediment transport hypothesis, reported in the followed sections. Moreover, three different models have been developed, based on the simplification of the hydrodynamic hypothesis. For all three the numerical models, the equations of water flow and sediment movement should be considered *quasi-coupled*. It however can be justified considering that the bottom variation are much slower than water surface variations.

2.1 HYDRODYNAMIC HYPOTHESIS

For all the models, channel cross sections are simplified as rectangles of bankfull channel width and no bank erosion or floodplain sediment contribution affect the bottom evolution. In the present formulation of the model the stream width (B_s) has been evaluated as a function of Q where $B_s = K_p Q^{0,5}$ (K_p is assumed to be constant). Each reach is schematized as a rectangular channel with uniform flow condition; water depth is calculated with the classical

Gauckler-Strickler equation (eq. 2.1), in which A is the wetted area (m^2), R the hydraulic radius (m), S_f the friction slope and K_s, the Strickler coefficient that may change in time and space (eq. 2.2):

$$Q = K_s A R^{2/3} S_f^{1/2} \tag{2.1}$$

$$K_s = 26/d_{90}^{1/6} \tag{2.2}$$

The three models present the same assumptions for the morphodynamic aspects but are different for the hydrodynamic characteristics (Table 2.1). The STE.RI.MOR model (STEep RIver MORphology model) is based on the hypothesis of local uniform flow and assume instantaneous adaptation in time of the water discharge in each branch of the network.

The second model, PLA.RI.MOR model (PLAin RIver MORphology model) is pretty similar to the first one but consider quasi-steady flow condition and a standard backwater formulation is employed to solve for flow characteristics.

The third model, UN.RI.MOR model (UNsteady RIver MORphology model) is based on the kinematic wave hypothesis. As a matter of fact, neglecting inertia and pressure differential terms in the dynamic equation for unsteady gradually varied flow in open channels and then combining it with the continuity equations we obtain:

$$\frac{\partial Q}{\partial t} + c_w \frac{\partial Q}{\partial x} = c_w q_l \tag{2.3}$$

in which Q is the water discharge (m^3/s), q_l is the input lateral water discharge per unit length (m^2/s) and c_w is the kinematic wave celerity (m/s) which is equal to (Cunge et al., 1980; Miller, 1984):

$$c_w = \left.\frac{\partial Q}{\partial A}\right|_x \tag{2.4}$$

Hyphotesis	Model	De St. Venant equation
Unsteady flow	UN.RI.MOR	$\frac{\partial}{\partial t}\left(\frac{Q}{A}\right)+\frac{\partial}{\partial x}\left(\frac{\beta Q^2}{2A^2}\right)+g\frac{\partial h}{\partial x}+g\left(J-I\right)=0$
Quasi-steady flow	PLA.RI.MOR	$\frac{\partial}{\partial x}\left(\frac{\beta Q^2}{2A^2}\right)+g\frac{\partial h}{\partial x}+g\left(J-I\right)=0$
Quasi-uniform flow	STE.RI.MOR	$\left(J-I\right)=0$

Table 2.1 Different hydrodynamic models and their applications.

In the Table 2.1 a summary briefly described the different models characteristics; in the De St. Venant equation x and t are the spatial and temporal axes; A is the flow area, Q is the flow discharge, h is the flow depth, I is the bed slope β is a correction coefficient for the momentum due to the nonuniformity of velocity distribution at the cross section; g is the gravitational acceleration and J is the friction slope.

2.2 SEDIMENT TRANSPORT HYPOTHESIS

For all models it is assumed that the motion equation for the *k-th* sediment fraction (k=1,2,…N), both as bedload and in suspension, is completely governed by the local parameters, such as discharge, energy slope, channel width, grain size, etc. (it means, instantaneous adaptation of the vertical sediment concentration in the water stream).

The bed material is divided into several layers to allow the computation of changes in bed-material gradation due to erosion or deposition. The sediment vertical exchange take place basically considering two layers (Armanini and Di Silvio, 1988): the transport layer, containing the particles transported in suspension and as bedload, and the active (or mixing) layer (Hirano, 1971) containing the particles that are not instantaneously in movement, but are liable to vertical movements to the upper transport layer (Fig. 2.1).

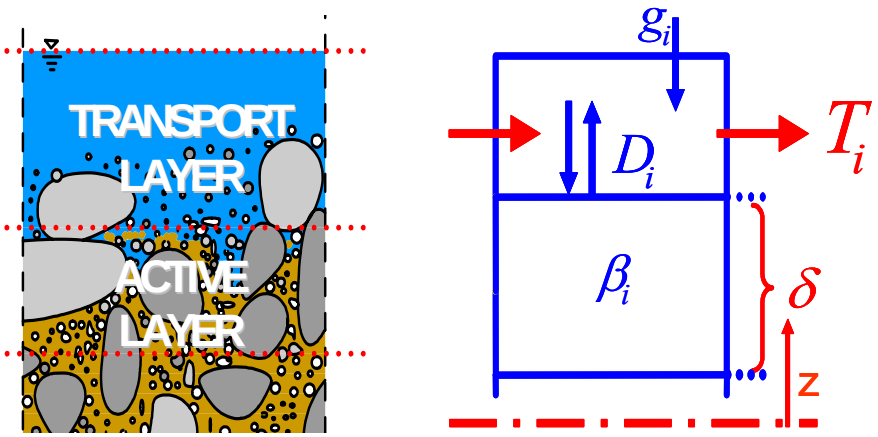

Fig. 2.1 Definition sketch for the sediment balance in the transport- and in the active-layer.

The balance in the transport layer between transport P_k and net deposition D_k, is written as eq. (2.5), where B is the active channel width (m) and g_k is lateral specific solid discharge (m^2/s).

$$BD_k + \frac{\partial P_k}{\partial x} = g_k \qquad (2.5)$$

Eq. (2.6) expresses the balance in the active layer and it leads to the computation of bed-composition changes. In this equation β_k is the percentage of the k-th class present in the

active-layer, β_k^s the percentage below the active-layer and β_k^* assuming different values during the erosion $D_k<0$ $\left(\beta_k^* = \beta_k^S\right)$ or deposition phase $D_k>0$ $\left(\beta_k^* = \beta_k\right)$

$$\frac{\partial\left(\delta\beta_k\right)}{\partial t} = D_k - \beta_k^* \frac{\partial Z}{\partial t} \tag{2.6}$$

Bottom level change is expressed by eq. (2.7) and the mixing layer thickness (δ) is assumed to be constant (order-of-magnitude about twice the representative diameters D_{90} of the coarsest particles).

Models consider 4 granulometric fractions (size class k) and the solid transport P_k (eq. 2.7) is approximated by a monomial expression, where α_c is a coefficient depending on the river category, β_k is the percentage of the k-th grainsize class d_k presents in the bottom and ζ_k the "hiding-exposure" coefficient (s=0.8) which reduces the larger mobility of smaller particles and vice-versa (eq. 2.8).

$$P_k = \alpha_c \frac{Q^m J^n}{B^p d_k^q} \beta_k \zeta_k \tag{2.7}$$

$$\zeta_k = \left(d_k \Big/ \sum_{k=1}^{n} \beta_k d_k \right)^s \tag{2.8}$$

3. NUMERICAL MODEL

The set of equations of the two–phase mathematical model was solved numerically using a finite difference approximation. A predictor-corrector method was used. The predictor step was performed with a FTBS (Forward Time Backward Space) scheme, while the corrector step was carried out with a Four-Points scheme.

3.1 PREDICTOR STEP: FTBS SCHEME

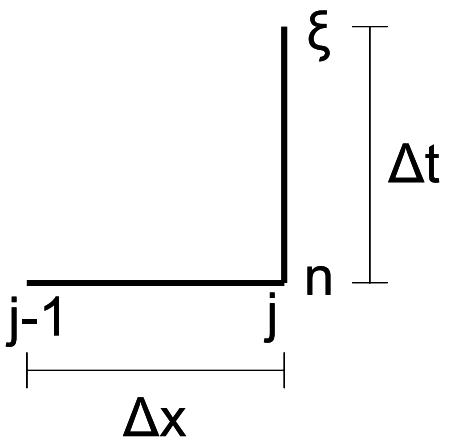

In the predictor step the time and space derivatives of the water discharge are approximated in the following way (superscript n is the present time level, superscript ξ is the predicted value, superscript $n+1$ is the new time level):

$$\frac{\partial Q}{\partial t} = \frac{Q_j^{\xi} - Q_j^n}{\Delta t} \tag{2.10}$$

$$\frac{\partial Q}{\partial x} = \frac{Q_j^n - Q_{j-1}^n}{\Delta x} \tag{2.11}$$

while the sediment continuity equation in the transport layer is solved by means of the following difference equation:

$$D_{k_j}^{\xi} = \frac{1}{B_j \Delta x}\left(P_{k_{j-1}}^n - P_{k_j}^n + G_{k_j}^n\right) \tag{2.12}$$

the difference equation for the temporal bed level changes is given by:

$$\frac{Z_{b_j}^{\xi} - Z_{b_j}^n}{\Delta t} = \sum_{k=1}^{4} D_{k_j}^{\xi} \tag{2.13}$$

and the vertical sediment balance in the mixing layer is discretized in the following manner:

$$\frac{\delta_j^n\left(\beta_{k_j}^{\xi} - \beta_{k_j}^n\right)}{\Delta t} = D_{k_j}^{\xi} - \beta_{k_j}^{*} \sum_{k=1}^{4} D_{k_j}^{\xi} \tag{2.14}$$

it is noted that in the predictor step the mixing layer thickness in equation (2.14) is considered constant in time.

3.2 CORRECTOR STEP: FOUR POINTS SCHEME

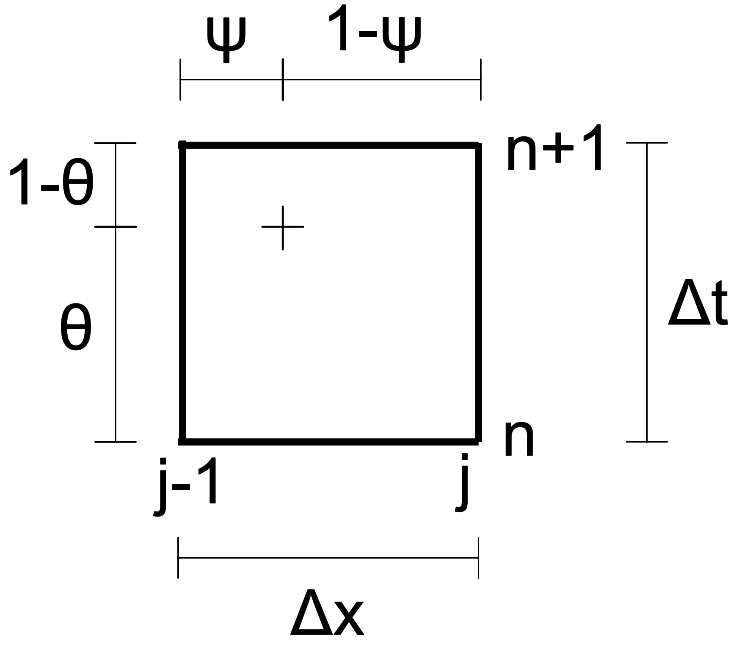

In the corrector step the time and space derivatives of the water discharge are approximated in the following way:

$$\frac{\partial Q}{\partial t} = \frac{\psi\left(Q_j^{n+1} - Q_j^n\right) + (1-\psi)\left(Q_{j-1}^{n+1} - Q_{j-1}^n\right)}{\Delta t} \tag{2.15}$$

$$\frac{\partial Q}{\partial x} = \frac{\theta\left(Q_j^{n+1} - Q_{j-1}^{n+1}\right) + (1-\theta)\left(Q_j^n - Q_{j-1}^n\right)}{\Delta x} \tag{2.16}$$

celerity c_w, weighted in space and time, is expressed as follows:

$$c_{w_j}^{n+1} = \theta\left[\psi c_{w_j}^{\xi} + (1-\psi) c_{w_{j-1}}^{\xi}\right] + (1-\theta)\left[\psi c_{w_j}^{n} + (1-\psi) c_{w_{j-1}}^{n}\right] \tag{2.17}$$

while the sediment continuity equation in the transport layer is solved with the following difference equation:

$$D_{k_j}^{n+1} = \frac{1}{B_j \Delta x}\left[(1-\theta)\left(P_{k_{j-1}}^n - P_{k_j}^n + G_{k_j}^n\right) + \theta\left(P_{k_{j-1}}^{\xi} - P_{k_j}^{\xi} + G_{k_j}^{n+1}\right)\right] \tag{2.18}$$

the difference equation for the temporal bed level changes is written as follows:

$$\frac{Z_{b_j}^{n+1} - Z_{b_j}^n}{\Delta t} = \sum_{k=1}^{4} D_{k_j}^{n+1} \tag{2.19}$$

and the difference equation for the vertical sediment balance in the mixing layer is given by:

$$\frac{\left(\delta\beta_k\right)_j^{n+1} - \left(\delta\beta_k\right)_j^n}{\Delta t} = D_{k_j}^{n+1} - \beta_{k_j}^{*}\left[\sum_{k=1}^{4} D_{k_j}^{n+1} - \frac{\left(\delta_j^{n+1} - \delta_j^n\right)}{\Delta t}\right] \tag{2.20}$$

The sequence of the numerical calculation is:

a) The water discharge is predicted (eqs. 2.10, 2.11) and corrected (eqs. 2.15, 2.16) considering for the celerity the mean value (eq. 2.17).

b) The motion equation for the sediment is applied at every grid point at time level *n*, in which the channel geometric data and the sediment data are known.

c) The predicted values D_k^{ξ} and β_k^{ξ} are computer at every grid point by using the sediment contuinuity equation (2.12) with the predictor-scheme and the vertical balance equation (eq. 2.14). Then the sediment transport P_k^{ξ} computed again at every grid point as a function of the predicted values β_k^{ξ}.

d) By applying again eq. (2.12) with the corrector-scheme the value of D_k^{n+1} is computer, and with eq. 14 the value β_k^{n+1} is computer at every grid point.

e) The sediment transport at time level *n+1* is now computed as a function of β_k^{n+1}.

f) At the end, the new bottom level is computed from eq. (2.13), with the value D_k^{n+1}.

3.3 LATERAL SEDIMENT INPUTS AND INTERNAL BOUNDARY CONDITIONS

In the model the lateral sediment inputs from tributaries and internal boundary conditions can be represented in different ways depending upon the kind of processes to be simulated. These are briefly described below.

3.3.1 Tributary conveying material as ordinary sediment transport

In this case the sediment transported by the water flow before the landslide event is computed (by the transport equation) with the local hydrodynamic and sedimentological characteristics of the final reach of the tributary.

3.3.2 Tributary conveying material from a nearby landslide as extraordinary sediment transport

In this case, to compute the sediment input as a function of the tributary water discharge it is assumed that the bed material composition of the tributary (slope less than 10-15 %), immediately after the landslide event, changes to that of the landslide material and remain that until the total volume is transported by the flow. However, it is possible to consider the input of a debris flow (tributary slope greater than 15-20%) by changing the composition of the riverbed to that of the debris material and by assuming a constant debris flow velocity entering the main stream. In both cases the landslide material composition and volume as well as the time of occurrence and the locations of the landslide events must be known before starting with the morphological calculations.

3.3.3 Fixed rocky bottom

In mountain rivers reaches, fixed rocky bottom are usually ecountered along the main streams; in this case erosion cannot progress below the rocky bottom and the sediment load coming from upstream is transferred to the downstream reaches as overpassing loads.

4. MODEL ANALYSIS

4.1 STABILITY CONDITION AND TIME STEP SIZE ADJUSTMENT

In the morphodynamic model the choice of the time step size Δt is subject to Courant-Friedrischs-Lewy (CFL) stability constraint:

$$\Delta t = \sigma \frac{\Delta x}{c_{\max}} \tag{2.21}$$

where $0<\sigma\leq 1$ and $c_{\max}$ is the maximum celerity at a relevant time step:

$$c_{\max} = \max\left\{c_w, c_{\beta_k}, c_{Z_b}\right\} \tag{2.22}$$

in expression 22, c_w is the celerity related to the flow which is given by the following equation:

$$c_w = \frac{5}{3}u \tag{2.23}$$

while c_{β_k} is the celerity associated to a disturbance in the bed material composition of the k-th class which can be expressed as follows:

$$c_{\beta_k} = \frac{P_k}{\delta B}\left(\frac{1}{\beta_k} - s\zeta_k^{1/s}\right) \tag{2.24}$$

and c_{z_b} is the celerity related to a disturbance in the bed level which is given by the following equation:

$$c_{Z_b} = \sum_{k=1}^{4} c_{\beta_k}\left[\left(D_k \Big/ \sum_{k=1}^{4} D_k\right) - \beta_k\right] \tag{2.25}$$

In order to avoid phase error and numerical diffusion in the constant σ in eq. (2.21) is generally set to values close to unity.

4.2 STABILITY AND ACCURANCY ANALYSIS

Some preliminary tests were performed as to analyze the stability of the numerical schemes as well as to check their accuracy against the theoretical evaluations of celerity and physical damping.

All the tests were performed by studying the behaviour of a channel in uniform conditions when a sudden variation of the bottom composition is introduced in its upper part. This variation simulates the input of fine materials in a mountain river, by landslides or debris flow (overfeeding); the availability of fine material in the bed generates a much higher transport (until the fine material is completely removed) and a rapid aggradation along the river.

The parameters used for the analysis, the granulometry of the initial bed (β_{k_0}) and of the landslide material (β_{k^*}) is given in the following Table 2.2. The mixing layer thickness was kept constant and equal to 1 m, not much different from the value of $2d_{90}$.

Fig. 2.2a and 2.2b gives an example of stability analysis, showing the progressive aggradation of the bottom along the channel caused by the stepwise disturbance at the upper end.

The distance along grid points is Δx=250 m while the time step is Δt=400 s in case *a* and Δt=250 s in case *b*. The weight coefficient in eq. 16 (the discharge was considered constant along the river reach) was θ.

Q [m^3/s]	300	m	1.8
B [m]	67	n	2.1
I [-]	0.02	p	0.8
α [-]	0.011	q	1.2
		s	0.0

	d_k [mm]	β_{k_0}	β_{k^*}
1^{st}	0.3	0.080	0.250
2^{nd}	3	0.240	0.520
3^{rd}	30	0.460	0.200
4^{th}	300	0.220	0.030

Table 2.2 Parameters used for the model stability analysis

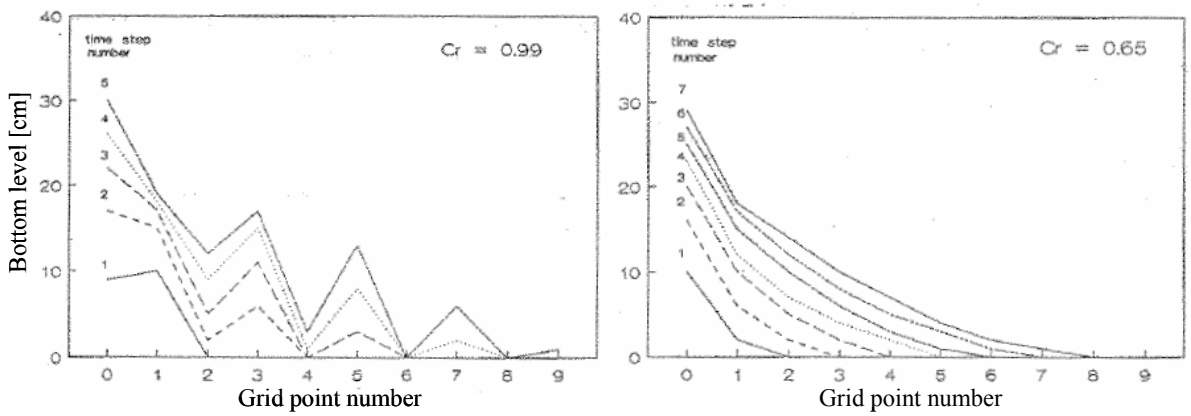

Fig. 2.2a and 2.2b An example of stability analysis. Propagation of a bottom level disturbance (stepwise variation of bottom composition) with different Courant numbers (Di Silvio and Peviani, 1989).

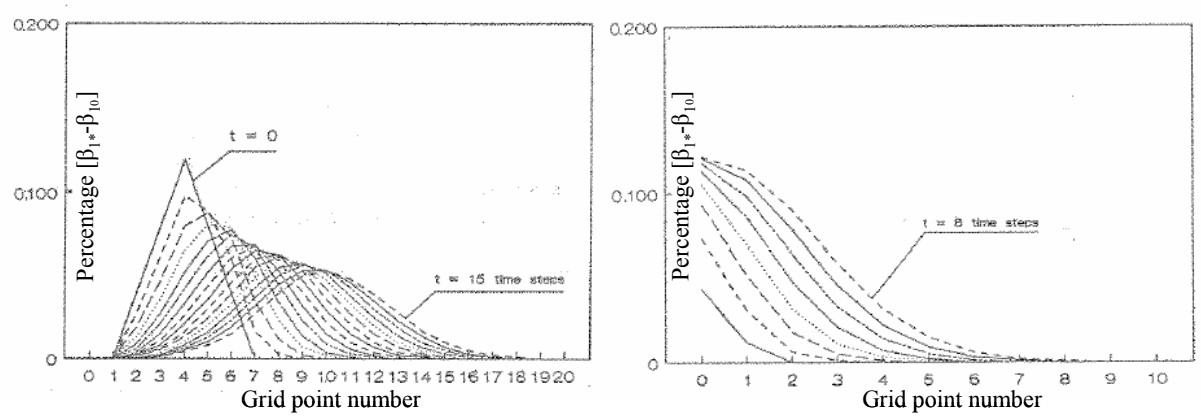

Fig. 2.3a and 2.3b An example of celerity analysis. Propagation of a bottom-composition disturbance: a) (left side) gradual variation and b) (right side) stepwise variation of the first fraction β_1 (Di Silvio and Peviani, 1989).

The result shows an actual upper limit for the Courant number, *Cr*=0.65.

Fig. 2.3a and 2.3b show the propagation of the disturbance of the bottom composition introduced in the upper part of the channel (only the propagation of the fraction k=1 is reported).

4.3 SENSITIVITY ANALYSIS OF THE PHYSICAL PARAMETERS

Some preliminary tests were performed to see the influence of the main physical parameters on the behaviour of the disturbance propagation. In particular, the celerity and height of the bottom aggradation was analyzed for different granulometries of the initial bottom and of the landslide material.

4.3.1 Influence of the initial bottom composition (β_{1_0})

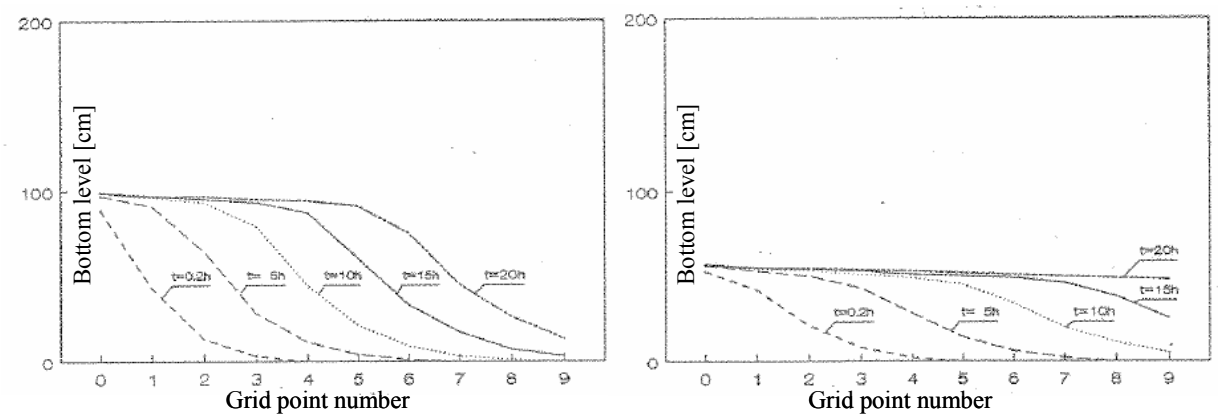

Fig. 2.4a and 2.4b Sensitivity analysis. Effects of the initial bottom composition β_{1_0} on the disturbance propagation (Di Silvio and Peviani, 1989).

In both simulations (Fig. 2.4a and 2.4b) the composition of the material at the upstream boundary is β_{1^*}=0.250, β_{2^*}=0.520, β_{3^*}=0.200, β_{4^*}=0.030, with $\delta=2d_{90}$ and s=0.6. The initial bottom composition in Case *a* is β_{1_0}=0.040, β_{2_0}=0.200, β_{3_0}=0.500, β_{4_0}=0.260. On the other hand, Case *b* has a finer material composed of β_{1_0}=0.120, β_{2_0}=0.280, β_{3_0}=0.420, β_{4_0}=0.180. It is possible to see that the disturbance wave propagates faster in case of finer initial bottom composition. As the transport at the upstream boundary is the same in both cases, the height of the wave is smaller in case of finer material.

4.3.2 Landslide material composition (β_{1^*})

In both cases (Fig. 2.5a and 2.5b) the initial composition of the bottom is β_{1_0}=0.080, β_{2_0}=0.240, β_{3_0}=0.460, β_{4_0}=0.220, with $\delta=2d_{90}$ and s=0.6.

The composition of the overloading material at the upstream boundary in Case a is β_{1^*}=0.463, β_{2^*}=0.349, β_{3^*}=0.168, β_{4^*}=0.020. In Case b there is a coarser material with composition β_{1^*}=0.250, β_{2^*}=0.520, β_{3^*}=0.200, β_{4^*}=0.030. The plots show a faster propagation disturbance in case of finer material; in spite of the difference on the upstream transport values (P=2.67 m^3/s in Case a, and P=1.55 m^3/s in Case b) the height of the wave remain quite constant.

Further tests confirm that the thickness of the *mixing layer* δ influences the celerity of the disturbance propagation on an inverse way: with smaller values of δ the celerity increases.

The *values of s* on the exposure-correction coefficient influences the sediment transport values of each fraction. In this way, for higher values of *s* the transported material becomes coarser.

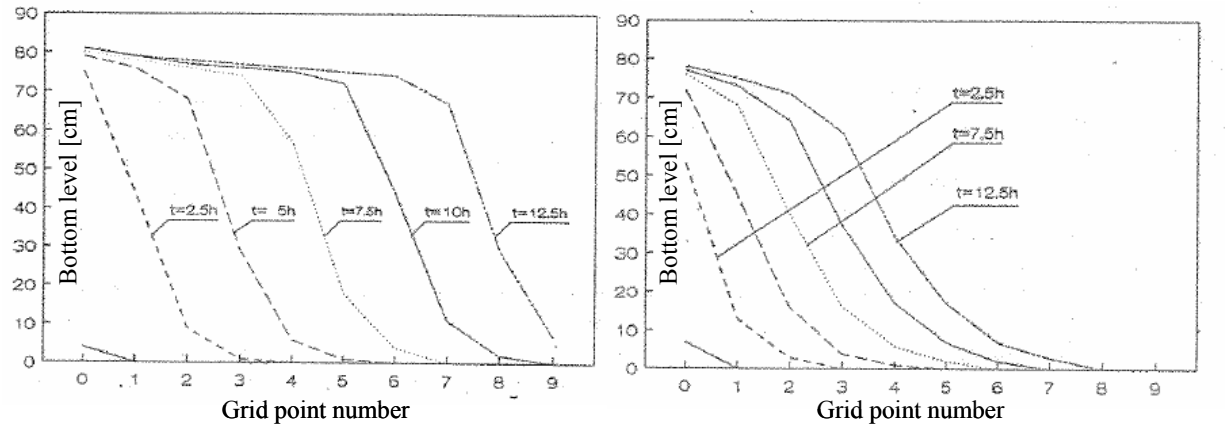

Fig. 2.5a and 2.5b Sensitivity analysis. Effects of the overloading composition β_{1^*} on the disturbance propagation (Di Silvio and Peviani, 1989).

5. APPLICATIONS

At present , the one-dimensional river models were applied mainly for mountain rivers to study the sediment transport and consequent morphological evolution of a stream during natural and artificial floods (Bonfigli et al., 1994; Peviani et al., 1995; Basile and Peviani, 1996; Fasolato et al., 2006) or during anthropologic activities from reservoirs (e.g. flushing operations) (*Chapter 5*, Fasolato et al., 2007). Another trend concerns expanding analysis to

long term evolution of rivers (Di Silvio and Peviani, 1991; Peviani, 2002; Ronco et al., 2007) and to large unsurveyed rivers (Ronco et al., 2008a).

Chapter 3

ONE-DIMENSIONAL ANALYTICAL MODEL OF RIVERS

SUMMARY

A one-dimensional analytical morphodynamic model for non-uniform grainsize material is discussed here. Besides the instantaneous propagation of the waterflow along the river reach, this model ("harmonic river") considers a sinusoidal variation of the boundary conditions at both ends (in time), as well as of the channel width (in space) and takes into account two grainsize classes of solid material. The objective of the model analysis is to study the effects of geometry, hydrology and sediment input unsteadiness and non-uniformities, by explicitly indicating the most important parameters that control their propagation and attenuation along the river. Apart from instantaneous propagation of waterflow, the information regarding the boundary conditions are conveyed along the river reach by three waves, two propagating in the downstream direction and one propagating upstream, independently from flow conditions. Moreover, except for extremely low values of Froude number, both the third and the second waves may be neglected in the middle of the reach and virtually all information is transmitted in the downstream direction by the first wave.

1. INTRODUCTION

The morphological behavior of a river reach is affected by the variability in space and time of its boundary conditions. Variability regards geometry (longitudinal and transversal bottom profile), hydrology (input of water and water levels), and sediment input (transport rate and grainsize distribution). In engineering applications, the variability of boundary conditions is often somehow filtered and an "equivalent" constant quantity is employed in lieu of the variable one. In most applications only the water flow input is assumed to be an independent boundary condition variable in time, while the sediment input and its composition are considered in equilibrium with the water flow. This, however, is not the case in nature, where the sediment input from the watershed slopes may vary in time in a total different way with respect to the runoff, depending upon the prevailing forms of erosion (mass movement, surface erosion, combination of the two forms, intermediate forms etc..).

The effects of the variability has been studied mainly by field observations, laboratory experiments and numerical models (Marin and Di Silvio, 1996; Cui et al., 1996; Cao et al., 2002; Papanicolaou, 2004; Wu et al., 2004; Cui and Parker, 2005; Curran et al., 2005; Wright and Parker, 2005a and 2005b) but not less helpful have been several analytical discussions (Seminara, 1997; Repetto et al., 1999; Lyn and Altinakar, 2002, Lanzoni et al., 2006).

The perturbations created by the variable boundary conditions at the two ends of the river propagate downstream and upstream along the river reach, following the characteristic lines of the governing equations. A discussion of the characteristics lines to evaluate the general behaviour of these perturbations has been initiated since almost one century for the fixed-bottom channels and reconsidered later for the case of uniform grainsize material (De Vries, 1965 and 1973; Lyn, 1987; Correia, 1992; Morris and Williams, 1996; Lyn and Altinakar, 2002). The discussion has subsequently been expanded and developed to include more and more aspects (non-uniform grainsize, adaptation length of suspended particles, two dimensional equations), with the purpose, among others, to single out the limits of different models' application (Sieben, 1997).

An analytical solution of the linearized one-dimensional equations for uniform grainsize has been found, for uniform sediments, by assuming sinusoidal variations in space and time (e.g. Ribberink and van der Sande,1985; Vreugdenhil, 1994).

The non-uniformity of grainsize material, however, is quite important for a correct description of river morphodynamics, as it has been clearly shown by Sieben (1997) and will be confirmed in the present Chapter. The "harmonic river" proposed here considers a sinusoidal variation of the boundary conditions at both ends (in time), as well as of the channel width (in

space) and takes into account two grainsize classes of solid material. The harmonic solution gives useful indications on the effects of unsteadiness and non-uniformities, by explicitly indicating the most important parameters that control their propagation and attenuation along the river.

2. THE LINEARIZED HARMONIC RIVER

2.1 BASIC EQUATIONS

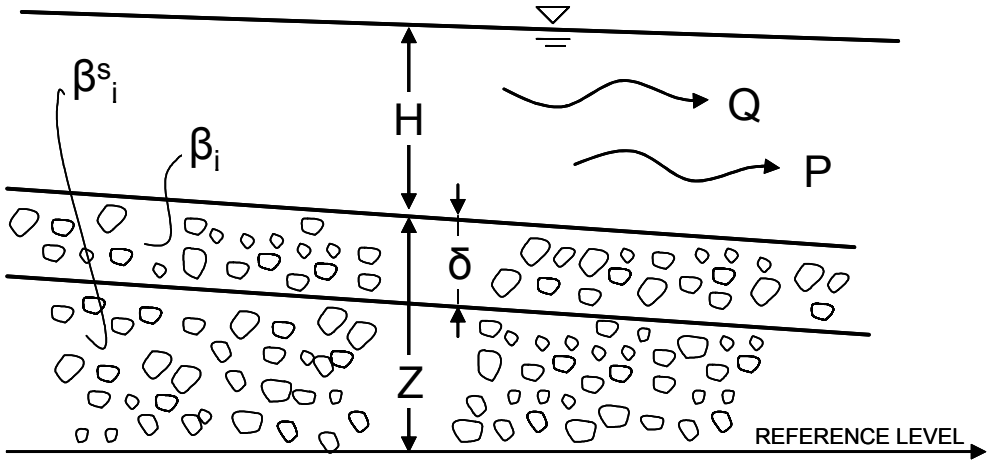

Fig.3.1 The one-dimensional model and its variables

The one-dimensional mathematical model (Fig. 3.1) for simulating the morphodynamic evolution of any river is characterized by a system of differential equations describing waterflow (De St. Venant equations, eq. 3.1 and 3.2), the sediment exchange between stream and bottom (Exner equation, eq. 3.3) and, for non-uniform sediments, the change of composition in the bottom "active layer" (Hirano equation, eq. 3.4).

$$\frac{\partial Q}{\partial x^*}+\frac{\partial A}{\partial t^*}=0 \tag{3.1}$$

$$\frac{\partial}{\partial x^*}\left(+H+Z+\frac{Q^2}{2gA^2}\right)=-\frac{1}{g}\frac{\partial U}{\partial t^*}-J \tag{3.2}$$

$$\sum_{k=1}^{N}\frac{\partial P_k}{\partial x^*}=-B\frac{\partial Z}{\partial t^*} \tag{3.3}$$

$$\delta B\frac{\partial \beta_k}{\partial t^*}=-\frac{\partial P_k}{\partial x^*}-B\beta_k^*\frac{\partial Z}{\partial t^*} \tag{3.4}$$

In eqs. 3.1-4, x^* and t^* are the (dimensional) space and time coordinate, Q is the water discharge, A is the wetted cross section area, H is the average water depth, Z the bottom elevation, g is the acceleration due to gravity, $U=Q/A$ the flow velocity, J the energy slope, P_k

is the solid discharge of the k-th class of sediment (k=1,2…N), $B(x^*)$ the channel width, δ is the thickness of the active-layer, β_k is the percentage of the k-th class present in the active-layer, β_k^s the percentage below the active-layer and β_k^* assuming different values during the erosion $\left(\beta_k^* = \beta_k^S\right)$ or deposition phase $\left(\beta_k^* = \beta_k\right)$.

For the water flow two important simplifications are assumed: an instantaneous propagation of the water flow discharge (simplified continuity equation, eq. 3.1') and quasi-steady flow condition (simplified momentum equation, eq. 3.2' with Coriolis coefficients equal to 1). Both conditions are satisfied in most rivers, whenever the flood wave length is quite longer than the distance between two major tributaries.

$$\frac{\partial Q}{\partial x^*} = 0 \tag{3.1'}$$

$$\frac{\partial}{\partial x^*}\left(\frac{Q^2}{2gA^2} + H + Z\right) = -J \tag{3.2'}$$

The hydraulic resistance is pounded by the Chézy formula, $Q = U \cdot A = C_h\sqrt{HJ}$.

Solid transport P_k is approximated by a monomial expression (Chapter 2, eq. 2.7), similar to the Engelund-Hansen transport formula, rounding some exponents (eq. 3.5); where α_c is a coefficient depending on the river category, β_k is the percentage of the k-th grainsize class d_k presents in the bottom and ζ_k the "hiding-exposure" coefficient (s=0.8) which reduces the larger mobility of smaller particles and vice-versa (eq. 3.6).

$$P_k = \alpha_c \frac{Q^2 J^2}{B d_k} \beta_k \zeta_k \tag{3.5}$$

$$\zeta_k = \left(d_k \Big/ \sum_{k=1}^{n} \beta_k d_k \right)^s \tag{3.6}$$

2.2 TWO GRAINSIZE MODEL

For sake of simplicity, the material has been assumed to be composed by only two representative diameters, d_1 and d_2. For selecting the two diameters, the hypothesis has been made that the bottom material of the *base configuration* of the river reach (see 2.3) has a Gaussian distribution with a mean (or median) diameter $\overline{d} = d_{50}$ and a standard deviation $\sigma^2 = \sum_{k=1}^{2} \beta_k \left(d_k - \overline{d}\right)^2$ (Fig. 3.2).

Under this hypothesis the representative grainsize diameters have been chosen as $d_1 = d_{16} = \overline{d} - \sigma$ and $d_2 = d_{84} = \overline{d} + \sigma$, being the compositions of the *reference river reach* β_1=β_2=0.5 (Fig. 3.2).

In the course of the morphological evolution, the effective compositions of the river, $\beta_1(x,t)$ and $\beta_2(x,t)$ will change in space and time, being $\beta_1 + \beta_2 = 1$. The non-dimensional parameters (characteristic of the *reference reach)* $\beta = \overline{\beta_1} / \overline{\beta_2} = 1$ and $d = d_1 / d_2 = \overline{d_{16}} / \overline{d_{84}}$ will also be introduced; the last one is corrected as $d^* = d^{1-s} = d_1/d_2 \cdot \zeta_1 / \zeta_2$ considering the hiding-exposure coefficient ζ_k (eq. 3.6) and s=0.8.

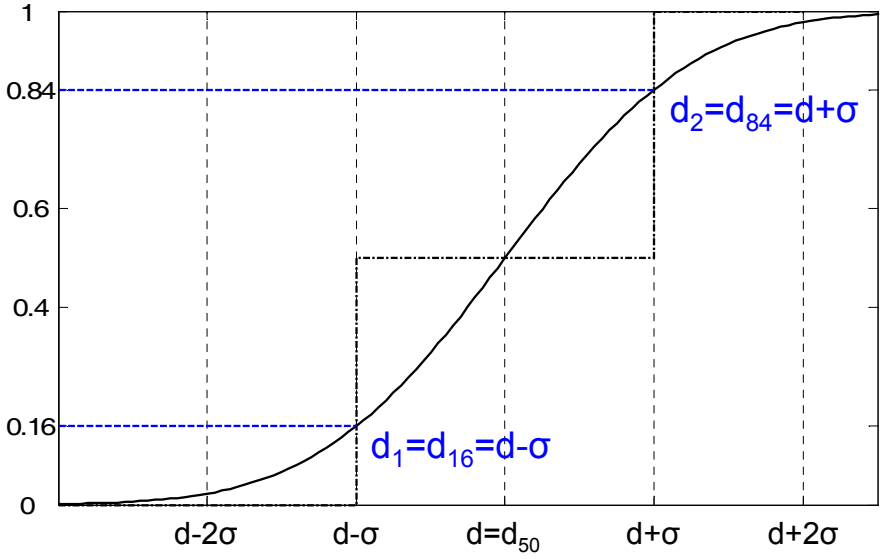

Fig. 3.2 Cumulative grainsize distribution function and representative diameters (d_1 and d_2).

2.3 LINEARIZED EQUATIONS

For an analytical approach to the problem, a linearization of the equations is necessary. This is made by assuming for each homogeneous river reach (e.g. between two major tributaries) a *base configuration* for river geometry (a finite rectangular channel with constant width B and slope J), river hydrology (constant water discharge Q) and river sediment (transport P and bottom composition β_k, i.e. grainsize percentage of a given particle size d_k). For each river reach, the base configuration it is assumed to be in equilibrium condition (*uniform waterflow, sediment transport and bottom composition*), so that a relationship, given by the transport equation (3.5), should exists between the quantities mentioned above.

In order to account for space and time irregularities, periodical perturbations will be introduced in the *base configuration*: river geometry (sinusoidally varying channel width),

river hydrology (sinusoidally varying water flow) and river sediment (sinusoidally varying classes). These perturbation (eqs. 3.7-12) will be in principle (albeit not always in nature) considered small with respect to their mean values, corresponding to the base configuration, indicated in the following by an underscore. In this way the model equations can be linearized around the mean value and an harmonic solution can be found satisfying the boundary conditions.

$$Q(t) = \underline{Q}\left(1 + q(t)\right) \tag{3.7}$$

$$B(x) = \underline{B}\left(1 + b(x)\right) \tag{3.8}$$

$$H(x,t) = \underline{H}\left(1 + h(x,t)\right) \tag{3.9}$$

$$P(x,t) = \underline{P}\left(1 + p(x,t)\right) \tag{3.10}$$

$$Z(x,t) = \underline{Z} + \underline{H} \cdot z(x,t) \tag{3.11}$$

$$\beta_1(x,t) = \underline{\beta_1}\left(1 + \beta_1^0(x,t)\right) \tag{3.12}$$

Under the above mentioned hypothesis and assuming q, b, h, p and β_1^0 much smaller than 1, the partial differential equations that describe the time- and space-evolution of the river (eqs. 3.1-6) can be written in terms of non-dimensional perturbation (eqs. 3.13-17), with the non dimensional temporal and spatial coordinates x and t ($t = t^* \underline{U}/\underline{H}$ and $x = x^*/\underline{H}$):

$$\frac{\partial q}{\partial x} = 0 \tag{3.13}$$

$$\alpha \frac{\partial h}{\partial x} + \frac{\partial z}{\partial x} - (1-\alpha)\frac{\partial b}{\partial x} = \varepsilon\left(h + \frac{2}{3}b - \frac{2}{3}q\right) \tag{3.14}$$

$$\frac{\partial z}{\partial t} + \psi \frac{\partial p}{\partial x} = 0 \tag{3.15}$$

$$p = 6q - 6h + \left(\eta^* + s\eta\right)\beta_1^0 - 5b \tag{3.16}$$

$$\frac{\partial \beta_1^0}{\partial t} + \frac{\psi}{\Delta} S^* \frac{\partial \beta_1^0}{\partial x} + \frac{\psi}{\Delta}\eta^* \frac{\partial p}{\partial x} = 0 \tag{3.17}$$

where the following constant coefficients pertain to the *base configuration* of the river reach, $\alpha = 1 - Fr^2$ and Fr is the Froude number ($Fr^2 = \underline{U}^2/g\underline{H}$); $\varepsilon = (3/2)EFr^2$ and E is the resistance coefficient ($E = 2g/C_h^2$); $\eta = (1-d)/(1+d)$ where d is the ratio $d = d_1/d_2$ between the diameters; $\eta^* = \left(1-d^*\right)/\left(1+d^*\right)$ depending on the "hiding-exposure" phenomena

through $d^* = d^{1-s}$ and $S^* = 1-\left(\eta^*\right)^2$; $\psi = \underline{P}/\underline{Q}$ represents the sediment concentration and $\Delta = \delta/\underline{H}$, is the relative mixing-layer thickness.

The system of five equations (eqs. 3.13-17) and five dependent variables, that describes the behavior of the *base configuration river* perturbed by sinusoidal waves, can be reduced to a system of three partial differential equations, function of space and time (Di Silvio and Marin, 1996). Therefore, the solution of the homogenous part of the system, for each variable, can be expressed in a general form as sum of *three basic damped harmonic waves* (eq. 3.18). A further (virtual) wave, with no damping and infinite celerity, is represented by the instantaneous propagation of Q (eq. 3.13).

$$f\left(x,t\right) = \sum_{n=1}^{3} \overline{f_{c_n}} \cdot e^{i\cdot\overline{k_n}\cdot x - i\cdot\omega\cdot t} \tag{3.18}$$

The parameter i represents the imaginary number, ω the forcing angular frequency, considered constant for all the variables, $\overline{f_{c_n}}$ and $\overline{k_n}$ complex coefficients. These coefficients will be found, respectively, using boundary conditions (par. 3.1) and solving the connected equations (par. 3.2).

The real part of the solution (eq. 3.19) is function of the imaginary and real part of $\overline{k_n}$ and of the modulus and argument of $\overline{f_{c_n}}$.

$$\mathrm{Re}\left\{f\left(x,t\right)\right\} = \left|\overline{f_{c_n}}\right| \cdot e^{-\mathrm{Im}\left\{\overline{k_n}\right\}\cdot x} \cos\left(\mathrm{Re}\left\{\overline{k_n}\right\} x - \omega t + Arg\left(\overline{f_{c_n}}\right)\right) \tag{3.19}$$

Terms $c_{f_n} = \omega/\mathrm{Re}\left\{\overline{k_n}\right\}$ and $L_{f_n} = 1/\mathrm{Im}\left\{\overline{k_n}\right\}$ (with n=1,2,3) represent, respectively, celerities and attenuation lengths of the *three basic waves* which propagate in the downstream direction (two waves) and in the upstream direction (one wave) along the river.

2.4 BOUNDARY CONDITIONS

In mobile-bed models, the number of upstream and downstream (independent) boundary conditions to be prescribed (Sieben, 1997) depends on the numbers of granulometric fractions and on the mode of sediment motion considered. For this model, with two sediment classes, local adaptation of transport and instantaneous propagation of flow discharge, the required independent boundary conditions are four and precisely three upstream and one downstream.

Sediment transport p, and sediment grainsize composition β_1, sinusoidally varying on time (eqs. 3.20-3.21) are two of the upstream boundary conditions (where $\overline{\beta_{1,c}^0}$ and $\overline{p_c}$ are complex coefficients).

$$\beta_1^0\left(x=0,t\right)=\overline{\beta_{1,c}^0}e^{-i\omega t}=\beta_{1,c}^0\cos\left(\omega t\right) \tag{3.20}$$

$$p\left(x=0,t\right)=\overline{p_c}e^{-i\omega t}=p_c\cos\left(\omega t\right) \tag{3.21}$$

Note that, due to the hypothesis (eq. 3.13), the non-dimensional water discharge perturbation q is only function of time (and not space) as it propagates instantaneously all over the river reach:

$$q=q\left(t\right)=\overline{q_c}e^{-i\omega t}=q_c\cos\left(\omega t\right) \tag{3.22}$$

The angular frequency ω is considered here corresponding to the typical flood event's period T_{wave} (expressed in a non dimensional form with the mean water depth $\underline{H}$ and velocity $\underline{U}$, eq. 3.22) as a function of the concentration time.

$$\omega=\frac{2\pi}{T_{wave}}\frac{\underline{H}}{\underline{U}} \tag{3.23}$$

Finally, the last sinusoidally varying boundary condition is to be imposed downstream and depends on the flow regime. For supercritical flow, the condition is the bottom elevation z (eq. 3.24/a), for subcritical flow the condition is the water elevation $z+h$ (eq. 3.24/b); l represents the non-dimensional length of the river ($l = L/\underline{H}$).

$$z\left(x=l,t\right)=\overline{z_c}e^{-i\omega t}=z_c\cos\left(\omega t\right) \tag{3.24/a}$$

$$\left(z+h\right)\left(x=l,t\right)=\left(\overline{z_c}+\overline{h}_c\right)e^{-i\omega t}=\left(z_c+h_c\right)\cos\left(\omega t\right) \tag{3.24/b}$$

In all the expressions mentioned above (eqs. 3.20-24) q_c, p_c, $\beta_{1,c}^0$, z_c and h_c represent the maximum values of the relative perturbations.

Also the geometric shape is considered sinusoidally varying and the cross width perturbation b can be expressed function of the non-dimensional spatial coordinate x, where $\Omega=\underline{H}/\lambda_b$ and λ_b is the wave length of the cross width oscillation.

$$b\left(x\right)=b_c\cos\left(2\pi\Omega x+\pi/2\right)=-b_c\sin\left(2\pi\Omega x\right) \tag{3.25}$$

3. THE HARMONIC SOLUTION

The harmonic solution of the system equations (eqs. 3.13-17) should be split into the homogeneous part and a particular solution of the system.

A particular solution can be determined considering the *morphodynamic stationary condition*s of the river. This is obtained by setting equal to zero the time variations of the morphological quantities $z(x,t)$ and $\beta_1^0(x,t)$. In this case (eqs. 3.26-29) the solid transport's perturbation $p(x,t)$

becomes only function of time (via water discharge *q(t)*) while the bottom's perturbation *z(x,t)* only function of space (via river width *b(x)*).

$$\beta_1^0(x) = 0 \tag{3.26}$$

$$p(t) = 2q(t) \tag{3.27}$$

$$h(x,t) = \frac{2}{3}q(t) - \frac{5}{6}b(x) \tag{3.28}$$

$$z(x) = \left(1 - \frac{\alpha}{6}\right)b(x) - \frac{\varepsilon}{6}\int_0^x b(x)\,dx \tag{3.29}$$

The morphodynamic stationary solution considers the effects of topographical and hydrological variations *b(x)* and *q(t)*, assuming the river at "equilibrium" conditions. It means that, along a river reach, sediment discharge is a univocal function of waterflow for any sections and time (Fasolato et al., 2006b). Note that this condition should eventually be attained by real river reaches, provided that sediment input is always in equilibrium with water input. This condition, however, is hardly satisfied in nature, especially on the small tributaries where the phase lag between runoff and sediment production (by surface erosion and mass movement) may be relevant.

The solution of the *homogeneous part* of the system, by contrast, considers the other perturbations which affect the morphodynamic equilibrium of the river due to variable boundary conditions. Variables *p(x,t)*, *h(x,t)*, *z(x,t)* and $\beta_1{}^0(x,t)$ can be expressed (in the form of eq. 3.18) as it follows:

$$p(x,t) = \overline{p_{c_1}} e^{i\overline{k_1}x - i\omega t} + \overline{p_{c_2}} e^{i\overline{k_2}x - i\omega t} + \overline{p_{c_3}} e^{i\overline{k_3}x - i\omega t} \tag{3.30}$$

$$h(x,t) = \overline{h_{c_1}} e^{i\overline{k_1}x - i\omega t} + \overline{h_{c_2}} e^{i\overline{k_2}x - i\omega t} + \overline{h_{c_3}} e^{i\overline{k_3}x - i\omega t} \tag{3.31}$$

$$z(x,t) = \overline{z_{c_1}} e^{i\overline{k_1}x - i\omega t} + \overline{z_{c_2}} e^{i\overline{k_2}x - i\omega t} + \overline{z_{c_3}} e^{i\overline{k_3}x - i\omega t} \tag{3.32}$$

$$\beta_1^0(x,t) = \overline{\beta_{1c_1}^0} e^{i\overline{k_1}x - i\omega t} + \overline{\beta_{1c_2}^0} e^{i\overline{k_2}x - i\omega t} + \overline{\beta_{1c_3}^0} e^{i\overline{k_3}x - i\omega t} \tag{3.33}$$

The complete harmonic solution is given by the sum of the non-homogeneous and homogeneous part, after having determined the values of the complex amplitudes $\overline{p_{c_n}}$, $\overline{h_{c_n}}$, $\overline{z_{c_n}}$, $\overline{\beta_{1c_n}^0}$ of the forcing perturbations and the propagation coefficients $\overline{k_n}$ (with *n*=1,2,3).

3.1 DEFINITION OF WAVES' AMPLITUDES AND PROPAGATION COEFFICIENTS

Substituting in the system (eq. 3.14-17), the expressions of the unknown quantities *p(x,t)*, *h(x,t)*, *z(x,t)* and $\beta_1^0(x,t)$, the system equations can be reduced to the following nine expressions (with *n*=1,2,3):

$$\begin{cases} \left(\frac{\varepsilon}{6}-\frac{\alpha}{6}\overline{k_n}i\right)\overline{p_{c_n}}+\overline{k_n}i\overline{z_{c_n}}+\left(\frac{\alpha}{6}\overline{k_n}i-\frac{\varepsilon}{6}\right)\left(\eta^*+s\eta\right)\overline{\beta_{1c_n}}=0 \\ -\omega\overline{z_{c_n}}+\psi\overline{k_n}\,\overline{p_{c_n}}=0 \\ \left(-\omega+\frac{\psi}{\Delta}S^*\overline{k_n}\right)\overline{\beta_{1c_n}}+\frac{\psi}{\Delta}\eta^*\overline{k_n}\,\overline{p_{c_n}}=0 \end{cases} \tag{3.34}$$

Eqs. 3.34 are determined in a first step substituting the variable *h(x,t)* (obtained from eq. 3.16) in the other equations of the system (eqs. 3.14, 3.15 and 3.17) and subsequently substituting in the equations so changed, the complete harmonic solution (expression of *h(x,t)* is for the moment omitted) (Madeo, 2002).

For a non trivial system solution, the nine equations (3.34) have to be rendered linearly dependent. This condition (as it is demonstrated below, par. 3.2) allows to determine complex coefficients $\overline{k_n}$.

In this way the system can be reduced to two linearly independent equations for each *n*, it means 6 equations, for 9 unknown complex quantities $\overline{p_{c_n}}$, $\overline{z_{c_n}}$, $\overline{\beta_{1c_n}^0}$ ($\overline{h_{c_n}}$ will be calculated later with eq. 3.16); other 3 equations are furnished by the boundary conditions (eqs. 3.20-22 and 3.24).

Amplitudes $\overline{z_{c_n}}$, $\overline{\beta_{1c_n}^0}$, $\overline{h_{c_n}}$ can be expressed as a function of the amplitude $\overline{p_{c_n}}$ in the following way (with *n*=1,2,3), apart from the flow conditions (*Fr*≥1 or *Fr*<1):

$$\overline{z_{c_n}}=\frac{\psi}{\omega}\overline{k_n}\,\overline{p_{c_n}} \tag{3.35}$$

$$\overline{\beta_{1c_n}^0}=\frac{1}{\left(\eta^*+s\eta\right)}\left[\frac{6\psi i\overline{k_n}^2}{\omega\left(\varepsilon-\alpha i\overline{k_n}\right)}+1\right]\overline{p_{c_n}} \tag{3.36}$$

$$\overline{h_{c_n}}=\frac{\psi i\overline{k_n}^2}{\omega\left(\varepsilon-\alpha i\overline{k_n}\right)}\overline{p_{c_n}} \tag{3.37}$$

On the other hand, the amplitude $\overline{p_{c_n}}$ can be expressed as a complex function of $\overline{k_n}$ that differs for supercritical and subcritical flow (*Appendix 3.A*); in this way, once calculated $\overline{k_n}$, it

is possible to univocally determine values of the 9 waves amplitudes and finding the complete non trivial system solution.

To rend equations 3.34 linearly dependent, the characteristic equation of the system (eq. 3.38) should be put equal to zero (*Appendix 3.B*):

$$i\overline{X}^2\left(\overline{X}S^* - 1\right) + \left(\overline{\varepsilon} - \overline{\alpha}\overline{X}i\right)\left(\gamma\overline{X} - 1\right) = 0 \qquad (3.38)$$

where (see eqs. 13-17) $S^* = 1 - \eta^{*2}$, $\gamma = 1 + s\eta\eta^*$, $\overline{\varepsilon} = \dfrac{\varepsilon\psi}{6\Delta^2\omega}$, $\overline{\alpha} = \dfrac{\alpha}{6\Delta}$ and $\overline{X} = \dfrac{\overline{k}\psi}{\Delta\omega}$.

This is a polynomial equation of the third degree with complex coefficients and it admits tree complex solutions; to determine the corresponding three solutions of $\overline{k}$, the relation $\overline{k_n} = \dfrac{\overline{X_n}\Delta\omega}{\psi}$ is to be considered (with *n*=1,2,3). For two of them, the real and imaginary part of the complex number are positive, while for the third solution both the real and imaginary part are negative.

3.2 WAVES' CELERITY AND ATTENUATION LENGTH

The three waves celerities and their attenuation lengths (expressed in a dimensional form) result so expressed:

$$c^*_{f_n} = c_{f_n} \cdot \underline{U} = \omega / \mathrm{Re}\left\{\overline{k_n}\right\} \cdot \underline{U} \qquad L^*_{f_n} = L_{f_n} \cdot \underline{H} = \underline{H} / \mathrm{Im}\left\{\overline{k_n}\right\}$$

The expressions above confirm what it has been already found regarding the number and direction of perturbations (Sieben, 1997): two of them (c_{f_1} and c_{f_2}) propagate from upstream to downstream; the third one (c_{f_3}, always negative, plotted in Fig. 3.3 as $\left|c_{f_3}\right|$) propagate on the contrary from downstream to upstream.

The graphs (a, and b), in Fig. 3.3, provide respectively the values of the tree celerities c_{f_n}, and of the three corresponding attenuation lengths L_{f_n}, as a function of Froude number.

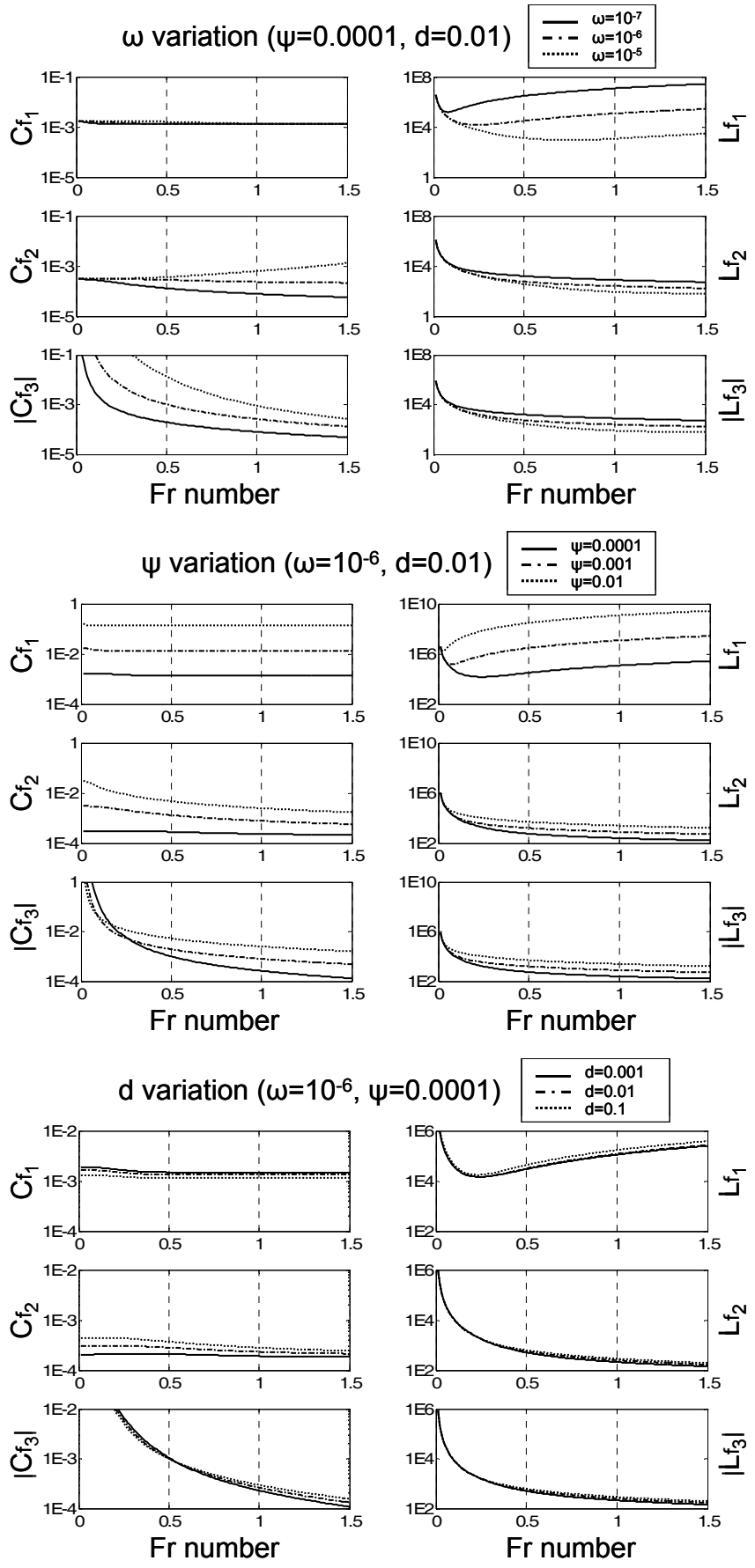

Fig. 3.3 Values of the three wave's celerities c_{fn} (a) and their attenuation lengths L_{fn} (b)

The graphs have been obtained from the numerical solutions of eq. 3.38 by varying the parameters ω (wave frequency, eq. 3.23), $\psi = \underline{P}/\underline{Q}$ (sediment concentration) and $d = d_1/d_2$ (grainsize uniformity) defined in eqs. (3.13-17). The parameters $E = 2g/C_h^2$ (resistance coefficient) and $\Delta = \delta/\underline{H}$ (non-dimensional mixing-layer) are assumed to be constant, respectively $E \approx 0.01$ [-] and $\Delta \approx 0.1$ [-].

Wave celerities represent the response time of the reach to the perturbations created at the boundaries. The only wave with negative celerity (n=3) propagates along the reach the perturbation created at the downstream end by water- and bottom-elevation.

For very low values of *Fr* the negative celerity c_{f_3} tends to be very fast while it becomes very slow for high *Fr*. In any case, with the exception of quite low values of *Fr* (dammed rivers) and definitely high values of ω (very short flood waves) and ψ (very high concentration), all three morphological waves have celerities many orders of magnitude slower than water flow. This means that even the fastest of the tree waves has a wave length ($\Lambda = c_f T_{wave}$) much shorter than the length of the river reach. As a consequence, in any given moment, one may recognize along a river reach a sequel of sinusoidal waves, more or less numerous, created by the combination of all three perturbations or, at least, by one or two of them. In other words, all the perturbations created at the boundaries with respect to the equilibrium conditions (in particular the input of sediment transport and its composition) propagate relatively slowly and do not reach, in general, the opposite end during the same flood event. The only exception is represented by the "wash load", constituted by extremely fine particles (loam and clay), which moves with the velocity of water and does not leave any trace on the river bottom. It should be noted in this regard that the "real" wash load is in general a negligible part of the total transport, even if it may be strongly visible for its brown or yellow color.

Even more interesting are the graphs of Fig. 3.3b, representing the *attenuation length* of the three perturbation waves, namely the distance, in the downstream (n=1,2) or upstream direction, over which the perturbation amplitude created at the boundaries is reduced $1/e$ times. This means that, at a very short distance from the upper end and from the lower end of the reach, we may respectively neglect the second (n=2) and third wave (n=3) with respect to the first one. In other words, no matter the celerity of propagation of the three waves, only the first wave is not destined to disappear very soon but to maintain a good part of its amplitude for the entire length of the reach. As it appears from the graphs, however, the attenuation length of the *first wave* tends to increase (namely its amplitude to persist longer) when the flood period is longer (small ω) and the sediment concentration higher (large ψ). By contrast,

appear to be less relevant on the attenuation rate both the grainsize non-uniformity (*d*) and the slope of the river reach (*Fr*).

3.3 AMPLITUDE OF THE FORCING WAVES

In the present model the boundary conditions in terms of sediment input, grainsize composition, bottom and water elevation are assumed to vary sinusoidally with frequency ω (eqs. 3.20-24). The respective amplitudes ($\overline{p_c}$, $\overline{\beta_{1c}^0}$, $\overline{z_c}$ and or $\overline{h_c}$) are arbitrary values depending on the intensity of the perturbations prescribed at both ends of the river reach. These amplitudes are given by the sum of the respective amplitudes of the propagating waves $\overline{p_{c_n}}$, $\overline{\beta_{1c_n}^0}$, $\overline{h_{c_n}}$, $\overline{z_{c_n}}$ (*n*=1,2 and 3) in eqs. 3.30-33.

In principle, *each* wave is affected by *all* the boundary conditions, as it appears from the expressions of $\overline{p_{c_n}}$ (reported in *Appendix 3.A*, $\overline{p_{c_x}}$ with *x*=1,2, and 3) and of $\overline{\beta_{1c_n}^0}$, $\overline{h_{c_n}}$ and $\overline{z_{c_n}}$ provided by eqs. 3.35-37. However, if we look at the different attenuation rates of the three waves (see par. 3.2), we recognize that only the first wave will be sufficiently persistent over the river reach, while the second one and the third one will substantially affect only the extreme zones of the reach, respectively near the upstream and the downstream end. Consequently it will suffice evaluating the effects of the boundary conditions only on the first wave. This can be made by computing the (complex) coefficients $\overline{A_1}$, $\overline{B_1}$, $\overline{C_1}$, $\overline{D_1}$, $\overline{E_1}$ and $\overline{F_1}$ in the following expressions (for subcritical flow) and in the analogous ones (for supercritical one):

$$\overline{p_{c_1}} = \overline{A_1}\cdot\overline{\beta_{1c}^0} + \overline{B_1}\cdot\left(\overline{p_c} - 2\overline{q_c}\right) + \overline{C_1}\cdot\left(\overline{z_c} + \overline{h_c} - 2/3\,\overline{q_c}\right) \tag{3.39}$$

$$\overline{\beta_{1c_1}^0} = \overline{D_1}\cdot\overline{\beta_{1c}^0} + \overline{E_1}\cdot\left(\overline{p_c} - 2\overline{q_c}\right) + \overline{F_1}\cdot\left(\overline{z_c} + \overline{h_c} - 2/3\,\overline{q_c}\right) \tag{3.40}$$

which provide the relative importance of the boundary conditions ($\overline{p_c}$, $\overline{q_c}$, $\overline{\beta_{1c}^0}$, $\overline{z_c}$ and or $\overline{h_c}$), respectively on the first-wave amplitudes, $\overline{p_{c_1}}$ and $\overline{\beta_{1c_1}^0}$, which convey along the river reach the perturbations of, respectively, sediment transport and bottom composition.

The graphs of the coefficients $\overline{A_1}$, $\overline{B_1}$ and $\overline{C_1}$ (Fig. 3.4, 1st, 2nd and 3rd row, respectively) have been obtained from the expression in *Appendix 3.A* while the graphs of the coefficients $\overline{D_1}$, $\overline{E_1}$ and $\overline{F_1}$ (Fig. 4.3, 4th, 5th and 6th row, respectively) have been obtained by eqs. 3.35-37, with *n*=1, by changing the values of *Fr* (for different values of the parameters ω, ψ and *d*).

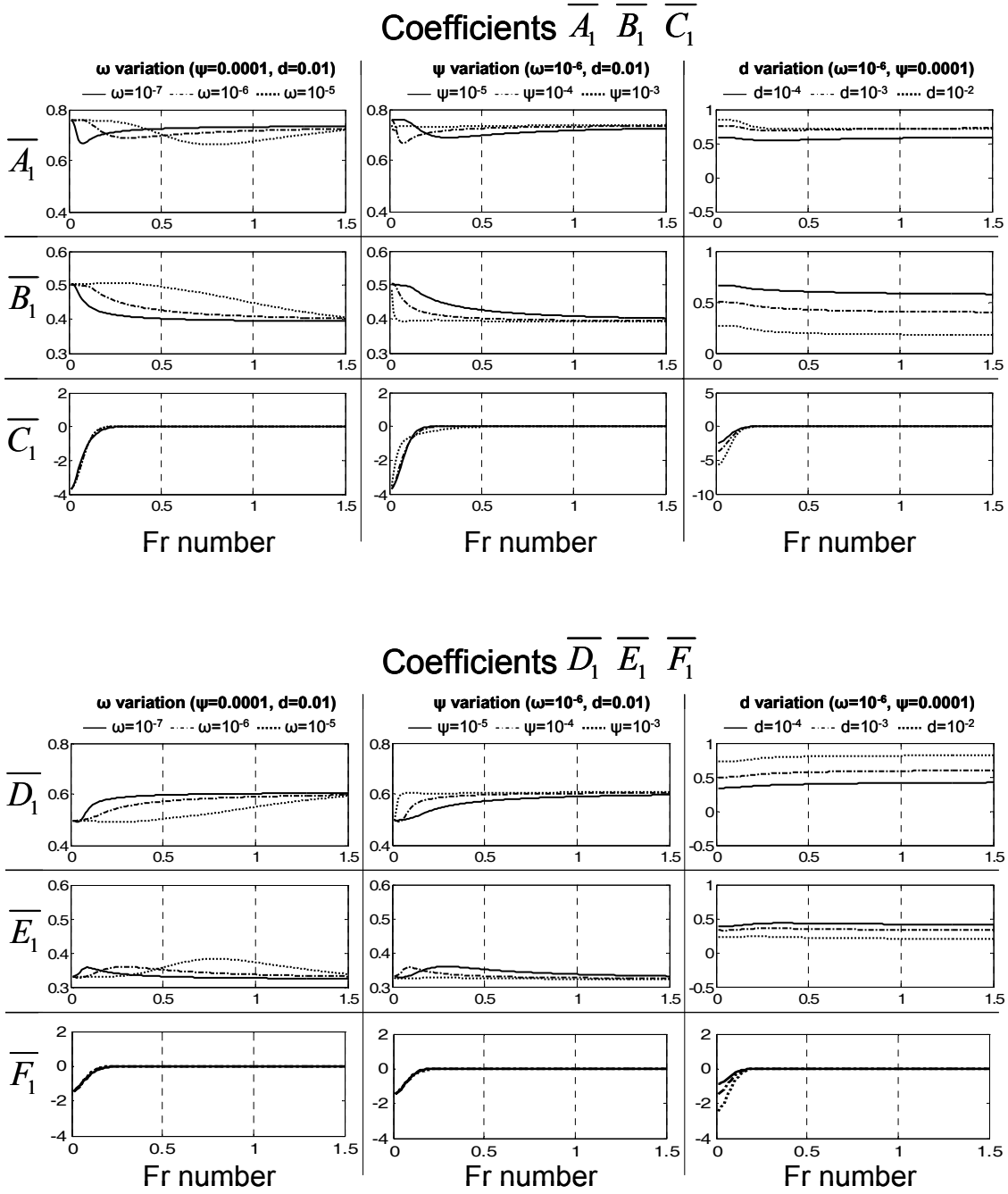

Fig. 3.4 Coefficients of the eq. 3.39 and 3.40 dependent on the Froude number (with varying *ω, ψ* and *d*).

The graphs indicate that for virtually any river (i.e. for any value of *Fr*, *ω, ψ* and *d*, with the only exception of *Fr*<0.2, corresponding to dammed rivers), the coefficients $\overline{C_1}$, and $\overline{F_1}$ are definitely much smaller than the coefficients $\overline{A_1}$, $\overline{B_1}$, $\overline{D_1}$ and $\overline{E_1}$. This means that both waves $\overline{p_{c_1}}$ (sediment transport) and $\overline{\beta_{1c_1}^0}$ (bottom composition) are practically unaffected by the boundary conditions prescribed at the downstream end (water and bottom elevation).

On the other end, the coefficients $\overline{A_1}$ are in general larger than $\overline{B_1}$; while the coefficients $\overline{D_1}$ are in general larger than $\overline{E_1}$. This means that the waves $\overline{p_{c_1}}$ and $\overline{\beta^0_{1c_1}}$ are affected by both the boundary conditions prescribed upstream, although the perturbation on the bottom composition ($\overline{\beta^0_{1c}}$) appears to be relatively more important than the perturbation on the sediment transport ($\overline{p_c}$).

4. SIMPLIFIED SOLUTIONS

4.1 QUASI UNIFORM MODEL

Simplification of *quasi-uniform model* can be generally considered when in a river, the energy variations from the bottom are considerably lower than the bottom slope (this is generally true for high value of the *Froude number*). Eq. 3.2 can be simplified in eq. 3.2' (where C_h is the Chézy coefficient, considering $Q=C_hBH^{3/2}$) and for the linearized system, eq. (3.14) can be reduced in eq. (3.14').

$$\frac{\partial Z}{\partial x^*} \cong -J = -\frac{Q^2}{A^2 C_h{}^2 H} \tag{3.2'}$$

$$\frac{\partial z}{\partial x} = \varepsilon\left(h + \frac{2}{3}b - \frac{2}{3}q\right) \tag{3.14'}$$

For very high values of *Fr*, also the parameter $\bar{\varepsilon} = \frac{E \cdot Fr^2 \psi}{4\Delta^2 \omega} >> 1$ and eq. (3.38) can be simplified neglecting terms with lower order of magnitude (*Appendix 3.C*). The correspond solutions for celerities c_{f_n} and L_{f_n} are reported below:

$$c_{f_1} = \frac{\psi}{\Delta}\gamma \qquad L_{f_1} = \frac{\varepsilon\psi^2}{6\Delta^3\omega^2}\frac{\gamma^4}{\left(\gamma - S^*\right)} \tag{3.41}$$

$$c_{f_2} = +\sqrt{\frac{12\omega S^*\psi}{\varepsilon\gamma}} \qquad L_{f_2} = +\sqrt{\frac{12S^*\psi}{\varepsilon\gamma\omega}} \tag{3.42}$$

$$c_{f_3} = -\sqrt{\frac{12\omega S^*\psi}{\varepsilon\gamma}} \qquad L_{f_3} = -\sqrt{\frac{12S^*\psi}{\varepsilon\gamma\omega}} \tag{3.43}$$

For the uniform flow (as it's also possible to observe in Fig. 3.3, for *Fr*>1) the celerity c_{f_1} is always (for any values of the perturbations' period T_{wave} and for the sediment concentration ψ) dominant compare to the other two celerities $c_{f_{2/3}}$. Moreover c_{f_1} doesn't depend on the perturbations' period, while $c_{f_{2/3}}$ tend to be neglected rising T_{wave}. Finally, $c_{f_1} \propto \psi$ while

$c_{f_{2/3}} \propto \sqrt{\psi}$ it means the difference between celerities rises increasing the sediment concentration ψ. Similar observations can be made for the attenuation lengths L_{f_n}; the first attenuation length is enough bigger than the others for any reasonable value of T_{wave} and ψ.

4.2 RIGID LID MODEL

The simplification of rigid-lid model can be instead considered when in a river, the longitudinal cinetic variations are considerably lower than the water depth slope (this is generally true for very low values of the *Fr* number). It means eq. 3.2 can be simplified in eq. 3.2'' and for the linearized system, eq. 3.14 can be reduced in eq. 3.14''.

$$\frac{\partial}{\partial x^*}\left(H+Z\right) \cong 0 \qquad (3.2'')$$

$$\frac{\partial z}{\partial x}+\frac{\partial h}{\partial x}=\varepsilon\left(h+\frac{2}{3}b-\frac{2}{3}q\right) \cong 0 \qquad (3.14'')$$

For very low values of *Fr* (*Fr*≈*0*), also the parameter $\bar{\varepsilon}=\frac{E\cdot Fr^2\psi}{4\Delta^2\omega} \cong 0$ and $\alpha = 1-Fr^2 \cong 1$; making an additional hypothesis of substantially different representative diameters for the two granulometric classes (S^*<<1) eq. 3.38 can be simplified neglecting terms with lower order of magnitude (*Appendix 3.D*). The correspond solutions for celerities c_{f_n} and L_{f_n} result:

$$c_{f_1}=\frac{\psi}{\Delta}\left(6\Delta+\gamma\right) \qquad L_{f_1}=\frac{6\Delta+\gamma}{6\varepsilon\Delta} \qquad (3.44)$$

$$c_{f_2}=\frac{6\psi S^*}{6\Delta+\gamma} \qquad L_{f_2}=\frac{6\Delta+\gamma}{\gamma\varepsilon} \qquad (3.45)$$

$$c_{f_3}=-\infty \qquad L_{f_3}=-\frac{1}{\varepsilon} \qquad (3.46)$$

For rigid lid model (as it's also possible to observe in Fig. 3.3, for *Fr*<<1) the celerity $c_{f_3} \to -\infty$ while $c_{f_{1/2}}$ don't depend on the perturbation period T_{wave} but they both result $c_{f_{1/2}} \propto \psi$ with $c_{f_1} >> c_{f_2}$ always.

4.3 COMPLETE ANALYTICAL SOLUTION

A complete and general solution of the harmonic system, it has been discussed in Chapter 3 with numerical results. It is important to underline that in general is not possible to find an analytical expression for the tree celerities and attenuation lengths without introducing some simplification of the system. Moreover it can be possible to represent the three roots of the eq.

(3.38) in a complex plane (a modified Cartesian plane, with the real part of complex numbers represented along the *x-axis*, and the imaginary part along the *y-axis*). It's important to underline how these solutions have a physical meaning for the tree perturbations waves, in fact:

$$\mathrm{Re}\{X_n\} = \frac{\psi/\Delta}{c_{f_n}} \qquad \mathrm{Im}\{X_n\} = \frac{\psi/\Delta}{L_{f_n}} \frac{\overline{U}}{\overline{H}} \frac{T_{wave}}{2\pi}$$

Qualitatively controlling the roots' variation, basically function of the four parameters of eq. (3.38), S^*, γ, $\overline{\alpha}$ and $\overline{\varepsilon}$ it's possible to describe variations and characteristics of the tree waves and so response of the river system to the equilibrium perturbations. While S^* and γ are function of the river granulometric features (in particular function of the ratio between diameters d and the hiding exposure coefficient s), the other two parameters $\overline{\alpha}$ and $\overline{\varepsilon}$, consider multiple river's characteristics. In particular, the last one results the most representative parameter for the river and can be explicitly expressed as $\overline{\varepsilon} = \frac{E \cdot Fr^2 \psi \overline{U}}{8\pi\Delta^2 \overline{H}} T_{wave}$; solutions are analyzed varying T_{wave} and consequently $\overline{\varepsilon}$.

In the following analysis the negative solution of X (it means $\mathrm{Re}\{X\} \le 0$) will be always represented as X_3, while the other two solutions X_1 and X_2 will be considered always as $\mathrm{Re}\{X_1\} \le \mathrm{Re}\{X_2\}$.

In the case of T_{wave}=0, also $\overline{\varepsilon}$ results equal to zero and solution of the system is similar to the rigid-lid hypothesis. The real and imaginary part of X_n, roots of eq. 3.38 (see *Appendix 3.D*) can be so summarized:

$$\mathrm{Re}\{X_{1/3}\} = 0 \qquad \mathrm{Im}\{X_{1/3}\} = 0 \qquad (3.47)$$

$$\mathrm{Re}\{X_2\} = \frac{\left(1+\gamma\overline{\alpha}\right) + \sqrt{\left(1+\gamma\overline{\alpha}\right)^2 - 4\overline{\alpha}S^*}}{2S^*} \qquad \mathrm{Im}\{X_2\} = 0 \qquad (3.48)$$

$$\mathrm{Re}\{X_{3/1}\} = \frac{\left(1+\gamma\overline{\alpha}\right) - \sqrt{\left(1+\gamma\overline{\alpha}\right)^2 - 4\overline{\alpha}S^*}}{2S^*} \qquad \mathrm{Im}\{X_{3/1}\} = 0 \qquad (3.49)$$

All solutions present the imaginary part equal to zero and so they are located along the *x-axis*. For any values of $\overline{\alpha}$ $\mathrm{Re}\{X_2\} > 0$, while, with $\overline{\alpha} > 0$ ($Fr<1$), $\mathrm{Re}\{X_{1/3}\} = \mathrm{Re}\{X_3\} = 0$ and

$\mathrm{Re}\{X_{3/1}\} = \mathrm{Re}\{X_1\} > 0$ and, with $\bar{\alpha} < 0$ ($Fr > 1$), $\mathrm{Re}\{X_{3/1}\} = \mathrm{Re}\{X_3\} < 0$ and $\mathrm{Re}\{X_{1/3}\} = \mathrm{Re}\{X_1\} = 0$.

In the case of $T_{wave} \to \infty$, also $\bar{\varepsilon} \to \infty$ and uniform-flow hypothesis can be considered. The real and imaginary part of X_n, roots of eq. (3.38) (see *Appendix 3.C*) can be so summarized as:

$$\mathrm{Re}\{X_1\} \approx \frac{1}{\gamma} \qquad \mathrm{Im}\{X_1\} \approx 0 \tag{3.50}$$

$$\mathrm{Re}\{X_2\} = \frac{\bar{\alpha}\gamma}{2S^*} + \sqrt{\frac{\gamma\bar{\varepsilon}}{2S^*}} \qquad \mathrm{Im}\{X_2\} \approx \mathrm{Re}\{X_2\} - \frac{\bar{\alpha}\gamma}{2S^*} \tag{3.51}$$

$$\mathrm{Re}\{X_3\} = \frac{\bar{\alpha}\gamma}{2S^*} - \sqrt{\frac{\gamma\bar{\varepsilon}}{2S^*}} \qquad \mathrm{Im}\{X_3\} \approx \mathrm{Re}\{X_3\} - \frac{\bar{\alpha}\gamma}{2S^*} \tag{3.52}$$

It's interesting to note the first solution X_1 is represented as a point on the x-axis and it depends exclusively from the granulometric composition of the bottom γ, while the other two solutions $X_{2/3}$ (particularly wide) are asymptotic (and with opposite sign) to a straight line, inclined of $\pi/4$ that intersects the y-axis on $-\bar{\alpha}\gamma/2S^*$. Because of the inverse proportion between L_f and X, the first wave presents a much bigger attenuation length than the other two so, also for high value of T_{wave} (as shown in Fig. 3.3), it is possible to neglect the second and third perturbation waves (in fact results $L_{f_1} \propto T_{wave}^2$ while $L_{f_{2/3}} \propto \sqrt{T_{wave}}$).

In an intermediate situation with a generic value of T_{wave} (and consequently $\bar{\varepsilon}$) it's possible to represent the qualitative trend of the tree solutions X_n for two main case; with positive and negative values of α and consequent $\bar{\alpha}$.

Both in the case of subcritical flow ($Fr < 1$ and $\alpha > 0$, Fig. 3.5a) and supercritical flow ($Fr > 1$ and $\alpha < 0$, Fig. 3.5b), increasing $\bar{\varepsilon}$, the two solutions X_3 and X_2, tend to the asymptote inclined of $\pi/4$ while X_1 is confined in a restricted area (with very low values compared to the other two solutions) around x-axis.

Therefore, considering the inverse relation $c_{f_n} \propto 1/\mathrm{Re}\{X_n\}$ and $L_{f_n} \propto 1/\mathrm{Im}\{X_n\}$, it's possible to find a sufficiently large value of T_{wave} (and consequently $\bar{\varepsilon}$), for any flow conditions, that both $c_{f_{2/3}}$ and $L_{f_{2/3}}$ can be neglected and the river system solution simplified on the determination of c_{f_1} and L_{f_1}.

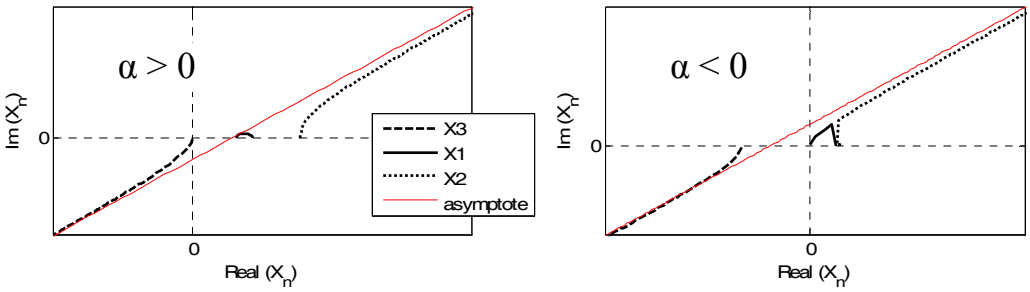

Fig. 3.5 Variation of the tree roots X_n for two hypothetical river with respectively α>0 (*Fr*<1) and α<0 (*Fr*>1) varying the parameter $\bar{\varepsilon}$. The thin continuous line represents the asymptote inclined of $\pi/4$.

5. NUMERICAL APPLICATIONS

Some numerical applications have been made to three rivers and basins with substantially different sizes and hydraulic characteristics; rivers' features and consequent analytical parameters are reported in Table 3.1.

Charac.s	River A: Comelico	River B: Piave	River C: Zambezi
L [m]	8,200	40,000	200,000
J [-]	0.0157	0.0030	0.0002
B [m]	20	100	600
Ch [$m^{1/2}/s$]	30	40	50
Twave [h]	10	50	4,000
Qeq [m^3/s]	100	900	4,000
$\beta = \beta_2/\beta_1$ [-]	1.0	1.0	1.0
ψ [-]	0.000324	0.000149	0.000003
Fr [-]	1.20	0.70	0.23
$d = d_1/d_2$ [-]	0.001	0.01	0.10
Δ [-]	0.05	0.05	0.05
E [-]	0.021791	0.012258	0.007845
H [m]	1.21	2.56	4.46
U [m/s]	4.13	3.51	1.49

Parameters	River A: Comelico	River B: Piave	River C: Zambezi
ω [-]	5.11E-05	2.55E-05	1.30E-06
α [-]	-0.44	0.51	0.95
$\bar{\alpha}$ [-]	-1.47	1.70	3.16
ε [-]	0.047	0.009	0.001
$\bar{\varepsilon}$ [-]	19.9	3.501	0.103
η [-]	1.00	0.98	0.82
η^* [-]	0.60	0.43	0.23
S^* [-]	0.642	0.815	0.949
$c^*_{f_1}$ [mm/s]	39.57	14.28	0.11
$c^*_{f_2}$ [mm/s]	7.34	2.73	0.02
$c^*_{f_3}$ [mm/s]	-4.35	-19.31	-335.12
$L^*_{f_1}$ [km]	17.454	7.452	98.379
$L^*_{f_2}$ [km]	0.033	0.230	7.61
$L^*_{f_3}$ [km]	-0.033	-0.223	-7.060

Table 3.1 Different rivers' characteristics and consequent analytical parameters

The first one (*River A*) is a Italian mountain river reach, part of the Piave river, with a catchment area of 372 km^2, subsequently called Comelico (Fasolato et al. 2007). The second one (*River B*) is a piedmont reach of the Piave river, located in the Eastern Alps, with a catchment area of 3,899 km^2. The last one (*River C*) is a lower reach of the Zambezi River, located in the Southeastern Africa, with catchment area of 1,332,412 km^2 (Ronco et al. 2006). Only Comelico (*River A*) has a Froude number larger than one, Piave (*River B*) has a Froude number slightly smaller than one, while the lower Zambezi river (*River C*) has a very low Froude number.

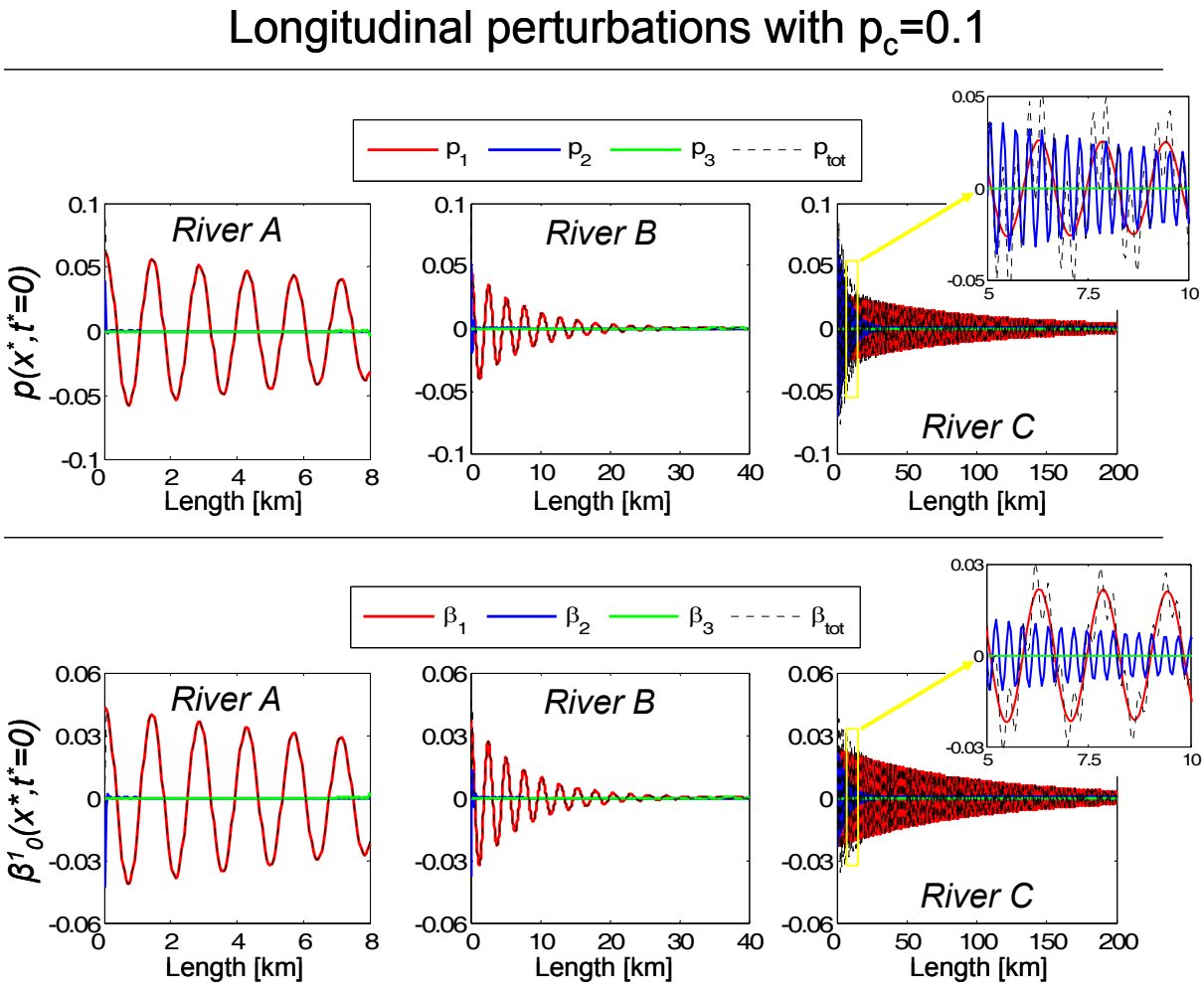

Fig. 3.6 Longitudinal variation of perturbations $p(x^*,t^*=0)$ and $\beta_1^0\left(x^*,t^*=0\right)$, as the sum of the tree perturbations $p_n(x^*,t^*=0)$ and $\beta_{1n}^0\left(x^*,t^*=0\right)$ for the three rivers analyzed, by assuming p_c=0.1 and $\overline{\beta_{1c}^0}=\overline{z_c}=\overline{h_c}$=0.

The length of the reach is the typical distance between major tributaries in that part of the respective river. In all rivers, the perturbations on width and water flow were put equal to zero ($b_c = 0$ and $q_c = 0$) while the downstream boundary conditions were considered $z_c = 0$ (*River A*) or $z_c + h_c = 0$ (*River B* and *C*). The only initial perturbation different from zero was considered, separately, $p_c = 0.1$ and $\beta_{1c}^0 = 0.1$.

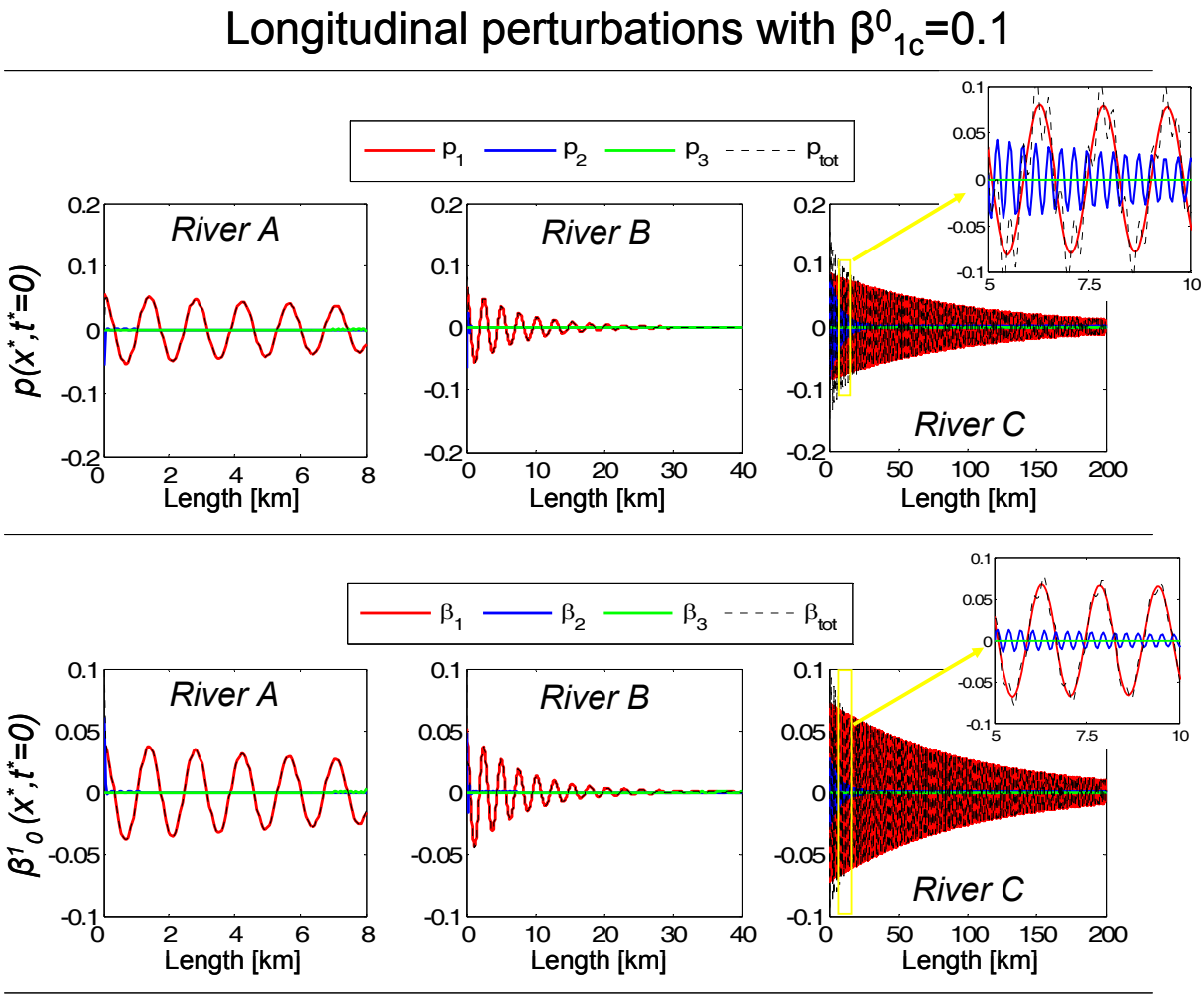

Fig. 3.7 Longitudinal variation of perturbations $p(x^*,t^*=0)$ and $\beta_1^0\left(x^*,t^*=0\right)$, as the sum of the tree perturbations $p_n(x^*,t^*=0)$ and $\beta_{1n}^0\left(x^*,t^*=0\right)$ for the three rivers analyzed, by assuming $\beta^0{}_{1c}$=0.1 and $\overline{p_c} = \overline{z_c} = \overline{h_c} = 0$.

The numerical results reported in Fig. 3.6 and Fig. 3.7, confirm the observations made in the preceding Sections 3.2 and 3.3. In all three rivers the third wave, propagating from the downstream end, is absolutely negligible, while the first one is definitely dominant. The effects of the second wave (propagating from the upstream end) is also quickly decaying, with

the only exception of the lower Zambezi river (having an extremely small Froude number), where its presence persists for about 10% of the river reach and at the beginning part of the reach seems to be dominant compared to the first wave (Fig. 3.5 *River C*).

As for the importance of the two upstream boundary conditions on the wave amplitude, it is confirmed that the perturbation of the river composition appears to be relatively more important than the perturbation on the sediment transport.

6. CONCLUSIONS

The harmonic solution of the morphodynamic equations provides the response of any homogeneous river reach (between the confluences of two subsequent large tributaries) to the forcing actions represented by the sinusoidal boundary conditions prescribed at its ends. The solution depends on four non-dimensional parameters, $S^* = 1 - \eta^{*2}$, $\gamma = 1 + s\eta\eta^*$, $\bar{\alpha} = \dfrac{\alpha}{6\Delta}$ and $\bar{\varepsilon} = \dfrac{\varepsilon\psi}{6\Delta^2\omega}$, which appears in the characteristic complex eq. (3.38). While the first three parameters are function of the mean morphological and fluvial characteristics (granulometric composition $d = d_{16}/d_{84}$, hiding and exposure coefficient *s*, mixing-layer thickness Δ and the Froude number *Fr*); the last one, is also function of the mean sediment concentration ψ and of the forcing perturbations' frequency ω.

The mean sediment concentration ψ is an important parameter in determining the amplitude of all perturbations, as well as their propagation's celerity. In all applications the celerity tends to increase when ψ increases, while it tends to decrease when *d* (grainsize non-uniformity) decreases or the mixing-layer thickness Δ increases.

The perturbations' frequency ω controls the time response of the river reach. As a matter of fact, an harmonic solution is strictly connected to the forcing frequency ω that, in this work, is considered to be the same for all the perturbations. This forcing frequency may be understood as the average recurrence of the major storms determining the variations of water discharge, sediment transport and bottom composition or, alternatively, as the frequency corresponding to the period of the annual largest flood wave. In real rivers, however, the independent boundary conditions present in general a large number of periodical components ranging from rainfall duration, to seasonal or annual periodicity, to the intermittence of rare catastrophic events.

Although the quantity ω is certainly important , a more significant parameter seems to be $\bar{\varepsilon}$ which is an interesting combination of frequency, Froude number and sediment concentration. As it will be shown in some papers (Fasolato et al., 2008b, Ronco et al., 2008a), when $\bar{\varepsilon}$ is large enough, the hypothesis of local uniform water flow can be accepted, in lieu of eq. 3.2, with substantial simplifications of the harmonic solution.

In any case, independently from the specific values of the parameters which characterize the river, a number of general conclusions can be drawn about the morphodynamic response of a river reach to variable boundary conditions. The information regarding the boundary conditions are conveyed along the river reach by three waves, plus one wave which represents the instantaneous propagation of the water flow. Of the three waves with finite celerity, only the third one propagates in the upstream direction but attenuates very quickly. Also the second wave, propagating in the downstream direction, has a rather strong damping. For this reason both the third and the second waves may be neglected, unless one is interested in the short extreme portions of the river reach.

Virtually all the information is transmitted in the downstream direction by the first wave. The first wave propagates along the reach with a finite celerity, $c^*_{f_1}$, which is three order of magnitudes slower than the water velocity and is more or less proportional to the value of ψ (Fig. 3.3a).

The attenuation length of the first wave (more or less corresponding to the halving distance) is comparable with the length of the reach and increases with larger values of wave period and sediment concentrations (Fig. 3.3b). This means that the first wave's amplitude generally persists all over the river reach with relevant values.

In conclusion, there is one "first" significant wave (initial amplitude $\overline{p_{c_1}}$) that conveys downstream the perturbations of sediment transport and one "first" significant wave (initial amplitude $\overline{\beta^0_{1c_1}}$) that conveys downstream the perturbation of bottom composition. It is important to note , that both amplitudes $\overline{p_{c_1}}$ and $\overline{\beta^0_{1c_1}}$ are affected in principle by *all* the boundary conditions prescribed at the upstream and the downstream end of the river reach (eqs. 3.39 and 3.40). As it appears from graph of Fig. 3.4, however, each amplitude is practically affected only by the boundary conditions of $\overline{p_c}$ and $\overline{\beta^0_{1c}}$, while the importance of the boundary conditions downstream results again to be negligible.

The harmonic solution provides a useful insight on the behavior of rivers and consents to assess the validity and limitation of "filtering" the space- and time- non-uniformities, as a common practice in numerical models.

Chapter 4

RIVER MORPHODYNAMIC EQUILIBRIUM AND UNIFORM-FLOW HYPOTHESIS

SUMMARY

A one-dimensional morphological model is applied to determine the altimetric and granulometric response of a movable-bed channel subject to prescribed sinusoidal variations of its width. Aim of the work is, on one hand, to analyze the morphodynamic equilibrium configuration of such a channel by varying the Froude number and the length of sinusoidal width variations and, on the other hand, to analyze the validity and limitations of the local uniform water flow hypothesis, an extremely useful simplification for large time- and space-scale computations. Analytical and numerical results suggest that, in equilibrium conditions, the configuration of the altimetric (bottom) profile with respect to the planimetric (bank) profile depends significantly on the Froude number and the wavelength of planimetric width variation. While for low values of these quantities, bed peaks correspond to the wide sections and bed troughs to the narrow sections, for higher and higher values, peaks and troughs of the bottom profile tend to move upstream.

Solutions in morphodynamic equilibrium also indicate that the local uniform water flow hypothesis is acceptable for large enough values of the Froude number and the width's wave length. The same criterion seems to work as well in (mild) non-equilibrium conditions.

The validity criterion of the local uniform water flow for a sinusoidal channel has been subsequently adapted to the case of irregular (natural) rivers (Ronco et al., 2008a).

1. INTRODUCTION

Many morphological processes in a river system basically controlled by its altimetric configuration (e.g. aggradation and degradation of the bottom and corresponding evolution of grainsize composition) can be described in terms of 1D (one-dimensional) equations of water flow (De St. Venant equations) and sediment transport of one or various granulometric classes (Cui et al., 1996; Cao et al., 2002; Papanicolaou, 2004; Wu et al., 2004; Cui and Parker, 2005; Curran et al., 2005; Wright and Parker, 2005a and 2005b).

When considering morphodynamic processes at very long (historical or geological) time-scale, however, the entire watershed should in principle be reproduced, and simplifications of De St. Venant equations become virtually necessary. In these cases, in fact, a complete one-dimensional morphodynamic model is still too much cumbersome and simplifying hypothesis must be applied (Di Silvio, 2006; Fasolato et al., 2006b).

The most interesting simplification to be possibly applied to a 1-D model for a river at watershed scale, is the so-called *local uniform water flow hypothesis* (Marin and Di Silvio, 1996). The hypothesis of local uniform water flow implies for the morphodynamic model a number of consequences which permit remarkable reductions of the computational time.

Local uniform flow means that, for a given discharge, water depth (and velocity), in any cross section, exclusively depends on the local slope of the bottom. This hypothesis is usually assumed to be valid whenever the river presents a reasonably regular shape and uniform bed slope (Di Silvio and Peviani, 1991). The idea is of course to consider as “uniform” the water flow averaged over a reach of finite length, but no criterion is available to evaluate the effects of the geometric irregularities both in width and depth (Ronco et al., 2008a). In the present chapter an attempt will be made to define the validity of the local uniform water flow hypothesis and the minimum length of the reach to be considered for the relevant averaging equations.

2. COMPLETE SIMPLIFIED AND LINEARIZED 1-D MORPHODYNAMIC MODEL

The complete one-dimensional mathematical model used to study the altimetric and granulometric evolution of a river (Chapter 3, Fig. 3.1) is the usual system of partial differential equations described before (Chapter 3, sect. 2).

To simplify the study, it is assumed that spatial variation of the waterflow is basically controlled by the main tributaries and that, along the reach between two main tributaries, (Chapter 3, eq. 3.1) may be substituted by:

$$\frac{\partial Q}{\partial x^*} = \frac{\partial Q}{\partial t^*}\frac{1}{c_w} \tag{4.1}$$

where $c_w = 3/2\,U$ is the (cinematic) celerity of the flood wave. For relatively long waves (or short reaches) one can even put $\partial Q / \partial x^* = 0$ (instantaneous flood wave propagation). It was also considered a wide rectangular cross section, the energy slope provided by the Chézy equation and a monomial expression, similar to the Engelund and Hansen's formula (Fasolato et al., 2006b), for the sediment discharge (Chapter 2, eq. 2.7) of the grainsize class *k-th*, including an "hiding-exposure" coefficient ζ_k (Chapter 2, eq. 2.8).

Eq. (2.7) implies that the transport of each sediment fraction, both as bedload and in suspension, is completely governed by the local parameters (it means instantaneous adaptation of the vertical sediment concentration in the water stream). The second De St. Venant equation (3.2) may be subject to further simplifications. First of all the "local" and, possibly, the "convective" acceleration term may be neglected. Even more radically, eq. (3.2) may be reduced to eq. (4.2)

$$\frac{\partial Z}{\partial x^*} = -J \tag{4.2}$$

which corresponds to the already mentioned *local uniform flow hypothesis*. This hypothesis will be discussed later.

For an analytical approach, the non-linear terms of equations (3.1-3.6) are to be linearized with respect to the *basic configuration* of the river reach (Chapter 3, par. 2.3).

The *basic configuration* corresponds to the stationary (equilibrium) conditions of a rectangular prismatic reach conveying a constant discharge (i.e. uniform water flow and corresponding sediment discharge). To evaluate the evolution in space and time, some small perturbations that affect the initial and boundary conditions of the reach were introduced. A complete (albeit rather complex) analytical solution of equations (3.13-3.17) has been found (Chapter 3, par. 3) by considering sinusoidal perturbations with respect to the basic configuration ("harmonic river).

A much simpler solution will be discussed in the following section with the hypothesis of morphodynamic stationary conditions.

3. ANALYTICAL SOLUTION IN MORPHODYNAMIC EQUILIBRIUM CONDITIONS

3.1 MORPHODYNAMIC STATIONARY CONDITIONS

A particular solution of the system (eqs. 3.13-17), that corresponds to equilibrium conditions, can be determined considering the stationary configuration for the bed profile and the bottom grainsize composition of the river reach. Namely, by putting equal to zero the time variations of the morphological quantities *z(x,t)* and $\beta_k^0(x,t)$. In this case eq. 3.17 becomes $\partial p/\partial x = 0$ and it means *p* is only function of the time *t* (eq. 4.3) while *z* is only function of the space *x* (eq. 4.6). Substituting this variables and solving the system, equations become:

$$\beta_k^0(x,t) = 0 \tag{4.3}$$

$$p(t) = 2q(t) \tag{4.4}$$

$$h(x,t) = \frac{2}{3}q(t) - \frac{5}{6}b(x) \tag{4.5}$$

$$\frac{\partial z(x)}{\partial x} = \left(1 - \frac{\alpha}{6}\right)\frac{\partial b(x)}{\partial x} - \frac{\varepsilon}{6}b(x) \tag{4.6}$$

By integrating eq. (4.6) from the origin of the reach to the distance *x*, one finds:

$$z(x) - z(0) = \left(1 - \frac{\alpha}{6}\right)\left[b(x) - b(0)\right] - \frac{\varepsilon}{6}\int_0^x b(x)\,dx \tag{4.6'}$$

This expression (eq. 4.6') will be simplified imposing that over the length *L* of the river reach the average deviation $\int_0^L z(x)\,dx/L$ is zero.

Eqs. 4.3-5 and 4.6' are valid for any river in equilibrium, not necessarily "harmonic" (sinusoidal variations).

An inspection of the solution allows for a number of interesting observations on the behavior of a *river in equilibrium*, namely in morphodynamic stationary conditions, in a channel with sinusoidally varying width. Some preliminary analysis have also been discussed for three and two dimensional models by Repetto et al. (2001, 2002) and for one dimensional model by Seminara (1997) but a more detailed discussion is necessary here.

First of all (eq. 4.3), the bottom composition does not change in time (i.e. when the water flow change) or in space (i.e. between narrow and wide cross sections). Secondly (eq. 4.4), the sediment transport does not depend on the local geometry and may only change if the water flow changes.

In equilibrium conditions, moreover the changes of water depth *h* depend exclusively on the changes of the channel width, with opposite sign of variation. Finally, contrary to the bottom profile *z*, the water depth doesn't depend on the Froude number (subcritical or supercritical flow).

Other relevant results of eqs. 4.3-4.6', regard the different behaviors of the longitudinal profiles of energy, water surface and bottom.

Defining as *j* the local energy slope $j = -\partial\left(H + Z + U^2/2g\right)\big/\partial x^*$, and as $i_w = -\partial\left(H + Z\right)\big/\partial x^*$ and $i_f = -\partial\left(Z\right)\big/\partial x^*$ respectively, the local slope of water surface and bottom, these variables can be expressed as a function of *b(x)*, (eqs. 4.7-9):

$$j(x) = \underline{J}\left(1 + \frac{1}{2}b(x)\right) \tag{4.7}$$

$$i_w(x) = \underline{J}\left(1 + \frac{1}{2}b(x) - \left(\frac{1-\alpha}{2\varepsilon}\right)\frac{\partial b(x)}{\partial x}\right) \tag{4.8}$$

$$i_f(x) = \underline{J}\left(1 + \frac{1}{2}b(x) - \left(\frac{6-\alpha}{2\varepsilon}\right)\frac{\partial b(x)}{\partial x}\right) \tag{4.9}$$

The local deviation of energy slope from the mean value $\underline{J}$ depends exclusively on the variation of the channel width *b(x)* (it results, eq. 4.7, exactly half of *b(x)*) and it doesn't depend on the flow conditions (Froude number). On the contrary, the water surface (eq. 4.8) and the bottom (eq. 4.9) slope depend both on the derivative of the longitudinal width variation and on the Froude number. For $Fr \to 0$ ($\alpha \to 1$) it's easy to observe that $i_w(x) \to j(x) \cong \underline{J}$ and therefore the water surface tends to a straight surface parallel to the basic configuration; this simplification is also called "rigid lid" hypothesis (Chapter 3, par. 4.2). For Fr >> 1 ($\varepsilon \to \infty$) it results that $i_w(x) \to i_f(x) \to j(x) = \underline{J}\left(1 + b(x)/2\right)$ and the locally quasi-uniform flow hypothesis can be applied (Chapter 3, par. 4.1).

Some of these results have also been found by Seminara (1997) who discussed the discordance between water depth and bottom elevation in equilibrium conditions. Now a question is in order: how much realistic are the equilibrium conditions for a real river?

Indeed, the solution (eq. 4.3-6') in morphodynamic stationary conditions corresponds to an effective configuration which a real river reach should eventually attain, provided that the water and sediment discharge are mutually related by a transport formula. This last condition, however, is not precisely fulfilled by the boundary conditions of a real river reach, especially in the steepest and farthest branches of the hydrographic network where the instantaneous

sediment input from the watershed slopes (by the surface erosion and mass movement) is rather independent from the contemporary runoff. We may expect therefore that the precise equilibrium conditions are never reached.

A detailed analysis of the effects of non-equilibrium boundary conditions in a river reach was made by Fasolato et al. (2008a). Yet, if the morphological configuration of a river reach remains substantially stationary, we may assume that it is in *quasi-equilibrium conditions* and its configuration is approximately described by eqs. (4.3-6').

3.2 SINUSOIDAL EQUILIBRIUM RIVER

For a preliminary evaluation of the morphodynamic equilibrium profiles, it was considered a series of simple cases with a sinusoidal variation of the cross width, in space and the water discharge in time, (eq. 4.10 and 4.11):

$$b(x) = -b_c \sin(2\pi\Omega x) \tag{4.10}$$

$$q(t) = q_c \cos(\omega t) \tag{4.11}$$

where $\Omega = \underline{H}/\lambda$ is the frequency of the spatial perturbation while $\omega = 2\pi\,\underline{H}/(T_{wave}\underline{U})$ is the angular frequency of the temporal perturbation; T_{wave} is the wave's period of the discharge oscillation and λ is the wave length of the cross width oscillation; b_c and q_c represent the maximum values of width and discharge perturbations.

In this way, considering for simplicity $q_c=0$ (no flow oscillations), is possible to write the water depth and bottom erosion/deposition oscillations as functions of Froude number (α and ε) and parameter $\Omega^{-1} = \lambda/\underline{H}$ (eqs. 4.12-13):

$$\frac{h(x^*)}{b_c} = +\frac{5}{6}\sin\left(2\pi\frac{x^*}{\lambda}\right) \tag{4.12}$$

$$\frac{z(x^*)}{b_c} = -\left(1-\frac{\alpha}{6}\right)\sin\left(2\pi\frac{x^*}{\lambda}\right) - \frac{\varepsilon}{6}\frac{\lambda}{2\pi\underline{H}}\cos\left(2\pi\frac{x^*}{\lambda}\right) \tag{4.13}$$

As it appears from eq. 4.12, the relative water depth (h/b_c) variation does not depend neither on the Froude number, nor on the width's wave-length (Fig. 4.1). Its relative amplitude is constant and equal to 5/6. This simply means that, to maintain the same sediment transport, water depth should increase more or less in the same proportion as the width decreases.

More complex is the behavior of the river bottom (z/b_c). The amplitude of the relative variation (peaks and troughs) tends to increase with the Froude number and with the length of the river width. These quantities also affect the position of peaks and troughs (Fig. 4.1).

For low Froude numbers the bottom peaks occurs at the wide section and the troughs at the channel narrowing. The bed profile is nearly in phase with the banks.

By increasing the Froude number, or the width wave-length, the peaks and troughs tend to anticipate the variation of the channel width and to locate themselves near to the flex of the width variation (Fig. 4.1).

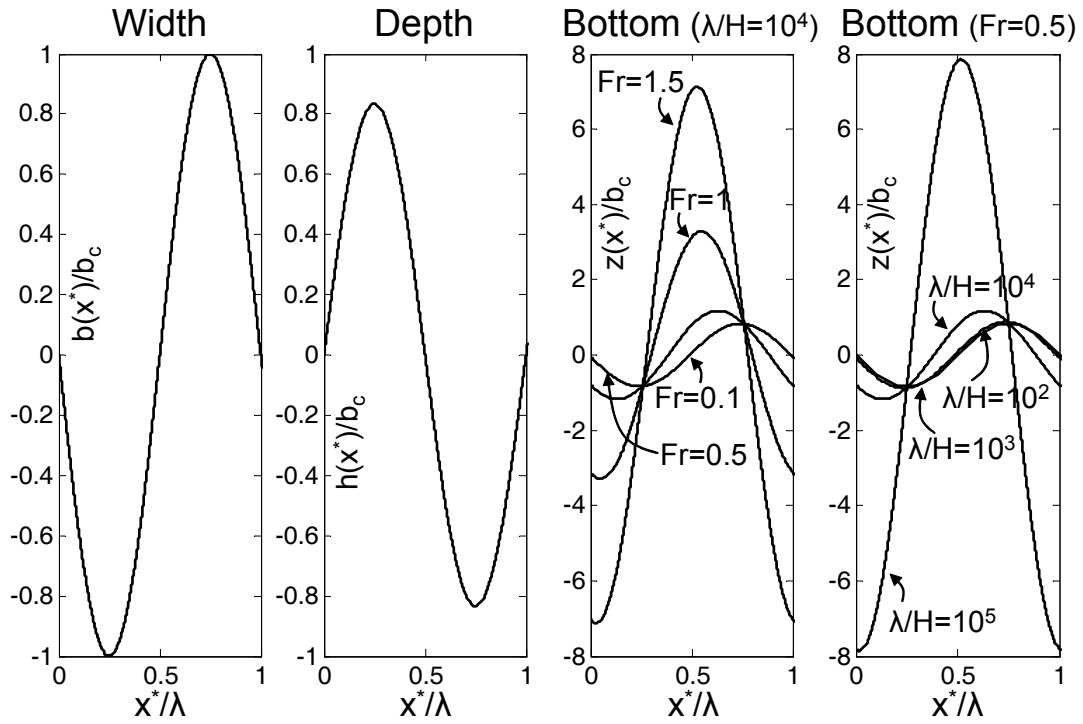

Fig. 4.1 Longitudinal water depth and bottom elevation (considering $q_c=0$), as a function of Froude number and $\Omega^{-1} = \lambda/\underline{H}$

Other parameters to be analyzed are local slopes (compared to the mean energy slope $\underline{J}$) of energy $j(x^*)$, water flow $i_w(x^*)$ and bottom slopes $i_f(x^*)$ (eq. 4.7'-4.8').

The relative graphs are reported in Fig. 4.2.

$$\left(\frac{j\left(x^*\right)-\underline{J}}{\underline{J}}\right)\Big/ b_c = -\frac{1}{2}\sin\left(2\pi\frac{x^*}{\lambda}\right) \tag{4.7'}$$

$$\left(\frac{i_w\left(x^*\right)-\underline{J}}{\underline{J}}\right)\Big/ b_c = -\frac{1}{2}\sin\left(2\pi\frac{x^*}{\lambda}\right)+\left(\frac{2}{3}E\right)2\pi\frac{\underline{H}}{\lambda}\cos\left(2\pi\frac{x^*}{\lambda}\right) \tag{4.8'}$$

$$\left(\frac{i_f\left(x^*\right)-\underline{J}}{\underline{J}}\right)\Big/ b_c = -\frac{1}{2}\sin\left(2\pi\frac{x^*}{\lambda}\right)+\left(\frac{6-\alpha}{2\varepsilon}\right)2\pi\frac{\underline{H}}{\lambda}\cos\left(2\pi\frac{x^*}{\lambda}\right) \tag{4.9'}$$

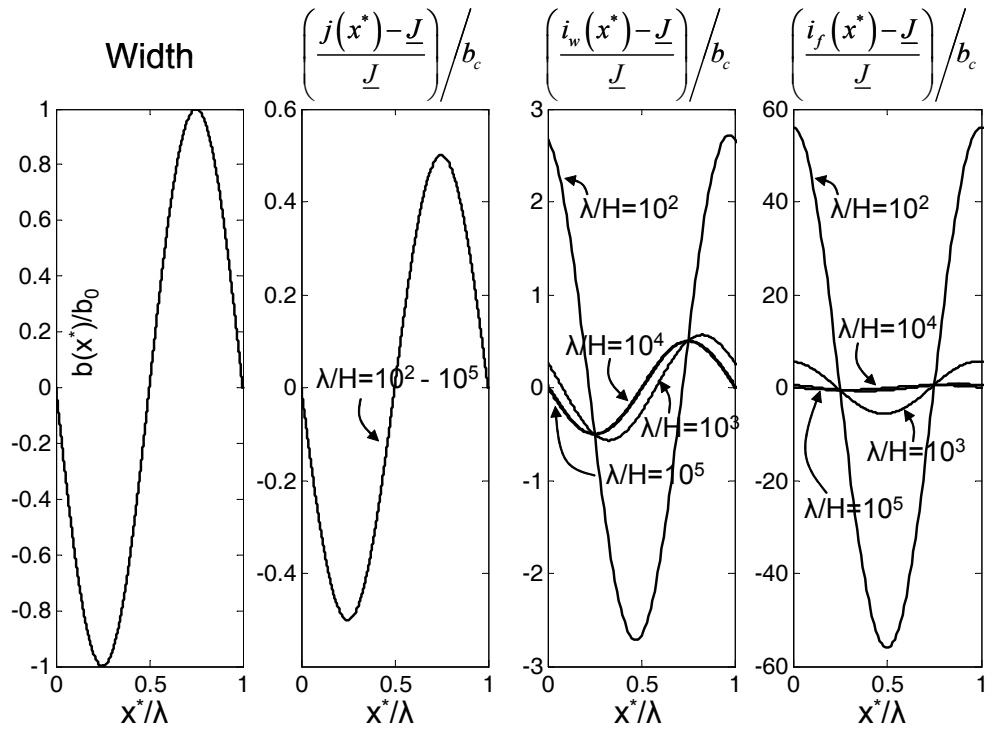

Fig. 4.2a Longitudinal slopes, respectively, of energy, water flow and bottom as a function of parameter $\Omega^{-1} = \lambda/\underline{H}$ (Fr is considered constant and equal to 0.5)

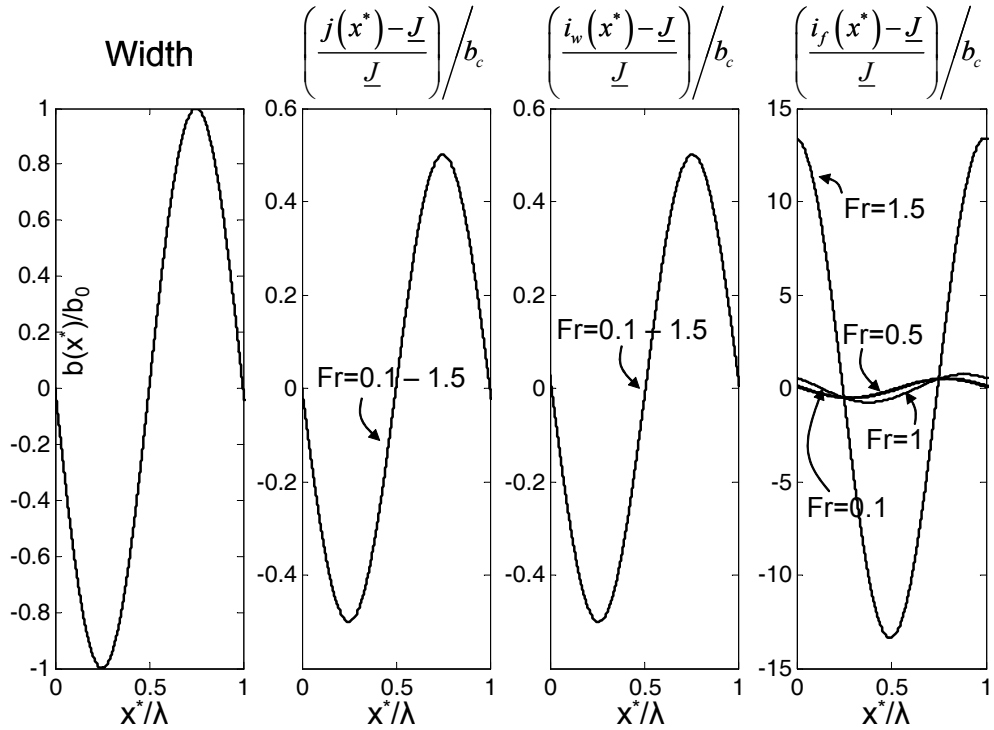

Fig. 4.2b Longitudinal slopes, respectively, of energy, water flow and bottom as a function of parameter Fr ($\Omega^{-1} = \lambda/\underline{H}$ is considered constant and equal to 10^4).

First of all, it is interesting to note that the oscillations of the energy slope are invariably very small (1/2 of the relative oscillations of the width). Oscillations of water surface by contrast, have a much larger amplitude and even more the oscillations of the bottom slope.

As shown by graphs, the slope of energy is in phase with the channel width variation, while, on the contrary, the amplitude and the phase lag of the water- and bottom-slope (eq. 4.9'), depends on $\Omega^{-1} = \lambda / \underline{H}$.

By increasing the parameter $\Omega^{-1} = \lambda / \underline{H}$ (Fig. 4.2), namely the length of the width wave, water flow and bottom slopes tend to the energy slope $i_w\left(x^*\right) \to i_f\left(x^*\right) \to j\left(x^*\right) = \underline{J}\left(1 + b\left(x^*\right)/2\right)$ (Fig. 4.2a, 4.2b and eqs. 4.8'-4.9'), while for low values of the ratio $\lambda / \underline{H}$ there is both an increase and an evident phase lag of the water and bottom slopes compared to the energy slope.

3.3 PEAKS AND TROUGHS OF THE BOTTOM ELEVATION

We have already observed that the bottom configuration is the most interesting morphological feature of an equilibrium river reach.

The bottom configuration is characterized by the amplitude of the peaks and troughs and by their position (phase lag) with respect to the forcing (width *b(x)*).

The maximum bottom elevation (peaks) of the bed morphological conformation at the equilibrium condition can easily be predicted analytically considering the value of $\overline{x^*_{\max}}$ (eq. 4.14) that maximizes $Z_{st}(x^*)$ (z_{st} is considered equal to z).

$$\overline{x^*_{\max}} = \frac{\lambda}{2\pi} arctg\left(\frac{6-\alpha}{\varepsilon}\frac{2\pi \underline{H}}{\lambda}\right) \qquad (4.14)$$

Both the amplitude and the phase lag of peaks and troughs depend on the Froude number and the length of the width-wave λ. This dependence is shown in Fig. 4.3; low values of both *Fr* and λ correspond, in physical terms, to prevailing "backwater effects". With prevailing "backwater effects" we tend to be close to the so-called "rigid lid approximation": namely a variation of the channel width does not produce any relevant variation of the water surface and therefore the change "*dz"* of the bottom elevation is practically equal to the change "*-dh"* of the water depth.

With high values of *Fr* and λ by contrast the "backwater effects" produced far away are rapidly damped and we move towards the *local uniform flow* approximation: namely the change of water depth "*dh"* produced by the change of the channel width corresponds to a relatively large variation of both the water level and the bottom elevation.

The corresponding phase lag, on the other hand, tends to be null with the *rigid lid approximation* and to anticipate till -90° for the local uniform flow hypothesis.

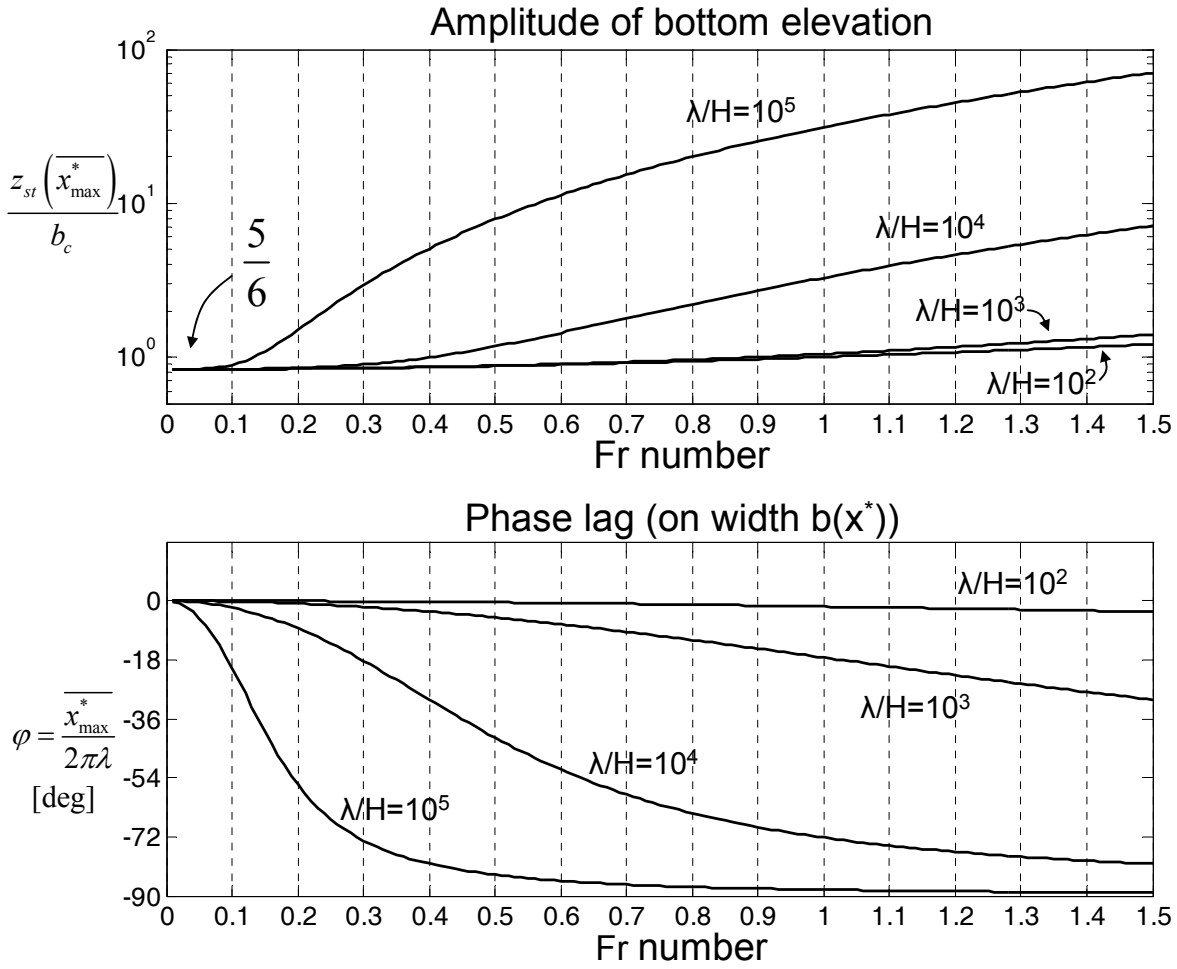

Fig. 4.3 a) Maximum oscillations of bottom deposition function of Froude number and wave length; b) phase lag (expressed in degrees) of the peaks of bottom oscillations as regards the width channel oscillations, function of the wave length and Froude number.

4. THE UNIFORM FLOW HYPOTHESIS

4.1 THE ONE-DIMENSIONAL EQUATIONS

The characteristic lines of the one-dimensional morphodynamic model (set of equations) introduced in Chapter 3 (eq. 3.1-4) has been thoroughly discussed since many years, initially in the case of uniform grainsize material (De Vries, 1965 and 1973; Lyn, 1987; Correia, 1992; Morris and Williams, 1996; Lyn and Altinakar, 2002) and, more recently, for the case of a sediment mixture (Marin and Di Silvio, 1996; Sieben, 1997; Fasolato et al., 2008a).

In its most complete form the set of equations implies the presence of (*2N+2*) characteristic lines, in the downstream and/or in the upstream direction, along which propagate the perturbations defined by the quantities that appear in the equations (Sieben, 1997).

For the mathematical model considered here (Chapter 3, eqs. 3.1-3.6) the hypothesis has been made that the sediment transport depends on the local hydraulic and granulometric conditions, namely that the adaptation length of the suspended particles is negligible. Moreover, note that for the analytical solution, (eqs. 3.13-17) only two grainsize classes (*N=2*) have been considered and one perturbation, with no damping and infinite celerity, is represented by the instantaneous propagation of *Q* along the river. So, only two *(N)* independent boundary conditions should be prescribed upstream and *1* boundary condition downstream (Sieben, 1997; Fasolato 2008a).

At least two grainsize classes (e.g. sand and gravel) are necessary to describe the space- and time- changes at watershed scale. However a further, extremely useful, simplification of the de St. Venant equations, can be introduced in the one-dimensional morphodynamic model to make it more adapt for watershed scale computations: namely the *local uniform flow hypothesis*. This consists in considering the local bottom slope almost equal to the energy slope:

$$\frac{\partial Z}{\partial x^*} \cong -J = -\frac{Q^2}{A^2 C_h{}^2 H} \tag{4.15}$$

which is valid whenever:

$$\frac{\partial Z}{\partial x^*} = \frac{\partial}{\partial x^*}\left(\frac{Q^2}{2gA^2} + H\right) \tag{4.16}$$

4.2 IMPLICATIONS OF THE UNIFORM FLOW HYPHOTESIS

The advantages of transforming the second de St. Venant equation (Chapter, eq. 3.2) into the much simpler (eq. 4.15) are many and mainly connected to the fact (Chapter 3) that, under this hypothesis, the effects of the perturbations moving downstream along the *N* characteristic lines, originating at the upstream-end of the channel, are invariably dominant with respect to the perturbations moving in the upstream direction along the only characteristic line originating at the downstream end.

This means that the solution along the channel depends prevalently on the boundary conditions prescribed upstream (waterflow input and bottom composition or, equivalently, waterflow input and sediment input of the *N* grainsize classes), rather than on the boundary condition prescribed downstream (bottom elevation or, equivalently, water elevation). It

should be noted, in fact, that the evolution of the bottom elevation is very slow while the water level (under the u*niform flow hypothesis*) is univocally related to the water flow. In uniform flow conditions, then, the effect of the boundary conditions at the downstream end is either transmitted instantaneously all over the channel (water depth) or propagates slowly and strongly attenuated in the upstream direction (bottom elevation). This circumstance permits to proceed with the numerical integration only in the downstream direction, with relatively large space- and time-steps.

Another, even more important, advantage of the uniform flow hypothesis is the possibility to compute the annual sediment transport P_S in any cross section of the channel, by integrating eq. (2.7) in the following way:

$$P_S = \sum_{k=1}^{N} P_k = \alpha \frac{J^n}{B^p} \sum_{k=1}^{N} \frac{\beta_k \zeta_k}{d_k^q} \int_{year} Q^m(t)\, dt \tag{4.17}$$

In eq. (4.17) it has been put $\underline{J} \cong -\partial Z / \partial x^*$ and it has been assumed that all the quantities remain practically constant during the year, except the waterflow *Q(t)*. This assumption, again, depends on the fact that the (*N*) perturbations basically related to the sediment boundary conditions move downstream with a much slower celerity and stronger attenuation than the perturbations related to the waterflow.

If one supposed a duration curve for the waterflow (eq. 4.18):

$$Q(t) = Q_0 \cdot e^{-\gamma t} \tag{4.18}$$

one finds (for great values of γ):

$$P_S = \frac{\alpha}{m} \frac{J^n}{B^p} \sum_{k=1}^{N} \frac{\beta_k \zeta_k}{d_k^q} \left(Q_0^{m-1} V_0 \right) \tag{4.19}$$

where Q_0 is the annual peak flow and V_0 the annual runoff volume (see Chapter 1, eq. 1.10). By using P_S as local sediment discharge, the morphodynamic evolution of the watershed can be simulated at much longer (year) time-steps (Chaper 1, par. 3.1).

4.3 LIMITATIONS OF THE UNIFORM FLOW HYPHOTESIS

In order to evaluate the errors made by applying the *uniform flow hypothesis* in river computations, let us consider the peak (or trough) created along a sinusoidal river reach, as discussed in the preceding sections. We may define the absolute error along that river reach as the difference between the maximum bottom elevations (peak or trough) computed with the steady flow model $Z_{st}(x^*)$ (supposed to be the exact solution) and the maximum peak elevation computed with uniform flow model $Z_{un}(x^*)$; this error e_{abs} can be expressed as (eq. 4.20):

$$e_{abs} = \left|\max\left|Z_{un}\right| - \max\left|Z_{st}\right|\right| = \frac{\left|\int_L \left|Z_{un}\left(x^*\right)\right| dL' - \int_L \left|Z_{st}\left(x^*\right)\right| dL'\right|}{L} \tag{4.20}$$

Then, let us define the relative error as the maximum absolute error scaled by the exact value of the peak (eq. 4.21):

$$Er_{rel} = \frac{\left|\max\left|Z_{un}\right| - \max\left|Z_{st}\right|\right|}{\max\left|Z_{st}\right|} = \frac{\left|\int_L \left|Z_{un}\left(x^*\right)\right| dL' - \int_L \left|Z_{st}\left(x^*\right)\right| dL'\right|}{\int_L \left|Z_{st}\left(x^*\right)\right| dL'} \tag{4.21}$$

where $\overline{x^*_{\max}}$ represents the distance from the reach origin where the bottom elevation ($Z_{st}(x^*)$) is maximum (eq. 4.14). As shown in Fig. 4.4, the maximum relative error is function both of the Froude number and of the wave length but doesn't depend on the wave amplitude b_c.

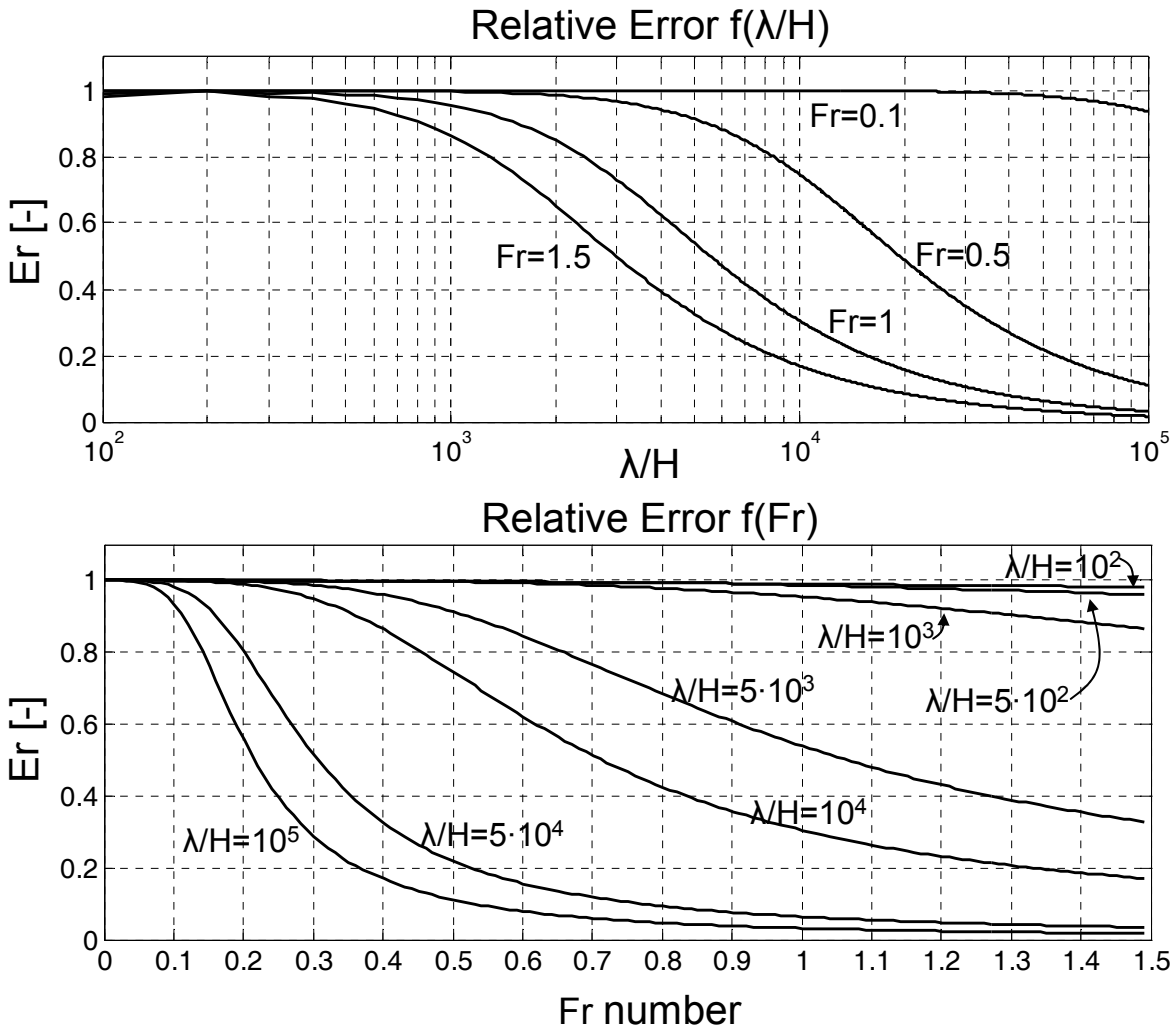

Fig. 4.4 Maximum relative error of the analytical solution between bottom elevation (function of Froude number and wave length).

5. NUMERICAL SOLUTIONS

The analytical solution provided in par. 3 (either based on the steady- or on the uniform-flow equations) has been obtained by a one-dimensional model which incorporates a number of simplifications. First of all, all the equations have been linearized; secondly, the flood wave propagation is assumed to be instantaneous $(\partial Q/\partial x = 0)$; and, finally, the grainsize distribution is limited to only two grainsize classes, while the exponents of the transport equation (eq. 2.7) have been rounded (m,n=2 and p,q=1; Chapter 3, eq.3.5).

In the present section the analytical solutions (both for the steady- and uniform-flow) have been compared with the non linear numerical model, under three different water flow hypothesis.

The numerical code STERIMOR (Fasolato et al., 2006a) was used for computation, integrating some modifications for water flow equations during different simulations (see Chapter 2, Table 2.1).

Note that, a model can be decoupled but still retaining some unsteady features of the waterflow equations as, for instance, the case of the *unsteady* model, where the cinematic wave hypothesis is made and unsteadiness is retained only by the continuity equation $\partial A/\partial t = -\partial Q/\partial x \neq 0$ but not by the momentum equation $\partial Q/\partial t = 0$.

For the characteristics of the three numerical models see Chapter 2.

Numerical analysis were made varying the mean bottom slope (and *Fr*) and the sinusoidal wave length of the width perturbation of an hypothetical river (river length 108 km, mean width 90 m, mean water discharge 100 m^3/s and Chézy coefficient 50 $m^{1/2}/s$).

5.1 NUMERICAL ACCURANCY

The space- and time-steps throughout all the present calculations are Δx=900 *m* and Δt=1000 *s*. Numerical tests show that this spatial and temporal step is appropriate since there is no appreciable difference among the computational results with finer steps, which moreover comply with Courant (CFL) stability requirement (Chapter 2). Note that Δx and Δt are much smaller of, respectively, the shorter spatial wave (9000 m) and the shorter temporal wave (about 350000 s) of the sinusoidal width and flow perturbation.

5.2 NON LINEARITY

A comparison of the analytical (linearized solution) and the non-linear numerical solution for the quasi-uniform and quasi-steady flow hypothesis is shown, respectively, in Fig. 4.5 varying the hydraulic conditions (*Fr*) and the wavelength of planimetric width variation.

In this way is possible to study different results (under exactly same boundary and initial conditions) and to consider negligible the numerical errors solely due to the non-linearity of the equations solved with the numerical model. As it can be seen, model results show slight underpredictions of the bed peaks and troughs. However, these discrepancies are at maximum less then 10%-15% and these values don't depend on the hydraulic (*Fr*) or planimetric variations (λ/H).

It must be emphasized that no calibration based on the analytical solutions was performed on the numerical models. The slight discrepancies (both for the *quasi-uniform* and for the *quasi-steady* flow) are totally caused by the non-linearity of the equations solved with the numerical model.

Numerical simulations confirm the peaks translation of bottom oscillations, function of *Fr* and λ/H in the case of *quasi-steady* flow (Fig. 4.5b) while the absence of this translation in the case of *quasi-uniform* flow.

5.3 NON EQUILIBRIUM CONDITIONS

Numerical simulations were made starting from a non-equilibrium river condition (initial bottom elevation), on one hand to verify if the final morphodynamic equilibrium corresponds to the theoretical one, on the other hand to analyze the differences between models in non-equilibrium, especially as far as the time to reach the equilibrium condition is concerned. For different simulations, the time to reach the equilibrium conditions depends both on the distance between the initial configuration and the final one and on the characteristics of the river (bottom slope, wave length etc.). So, to compare a non-dimensional time $\hat{t}$ was defined in such a way that $\hat{t} = 1$ when the bottom peaks' amplitude, calculated with the *quasi-steady* model, is half of the theoretical one (Fig. 4.6a). It was than assumed that at $\hat{t} \geq 5$ the (quasi-) equilibrium conditions were reached by the numerical model solutions.

A systematic series of numerical simulations in non-equilibrium conditions has also been carried on with different boundary conditions (e.g. by feeding the river with a sinusoidal input of sediments and waterflow). As for the non-equilibrium initial condition, also in this case the numerical relative error between steady- and uniform-flow hypothesis varies with Froude number and wave length in the same way as the analytical solution. Moreover, the *maximum* numerical error generally occurs at the beginning of the simulation, when is largest the distance from the equilibrium conditions. In any case, the maximum error is only slightly larger than the analytical one (Fig. 4.7).

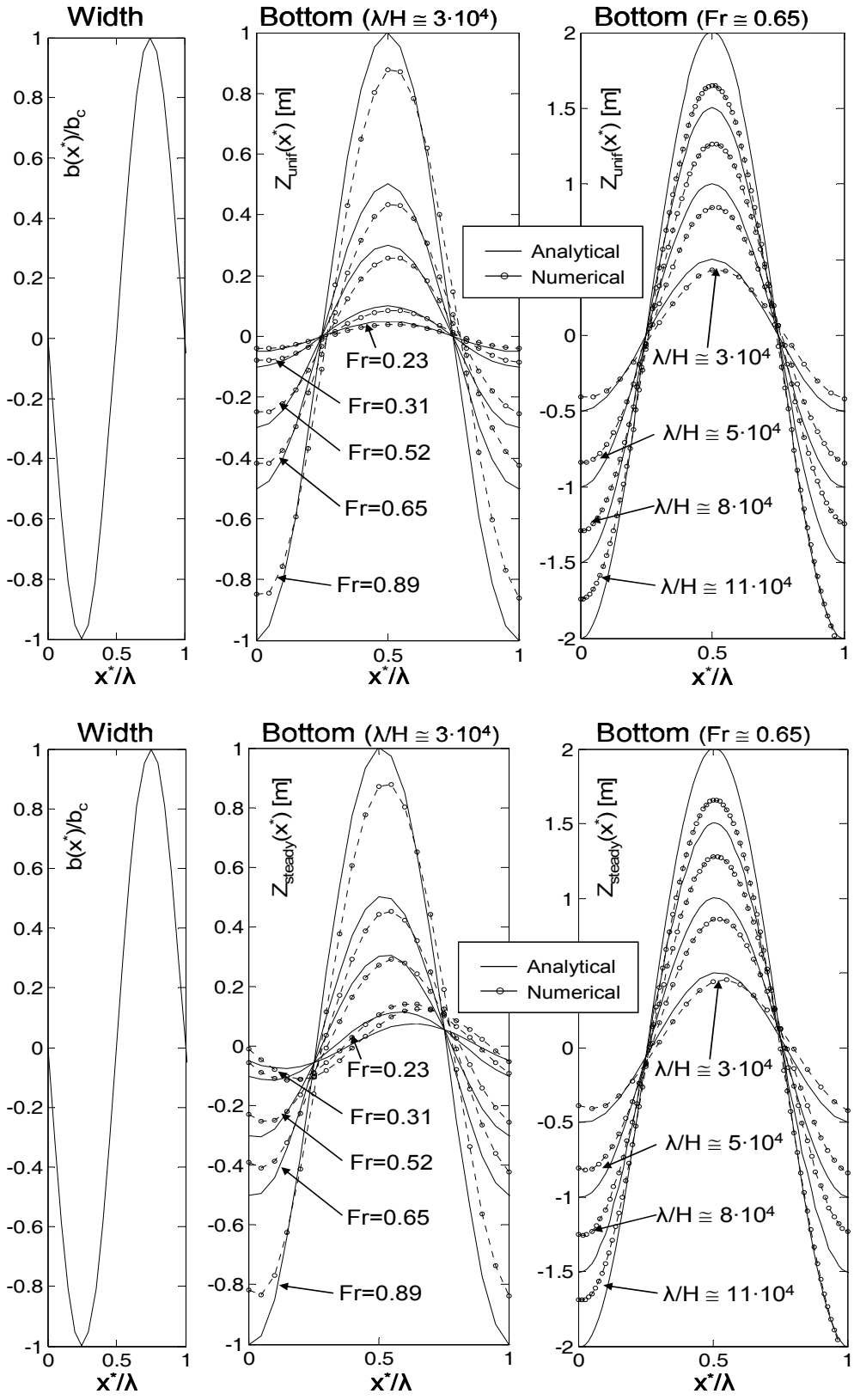

Fig. 4.5. Comparisons between bottom elevation calculated numerically and theoretically (analytically) for the *quasi-uniform* flow models (a) and *quasi-steady* flow models (b) varying Froude numbers and wave lengths.

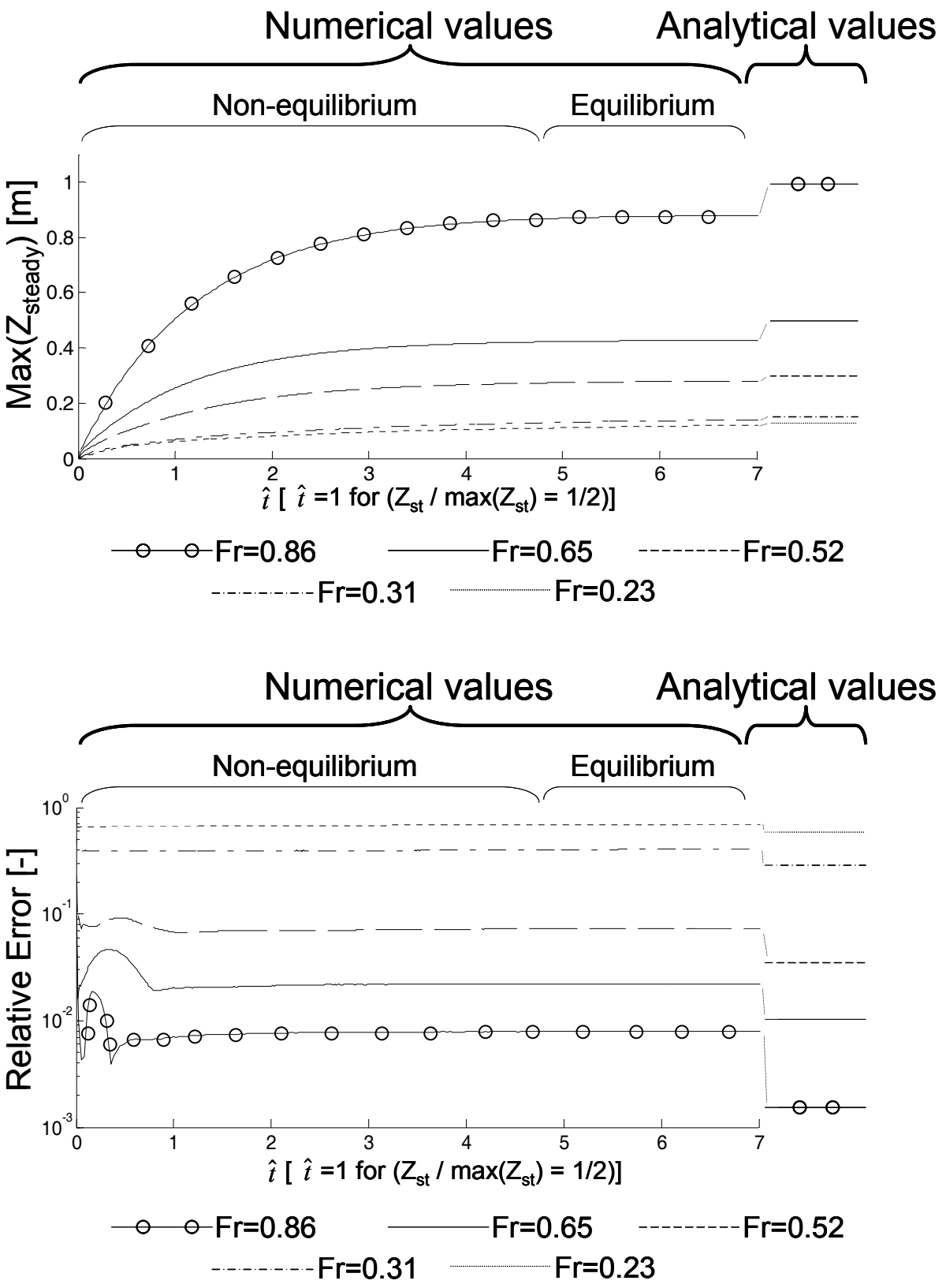

Fig. 4.6 a) Maximum bottom peak simulated with *quasi-steady* model and b) numerical errors between *quasi-steady* and *quasi-uniform* models, compared to the analytical ones considering different values of Froude number (λ/H=2.7·10^4 for all the simulations).

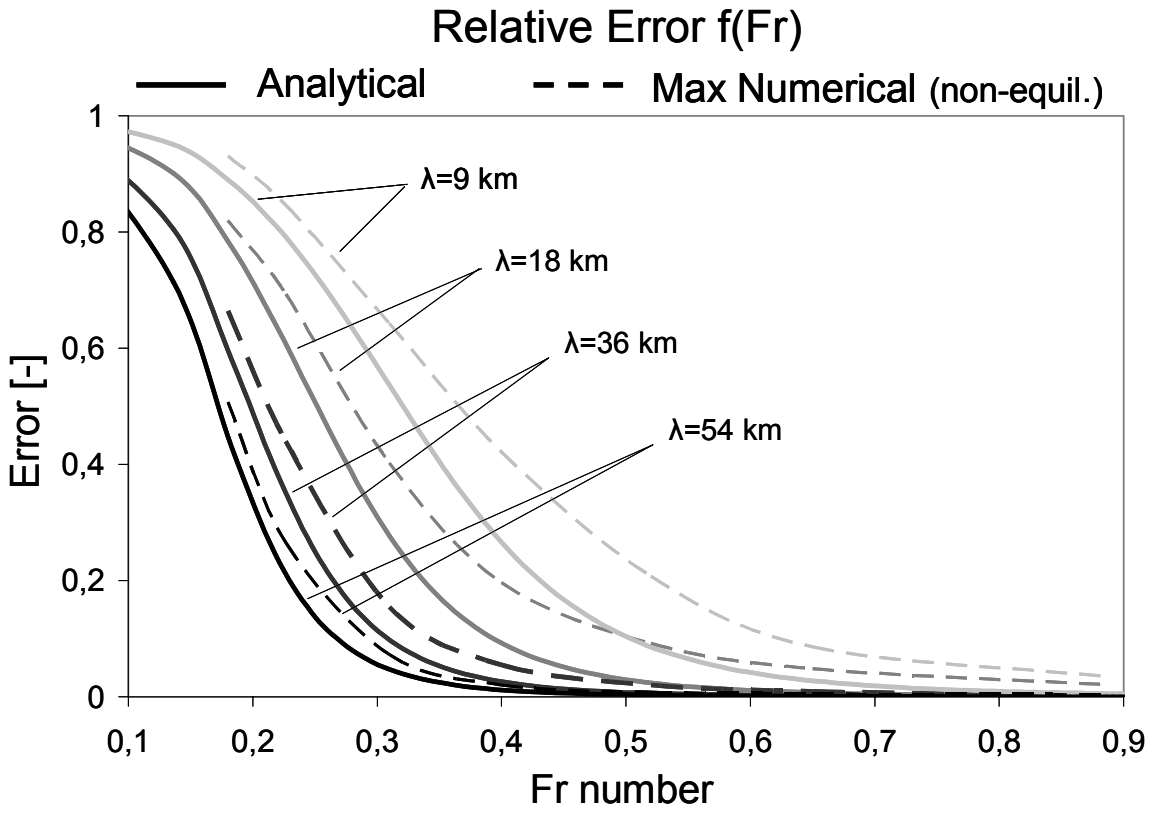

Fig.4.7 Numerical error (maximum in non equilibrium conditions) and analytical one function of Fr number and the wave length λ.

6. CONCLUSIONS

The analytical solution of the linearized 1-D morphodynamic equations applied to a sinusoidal river in equilibrium conditions has permitted to investigate the variation of bottom elevation, water depth, and energy slope along the river as a function of the river width. The same solution provides a general criterion to predict the maximum relative error between the *steady-* and the *uniform-flow* hypothesis. The theoretical solution has been numerically checked for evaluating the effects of *non-linearity* and *non-equilibrium*. In the case of sinusoidal perturbations of the river width, the numerical analysis confirm the theoretical criterion: namely the relative error decreases when the wave length of the width perturbation and the Froude number of the river increase.

Therefore the analytical criterion also permits, for a given Froude number, to define a "minimum" wave length above which the error is less than a prescribed values. Based on this criterion, in another paper (Ronco et al., 2008a) has been developed the concept of "morphological box" to be applied to the case of natural rivers with an irregular configuration.

Chapter 5

EVOLUTION OF A RIVER DUE TO SEDIMENT FLUSHING FROM A RESERVOIR

SUMMARY

Is presented here a comprehensive study combining field measurements and numerical modelling of an upper area of the Piave Basin (Eastern Alps, Italy) where flushing operations from an alpine reservoir (Comelico reservoir, capacity of 1.4 10^6 m^3) were performed periodically in the past decades. Boundary conditions (partially controlled by management) for the downstream channel of this reservoir are known; further downstream, this channel empties into the Pieve di Cadore reservoir.

Two numerical morphodynamic models (CCHE1D from University of Mississippi, based on unsteady flow and STERIMOR from University of Padua, based on quasi-uniform flow) were applied to simulation of the chronological sequence of strong deposition, subsequent erosion-phases of the river downstream and sediment transport caused by sediment flushing operations. The simulation results make it possible to better understand the sediment transport and morphological change processes in the channel and improve sediment flushing practices; as well as to analyze the validity and limitations of the local-uniform-flow hypothesis by comparing the two models' simulation results.

1. INTRODUCTION

The annual rate of reservoir storage capacity loss to sedimentation in the world is 0.5–1%, and it varies dramatically from one river basin to another due to different forest cover and geological conditions. In order to control reservoir sedimentation, different approaches such as bypassing, dredging, flushing, sluicing, and upstream sediment trapping have been developed. Although combinations of these sediment control measures are usually adopted to retain the maximum capacity. The flushing approach, among others, is an efficient hydraulic sediment removal technique to restore the reservoir storage capacity.

In this study, two numerical morphodynamic models (CCHE1D from University of Mississippi, based on unsteady flows and STERIMOR from University of Padua, based on quasi-uniform flow) have been developed and applied to simulate flushing operations performed in the alpine reservoir in the last decade. The simulation results were compared with the measurements during and after the sediment flushing operations and were used to evaluate the impacts of these operations on the river downstream. Finally, once calibrated and validated, the more efficient STERIMOR model was also used to reproduce the long-term tendency of the morphology of the river.

2. STUDY SITE

The study area (Fig. 5.1) is located in the upper part of the Piave basin, between Pieve di Cadore reservoir ($64.3 \cdot 10^6$ m^3) and Santa Caterina reservoir ($6.7 \cdot 10^6$ m^3) and Comelico reservoir ($1.4 \cdot 10^6$ m^3).

In this area the present physiographic setting of the river results mainly from the evolution of the drainage system during the Lateglacial and the Holocene (Surian, 2002). The drainage basin is mainly composed of sedimentary rocks (predominantly limestone and dolomite) and the river is incised in the bedrock and presents a quite narrow channel.

All the released sediments (from Comelico dam, during flushing operations) moreover, are intercepted by the Pieve di Cadore reservoir. The catchment collected by the lake has a total area of about 860 km^2 but excluding basins collected by the two upstairs dams (in which the discharge released is partially controlled by management), the watershed area directly draining to the lake is about 230 km^2. Some mountain peaks are higher than 3,000 m, the snow and glacial ice constitute an important mountain source of water for power generation.

Until the year 2005, about $18.0 \cdot 10^6$ m^3 of sediments were deposited in the Pieve di Cadore lake, causing the progressive reduction of the reservoir water storage capacity with an annual rate of about 0.5%.

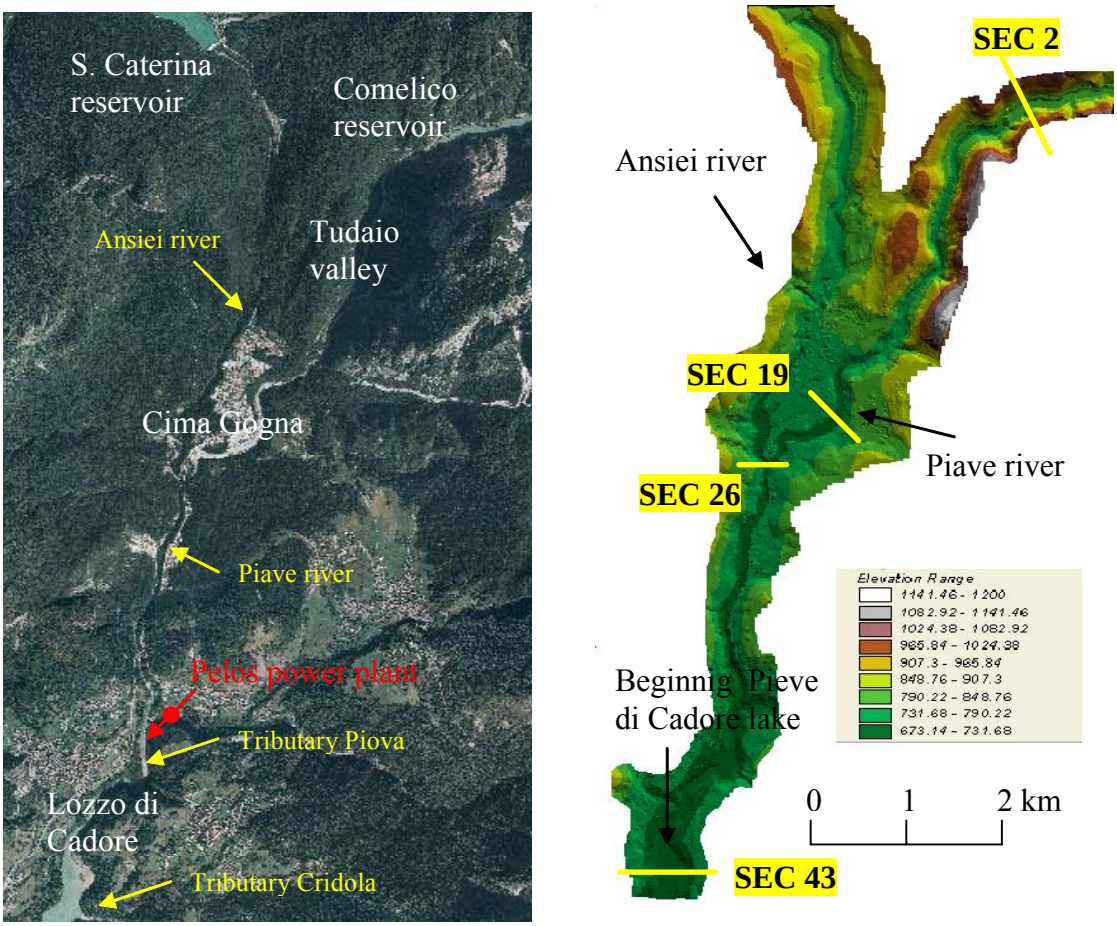

Figure 5.1. Location of the study site in the upper course of Piave river. (a) Aerial photos (2000) and (b) Digital elevation map (extract from .dxf files 1:5.000) with some sections (the number of sections are related to the computation grid point) of the rivers.

3. FIELD MEASUREMENTS AND DIGITAL DATA

3.1 HYDROLOGICAL DATA

The alternate operations of flushing and flood at the Comelico dam have continued probably for 70 years (the dam was built in 1931), but they have been quantitatively recorded only in the last decades (1994 to 2005). By analyzing the water discharges released from Comelico dam (from 1990 to 2005), it was possible to identify three distinct regimes: (i) flushing periods, (ii) very long minimum flow periods and (iii) moderate flow (from April to May, due to the melting of snow) and flood periods (about one flood event per year). From autumn

2003, however, the water flow management of Comelico dam has changed because of a new Italian regulations, prescribe a "vital minimum discharge" to be released downstream.

From the Comelico dam and before the beginning of the Pieve di Cadore lake there are (besides the Ansiei river) two other significant tributaries reaching the Piave river; the Piova river and the Cridola river (Fig.5.1a). For these rivers the daily average discharge data are not available; this information had to be obtained indirectly from the other available hydrological data. Since Piova and Cridola's watershed areas are respectively of 36 and 19 km^2, the monthly average discharges are noticeably smaller than the others and for these reasons, during these first series of simulations, were neglected. At the same time, an important contribution of water discharge is supplied by the Pelos power plant (Fig. 5.1a) that returns the water diverted from the two lakes upstream after its use. While the discharge released from the Pelos power plant is obviously lacking in sediments, the solid transport supply from the Cridola river (particularly during flood events) aids considerably the sedimentation of the Piave di Cadore reservoir and its influence has to be studied in depth in the future.

Fig. 5.2 indicates the time series of water surface elevation of the Pieve di Cadore Lake. The time series do not show a clear periodic behavior (they are artificially controlled) but is interesting to note that the minimum annual levels of the lake were always occurred during the same period (March of every year), due to the necessity to make the most of the storage reservoir capacity for the spring, the snow and glacial ice melting season.

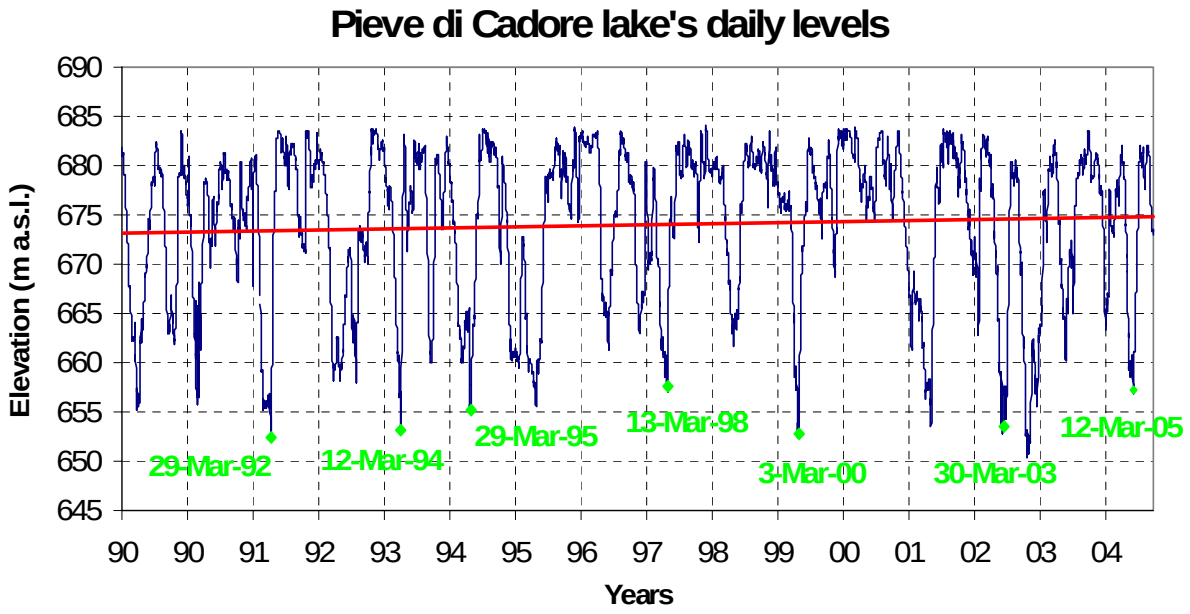

Figure 5.2. Time series of daily lake levels (From 1st January 1990 to 30th June 2005); the red line fits the entire data and its slope indicates a positive trend.

The mean annual levels vary between 668.2 m and 676.5; it is also important to underline that over the years, levels of the Pieve di Cadore lake have slowly but gradually increased (as shown by the red line in Fig. 5.2) and this is probably due to sedimentation.

3.2 TOPHOGRAFIC DATA

The extraction of cross sections, the coordinates of the thalweg, the longitudinal profile and other useful information, such as the locations of various important landmarks, confluences with tributaries had to be determined using various maps (electronic and paper format) and were integrated with photographic survey made by authors in the last two years. A set of detailed cross sections and thalweg elevations were surveyed in the summer of 2005 for the first few kilometres downstream Comelico Dam (Fig. 5.3) validate and complete information extracted from maps but unfortunately covered just a limited part of the studied river.

For the simulations, the cross section geometries at various locations were mainly extracted from aerial and digital data (1:5000, .dxf files, contour maps with a contour-line interval of 5m). Due to the insufficient resolution of the existing contour map (5 m), the lower parts of the cross-sections were completed artificially by assuming a parabolic shape. Obviously this assumption is a rough estimate of the real profile. Neverthless, as much as possible these cross section geometries were modified based on the surveyed cross section data (2005), which was available only for the upper part of the study reach.

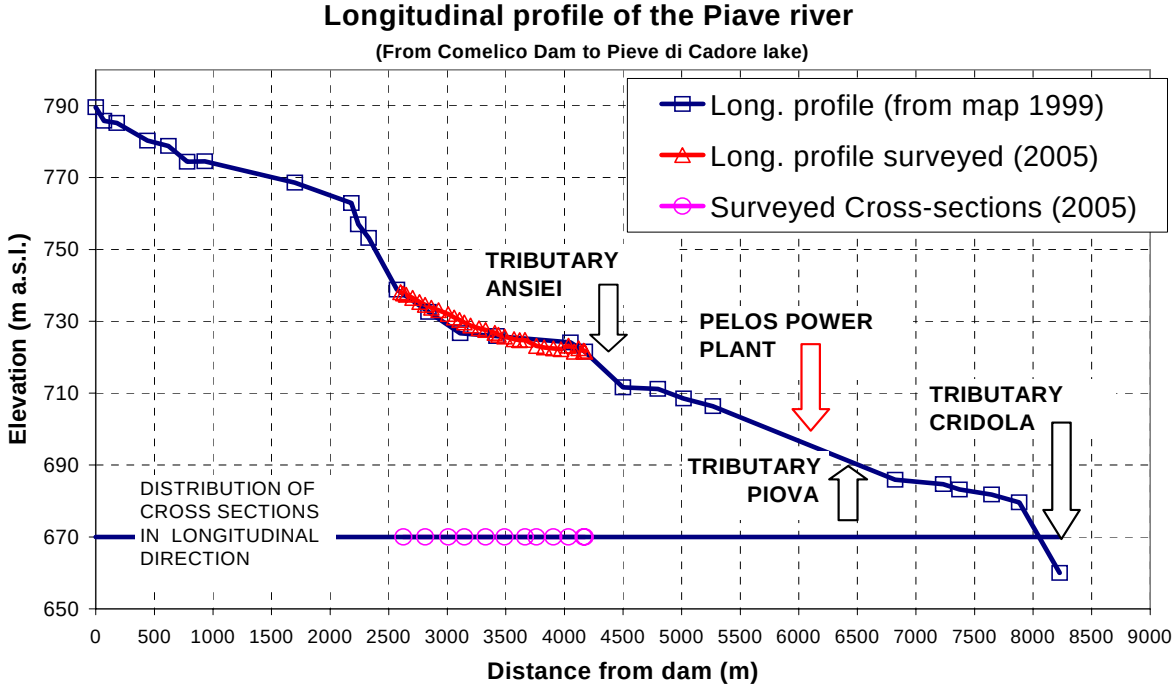

Figure 5.3. Piave river's (from Comelico dam to the beginning of Pieve di Cadore Lake) channel thalweg elevation (from map and surveyed) and locations of cross sections surveyed.

3.3 GRANULOMETRIC DATA

The sampling method was designed to investigate longitudinal, vertical (armouring) and temporal variations in the bed material. Along the study reaches, surface and volumetric material was sampled in different sites and in different times (Table 5.1 and Fig. 5.4).

Study reach	Location (Fig. 1b)	Surveyed period	Number of samplings	Type of sampling
Piave river	Tudaio valley (Sect. 2)	August 2005	5	Surface
Piave river	Cima Gogna (Sect. 19)	August 2005	1	Vol. & Surf.
Ansiei river	Cima Gogna (Sect. 19)	August 2005	1	Vol. & Surf.
Piave river	Tudaio valley (Sect. 2)	November 2005	1	Surface
Piave river	Cima Gogna (Sect. 19)	November 2005	1	Surface
Piave river	Pelos	November 2005	1	Surface
Piave river	Cima Gogna (Sect. 19)	August 2006	4	Volumetric
Ansiei river	Cima Gogna (Sect. 19)	August 2006	1	Volumetric
Cridola river	Lozzo di Cadore	August 2006	2	Volumetric
Pieve di cadore lake	Lozzo di Cadore (Sect. 43)	August 2006	2	Volumetric
	TOTAL SAMPLINGS		**19**	

Table 5.1. Location, number and type of granulometric sampling in study reaches (2005/2006).

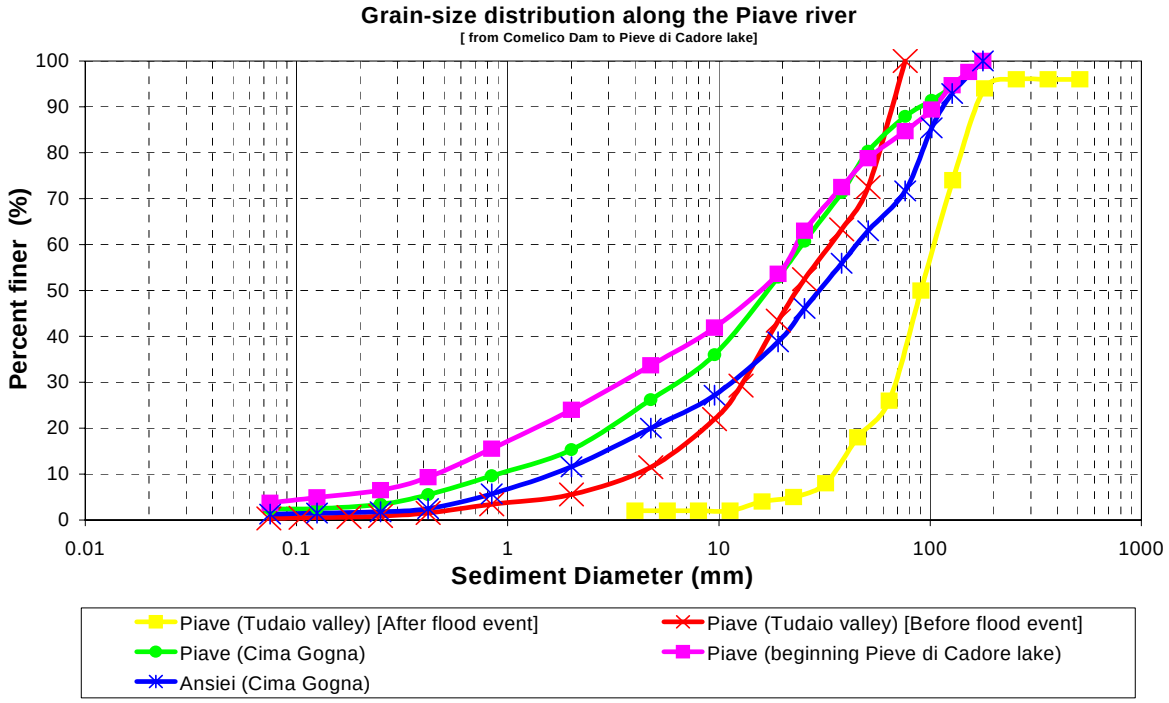

Figure 5.4. Grain size composition along the Piave river

Surface material was sampled using the grid by number method (Surian, 2002). Gravel samples were taken from exposed bars (lateral, mid-channel or point bars) and close to active

channels. Since this method doesn't allow to sample fine materials, some volumetric samplings were made in the same places to characterize the bed complete granulometry.

The tributary Ansiei (where virtually flows only clear water) presents an armoured bed with definitely coarse material (Fig. 5.4). The Piave reach below the Comelico dam, by contrast, presents a more complex pattern, with layers of different material caused by the chronological sequence of strong deposition and subsequent slow erosion-phases.

In particular, two series of samplings were made in the Piave river before and after the flood event of October 2005. In this way it was possible to distinguish the finer material of the stratified thick layer (yellow line in Fig. 5.4) (deposited during flushing periods) from the coarser material of the bottom (red line in Fig. 5.4).

4. NUMERICAL MODELING

The CCHE1D is an unsteady model, it was used to reproduce both the quick chronological sequences of strong deposition (hours) due to flushing activities (or strong erosion due to flood events) and subsequent slow erosion-phases (months) with relatively small flow (the so-called "vital minimum discharge").

A simpler but more efficient model (STERIMOR, from University of Padua, see Chapter 2) were used for simulating the long-term tendency (years or decades) of the morphology of the river. The STERIMOR model (STEep RIver MORphology) is based on quasi-uniform flow hypothesis and consent, filtering the morphological fluctuations due to short term components, to predict the long-term evolution (time-averaged values over a year or number of years) of the study reach.

4.1 CCHE1D MODELING SYSTEM

The CCHE1D model is a one-dimensional model but it includes a (quasi 2D) component for simulating the cross-sections evolution of the channel (with bank erosion procedures). It simulates the non-equilibrium transport of non-uniform total load under unsteady flow conditions in dentritic channel networks (Wu et al., 2004).

The model offers four method for the determination of sediment transport capacity; for the purpose of this work, the modified Engelund and Hansen's 1967 formula was choice. The hiding and exposure correction factor ε_k for non-uniform material is determined with Wu et al's (2000a) method.

4.2 STERIMOR MODELING SYSTEM

The STERIMOR model is based on a relatively simple hydrodynamic component, while much attention is devoted to the non-uniform distribution of sediment grainsize (see Chapter 2). Model consider 4 granulometric fractions (size class *k*) and the transport equation (Chaper 2, eq. 2.7) is:

$$P_k = \alpha_c \frac{Q^m J^n}{B^p d_k^q} \beta_k \zeta_k \tag{5.1}$$

where Q is the water discharge, B is the active channel width and J is the energy slope of the flow. The exposure-correction coefficient is the same of CCHE1D ($\zeta_k = \varepsilon_k$).

The formula is similar to the Engelund and Hansen's transport formula (Di Silvio, 1991) with the following values of the exponents

m=17/10=1.7 n=33/20=1.65 p=7/10=0.7 q=1

The value of α_c is equal to the following equation (eq. 5.2) and in all simulations carried out is considered

$$\alpha_c = 0.1\left(\frac{\gamma}{\gamma_s - \gamma}\right)^2 \frac{1}{2\sqrt{g}} \cdot k_s^{0.3} \tag{5.2}$$

5. SHORT TERM SIMULATIONS

One-year simulations were conducted for the entire 2004 (Fig. 5.5a, reported the event starting the 100th day of the year) and the entire 2002 (Fig. 5.5b, reported the event starting the 300th day of the year).

Several important parameters were evaluated according to the CCHE1D computational limits (Wu et al., 2004). Because of the lack of detailed surveying data, Manning's roughness coefficient was considered constant and proportional to the representative diameters of the bed material. The non-equilibrium adaptation length of bed load was calibrated as 100 m. The mixing layer thickness is assumed to be twice the representative diameters of the coarsest particles d_{90} (it was set equal to 0.2 m). Several computational time-step were tested (from 1 minute to 15 minutes) and it was found that the simulations results are not particularly sensitive to the length of this range. Therefore, only the simulation results with 10-minute time-steps are presented in this paper.

5.1 ONE-YEAR SIMULATIONS

In the upper reach of the Piave River, (Fig. 5.5a, section 2) the consequence of flushing operation is a strong deposition of stratified material that is partially eroded by the subsequent

low water flood. Thalweg elevation can increase of about 4-5 meters at the end of the operation. The deposited material rapidly lessened with distance from the dam and in the proximity of Cima Gogna, about 3,500 meters below the dam (Fig. 5.5a, section 19), the bed area change is still evident but much smaller (thalweg elevation increases just 0.5-1 meter). Finally, about 800 meters below, after the confluence with the tributary Ansiei, the effects of this deposition are rapidly removed by the tributary river (Fig. 5.5a, section 26) and almost all the deposited sediments are washed out by the incoming water.

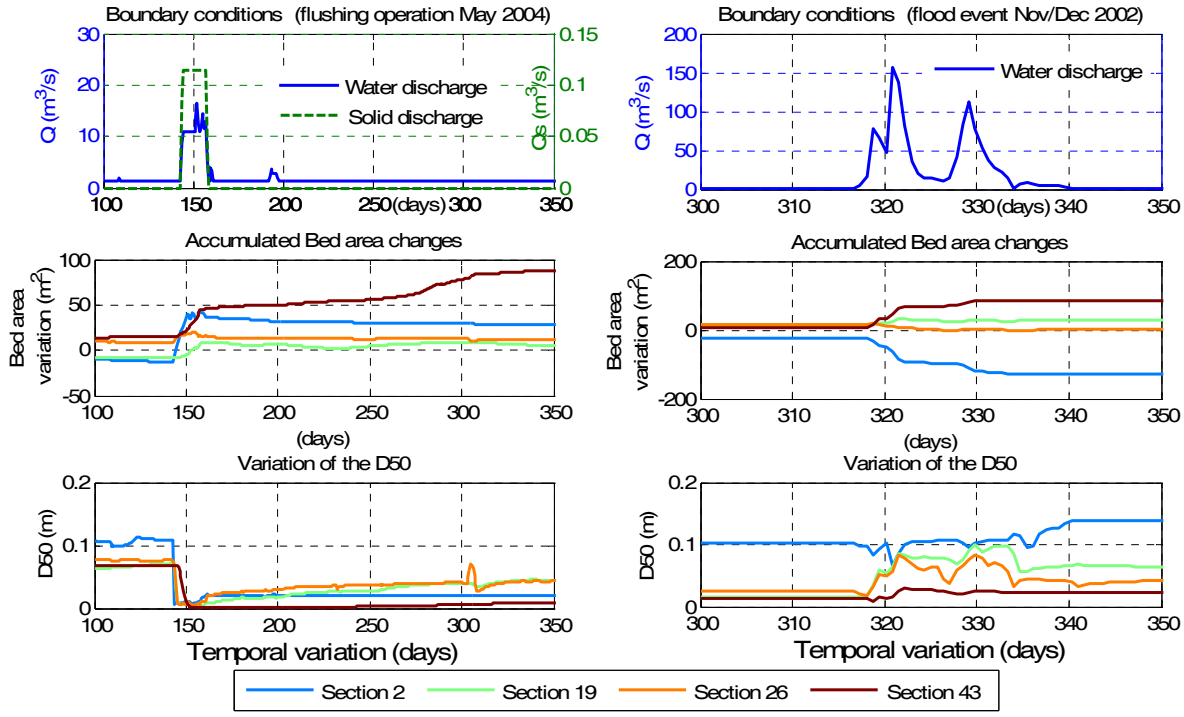

Figure 5.5. Upstream boundary conditions (1) and consequent evolution of (2) bed area and (3) grain-size at different sections, respectively during (a, left side) flushing operation of May 2004 and (b, right side) flood event of Nov\Dec 2002. [As shown in Fig. 5.1b, the 2,19, 26 and 43 sections are located respectively 200, 3500, 4250, and 8250 meters below the Comelico Dam]

What is more interesting is that the flushing operations affect also the lower part of the reach (part of the released sediments starts to reach the lake after about seven days), in proximity of the Pieve di Cadore Lake (Fig. 5.5b, section 43, outlet section). The effects are considerable and the material continue to settle also after the flushing events. This phenomena is probably due to the moderate flow (prescribed by environmental regulation) that partially eroded the deposited material and transport it to the Pieve di Cadore Lake.

Analyzing the variation of the bed material composition, the granulometric size (D_{50} , Fig. 5.5a – 3) decreases as a consequence of the finer material deposited by flushing and increases during the erosion with moderate flow (for the armouring tendency).

In the year 2002, there were flushing operations (May 2002) and a strong flood event (Fig. 5.5b) during the end of the year (Nov/Dec 2002). The flood period caused a strong erosion in the upper part of the Piave (Fig. 5.5b, Sec 2) and consequent coarsening of the bed material. The flood effects also can be noticed at the outlet section (beginning of the Pieve di Cadore Lake, Fig. 5.5b, Sec 43) where sediments transported seem to reach the lake.

5.2 MULTIPLE-YEAR SIMULATIONS

In order to extend the study to the long-term morphodynamic effects of the chronological sequence of strong deposition and subsequent erosion-phases, the last six years (from July 1st 1999 to June 30th 2005) were simulated with the CCHE1D model (Fig. 5.6).

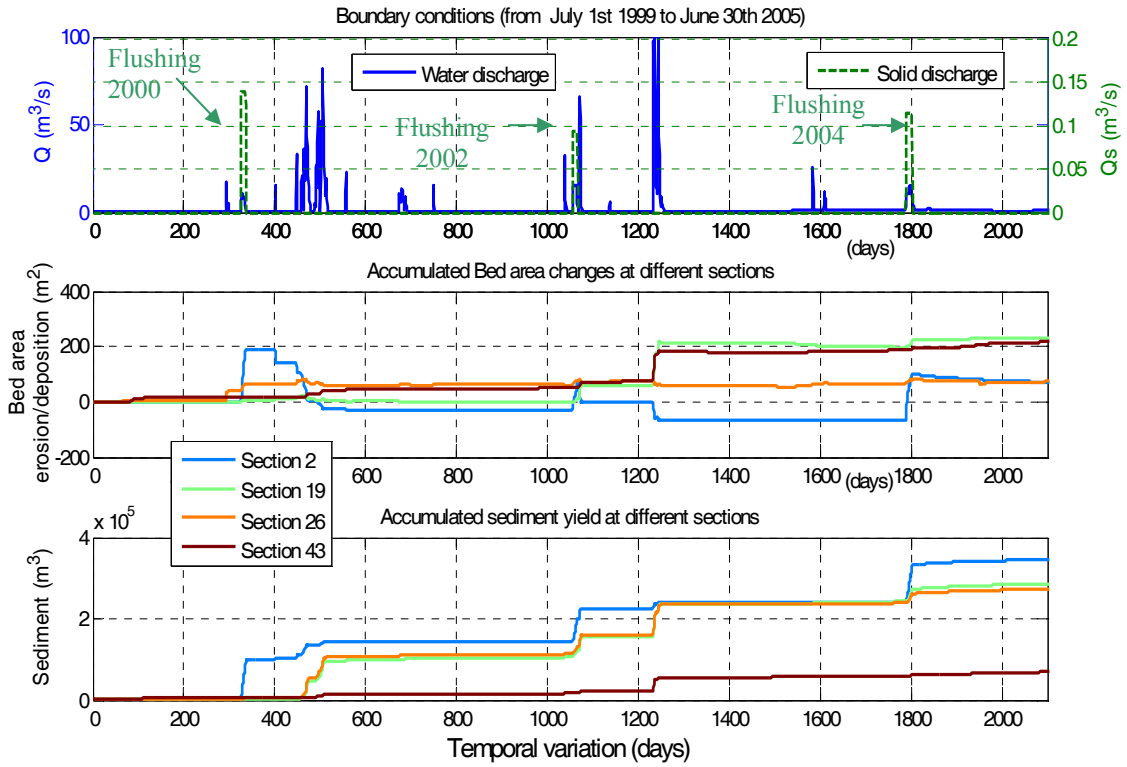

Figure 5.6. Upstream boundary conditions (1) and consequent (2) bed area evolution and (3) accumulated volumetric sediment yield at different sections, simulated from July 1st 1999 to June 30th 2005.

During this period three flushing operations were carried out and several strong flood events were recorded. As shown in Fig. 5.6, the results of this six-years simulation confirmed what

was previously underlined; as a consequence of the flushing operations, considerable amounts of sediment deposit in the first few hundreds meters downstream of the release point (section 2); the moderate and low flow (normally released from the dam) are not sufficient to carry all the sediments downstream.

6. LONG TERM SIMULATIONS

To reproduce the long-term (decades or centuries) tendency of the morphology of the river downstream of the dam it was necessary to apply a simplified model (STERIMOR) that enable us, to reduce the computational time for long-term simulation, and avoid using an unsteady model to run with low efficiency.

The validity and limitations of the local-uniform-flow hypothesis, were in detail discussed in Chapter 4 but, generally, quasi-uniform models can be applied to mountain rivers (as the upper Piave River), characterized by quite high values of Froude number (larger than or close to 1).

Considering, for instance, one-year simulation (2004, with the flushing event of May) and comparing the simulation results between CCHE1D and STERIMOR models (Fig. 5.7), the trend is similar and the difference between the total material discharge in every section was less than 20% (Fig. 5.7, green line). Moreover, this difference, seems to decrease with decreasing time and spatial resolution.

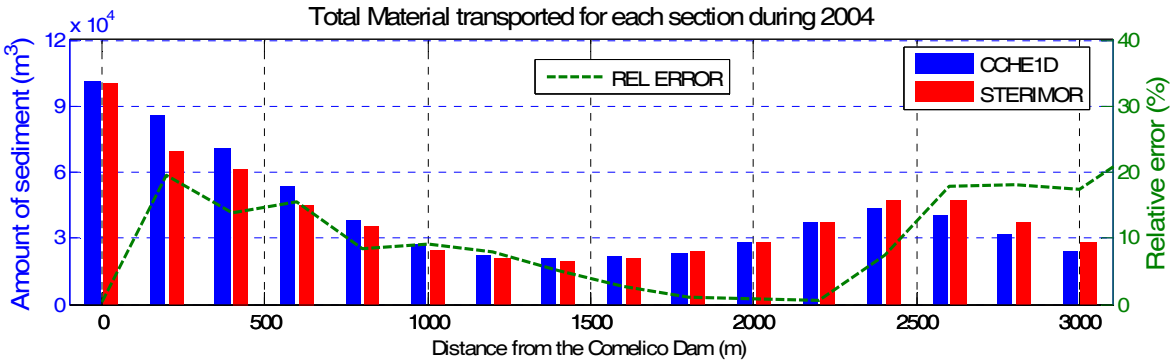

Figure 5.7. Comparison between results of the STERIMOR and CCHE1D models for simulation of the flushing event of 2004 (total amount of sediment discharged for each section and relative error).

By assuming an hypothetical year with two wet periods (a moderate flow and a flood period) and flushing events alternating every two years, twenty years were simulated (Fig. 5.8).

Preliminary results shown the upper part of the river, in spite of the fluctuation due to the flushing and flood events, during the long period seems to preserve (except a slight degradation) the current elevation. Instead, the middle course of the river has been incising by the tributary Ansiei. In fact, the clear water, incoming from the S. Caterina Dam, can be referred to as hungry water and causes a slow but constant degradation of the River bed and coarsening of the bed material.

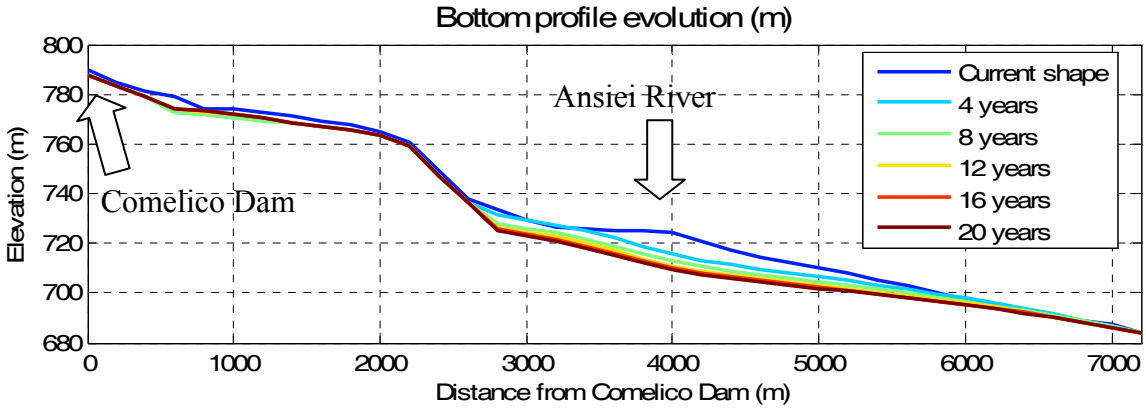

Figure 5.8. Simulation of the bottom profile evolution for long term simulation (20 years).

7. CONCLUSIONS

One-year simulations (2002 and 2004 year) were conducted to calibrate and validate the models with the available data. These simulations were also for investigating the fate and transport of the flushed sediment. After the flushing operations, thalweg elevation increases considerably in the upper part of the river, but the deposited material rapidly lessened with distance from the dam and in proximity of the confluence with the tributary Ansiei, the effects of this deposition are rapidly vanished. Simulations results also show that the flood period caused a strong erosion in the upper part of the river (with coarsening of the bed material) but the effects can also affect the outlet section (Pieve di Cadore Lake).

The six-years simulations (from July 1st 1999 to June 30th 2005) were conducted to study the middle-term consequences of strong deposition and subsequent erosion-phases. Simulations show that after six years only part of the sediments released from the dam reach the outlet zone. This is in part due to the particular dry years (2003 and 2004) but maybe also the simplified hydrology underestimates the total sediment transport along the reach. Analyzing the variation of the bed material composition, during this six years, the granulometry of the bed decreases as a consequence of the finer material deposited by flushing and increases during moderate and flood period (it's more evident in the upper part of the study reach).

Besides this distinction, along the study reach it is possible to distinguish a progressive reduction of bed material size ("downstream fining") in spite of some irregularities probably due to the tributaries' modifications in the sediment texture.

The twenty-years simulations (as hypothetical future scenario) show that while for the long-term period, alternating flushing and flood events doesn't affect the mean bottom slope, the tributary Ansiei, with his "hungry" water, seems to incise the Piave bed elevation. This general trend seem to affect also the lower part of the river, where recent measurements demonstrate a reduction of the bed elevation and coarsening of the bed material.

Is necessary to underline that the simplified hydrology considered and neglecting the finer transport material, limits the study of the Pieve di Cadore Lake's sedimentation. As a matter of fact, the sedimentation rate of the lake reproduced with simulations is about 120,000-150,000 m^3/year, while from the field measurements, results of about 180,000-200,000 m^3/year in the last 6 years (in the past decades it was more than 300,000 m^3/year).

In the future the models so calibrated, will be applied also to the study of the sedimentation process inside the Pieve di Cadore Lake.

Chapter 6

GENERATION AND EVOLUTION OF A TIDAL NETWORK

SUMMARY

The branching channel generation in a short tidal basin has been modeled (Fasolato et al., 2004) by a long term morphological model based on the notion of long term equilibrium concentration, intertidal diffusion coefficient (Di Silvio, Padovan, 1998) and on the simplification of the two-dimensional shallow water equations. The model consents to reproduce, in a schematic lagoon, the network ontogeny and the subsequent morphological bottom evolution, as a consequence of a breaching of the littoral dune line. As the channels evolve, the system tends asymptotically toward a quasi-equilibrium condition apparently characterized by a stable planimetric configuration of the channel network. Numerical channel structures and their watersheds are qualitatively similar to the Venice Lagoon's ones. It has been also shown that the simulated lagoon embayment tends to develop towards an increasingly lower state of energy.

1. INTRODUCTION

Channels, shoals and marshes are important features in estuaries and tidal inlets. The tidal network controls the hydrodynamics and sediment exchange of the entire tidal basin while the intertidal areas are of great ecological importance, being the feeding and breading grounds for a varieties of species.

Human action (hydraulic constructions or dredging activities) and long term natural events (sea level rise or subsidence) can alter and change the natural equilibrium of the morphological and hydraulic tidal environment, therefore it is important to understand and predict the morphodynamic behavior of these complex systems. Recent developments for automatic extraction of the tidal channel network from digital terrain maps (Fagherazzi et al., 1999) have improved the possibilities to study these systems (Rinaldo et al., 1999a, 1999b). Using this technique, it was shown that tidal networks exhibit a great variety of geometrical and topological forms, and that channels in different tidal basins exhibit quite different overall scaling characteristics (Fagherazzi et al., 1999; Rinaldo et al., 1999a).

At the same time, typical timescales for adjustment of the channel/shoal pattern after completion of major works are in the range of decades but in the case of environmental or geological changes can go over centuries (de Vriend, 1996).

Object of the present paper is the morphological evolution of tidal systems (with all their components of channels, shoals and marshes), initiated by a persistent large breach trough the littoral dunes protecting the adjacent coastal plain. The evolution may be affected by possible changes of the forcing action (e.g. sea level rise) as well by anthropogenic action (dredging and construction).

The conventional approach to lagoon morphodynamic is based on the repeated application of “tidal scale” models (Marciano, 2005). It is interesting, however, exploring the possibilities offered by long-term morphological models, defined also as *conceptual models*, that consent to simulate and reproduce the long term (centuries) system’s evolution with a relatively light computational effort.

Conceptual models filter the morphological fluctuations due to short term components and reproduce all the processes (with time-averaged values over a year or a number of years).

They incorporate many physical (and even biological) processes via a number of algebraic or differential equations containing semi-empirical coefficients, which can be calibrated by direct comparison with experiments or with specific short-term models.

The simplified two-dimensional conceptual model presented here, simulates the long term contributions of tidal currents and wind waves to the sediment transport and bottom evolution in a tidal basin. The effect of halophyte vegetation or marshes is also put into account.

2. CONCEPTUAL MODEL

2.1 HYDRODYNAMICS

In the present conceptual model (Di Silvio, Padovan, 1998) sediments are not physically conveyed to an fro by tidal currents but their "net" (long term) transport is given in the form of intertidal dispersion. Tidal currents, however, are utilized to define the intertidal dispersion coefficient D_{ij} (eq. 6.8).

For this purpose the waterflow model may be relatively crude as it should provide only the velocity field in maximum flood conditions. It is based on a simplification of the two-dimensional shallow water equations, similar to the dimensionless Poisson form obtained by Rinaldo et al. (1999b).

In a relatively "short" tidal lagoon (with propagation time between inlet and lagoon basin lower than a quarter of a tidal period T_m), one can assume that at maximum flood conditions friction terms dominate inertial effects in momentum equations and the flood velocity of tidal elevation ($\partial\eta/\partial\tau$) is constant (and equal to the maximum rising velocity in the sea) in each part of the lagoon (Fig. 6.1).

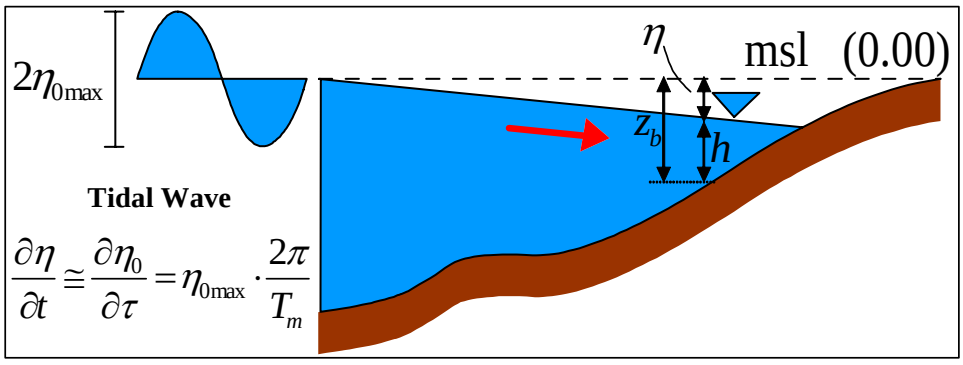

Fig. 6.1 Tidal elevation at maximum flood conditions.

The friction term, under this hypothesis, has been linearised using the energy criterion first introduced by Lorentz (1926), which allows one to write the depth averaged velocity as:

$$U = -\frac{h \cdot C_h^{\,2}}{\sqrt{U^2 + V^2}} \frac{\partial\eta}{\partial x} \qquad (6.1)$$

$$V = -\frac{h \cdot C_h^{\,2}}{\sqrt{U^2 + V^2}} \frac{\partial \eta}{\partial y} \tag{6.2}$$

where (U, V) denote the depth-averaged flow velocities in the (x, y) directions respectively, $h=z_b - \eta$ is the local water level, z_b is the bottom depth, η the local surface elevation and C_h is Chezy's coefficient.

To put into account the resistance due to vertical walls in the inlet and along the barrier island the Chezy's coefficient is considered linearly increasing from 30 to 50 $m^{1/2}/s$ over a distance of 500 m from the wall. In all the other part of the lagoon is considered constant and equal to 50 $m^{1/2}/s$ (D'Alpaos et al., 2007).

The two-dimensional continuity equation can be written as:

$$\frac{\partial \eta}{\partial \tau} + \frac{\partial (hU)}{\partial x} + \frac{\partial (hV)}{\partial y} = 0 \tag{6.3}$$

Local surface elevation $\eta(x,y)$ in the basin lagoon can be defined substituting expressions (6.1) and (6.2) into (6.3) and the governing equations can be simplified with a dimensionless Poisson form. The Poisson form equation can be correctly used for determining the velocity field in the shoals in which the depth is more or less uniform. As the boundary conditions for the shoals it can be assume that the level η_0 in the sea propagates instantaneously and without damping along the deeper channels (Rinaldo et al. 1999b).

This procedure can be applied if the planimetric structure of the channels is known and stable. The different behaviour of channels and shoals, however, cannot be postulated during the generation of the very same channel network.

If one wants to calculate local surface elevation and field velocity all over the lagoon without distinguishing between channels and shoals, it is not possible to neglect bathymetric gradients in direction x and y. So it is necessary to solve the system of equations (6.1), (6.2) and (6.3) obtaining the following expression (6.4) and using "under-relaxation" approximation method for the convergence;

$$\eta_{0\max} \frac{2\pi}{T_m} + \frac{\partial}{\partial x}\left[\left(\frac{-h^2 C_h^{\,2}}{U_0}\right)\frac{\partial \eta}{\partial x}\right] + \frac{\partial}{\partial y}\left[\left(\frac{-h^2 C_h^{\,2}}{U_0}\right)\frac{\partial \eta}{\partial y}\right] = 0 \tag{6.4}$$

where $U_0 = \sqrt{U^2 + V^2}$.

2.2 SEDIMENT TRANSPORT

The two-dimensional intertidal balance equations for the sediments (Chapter 1, eq. 1.18) are written as:

$$\frac{\partial Ch}{\partial t}+\frac{\partial T_x}{\partial x}+\frac{\partial T_y}{\partial y}=E \qquad (6.5)$$

where T_x and T_y are the "net" sediment transport (averaged over a number of tidal oscillations) in the direction x and y respectively; E is the long-term entrainment or deposition rate and the first term $\partial Ch/\partial t$ (the accumulation term) is neglected because much smaller then E (Fig. 6.2).

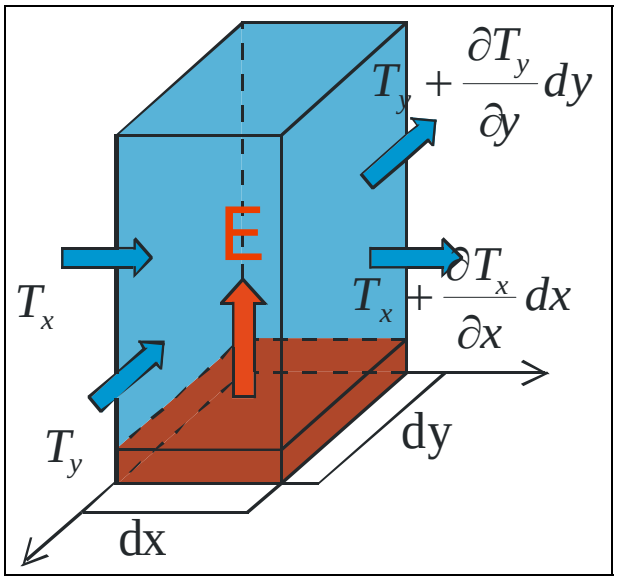

Fig. 6.2 Long-term balance of sediment trough a infinitesimal element of the lagoon.

The following expressions for the "net" sediment transport are obtained by integrating the suspended transport equations, over a long period of time:

$$T_x = h\cdot\left(\cancel{C\cdot U}-D_{xx}\frac{\partial C}{\partial x}-D_{xy}\frac{\partial C}{\partial y}\right) \qquad (6.6)$$

$$T_y = h\cdot\left(\cancel{C\cdot V}-D_{yx}\frac{\partial C}{\partial x}-D_{yy}\frac{\partial C}{\partial y}\right) \qquad (6.7)$$

where h is the averaged water depth, C the intertidal averaged sediment concentration in the water column, U and V denote the depth-averaged residual (intertidal) flow velocities in the x and y directions, D_{ij} the intertidal dispersion tensor.

In the chosen lagoon basin, the residual terms of advection $C\cdot V$ and $C\cdot U$ can be neglected in comparison with the intertidal dispersion transport.

2.3 INTERTIDAL DISPERSION

The intertidal dispersion is the dominant mechanism of transport in a long time period. It determines the spatially distribution of lagoon's suspended sediments and it is controlled by the gradient of the long term averaged sediment concentration.

For a tidal lagoon formed by a network of deep channels cut in broad and shallow areas, the dominant intertidal mixing is due to the alternate "trapping and pumping" phenomena between channel and shoals during the entire tidal cycle (Schijf and Schönfeld, 1953).

To understand this mechanism, let suppose that any tracer (not necessarily a sediment) is continuously discharged in the lagoon and from there to the sea.

In tidal flood conditions clear water enters from the sea to the lagoon basin transported by the channel. The tracer concentration in the channel is smaller than in the shoals, so the clear water is transported to the shoals from the channel. In ebb tide conditions the concentration in the shoals is higher and the tracer is transported to the channel and eventually to the sea (Dal Monte, 2004).

The same mechanism applies to suspended sediment if the concentration in the sea is lower than within the lagoon (degrading lagoon). The sign of transport is inverted if the concentration in the sea is higher than within the lagoon (silting lagoon).

The tensor of intertidal dispersion D_{ij} expresses the physics of this exchange through a square proportionality with the field velocity (Dronkers, 1978):

$$\overline{\overline{D}} = \begin{pmatrix} D_{xx} & D_{xy} \\ D_{yx} & D_{yy} \end{pmatrix} = k_e \begin{pmatrix} U^2 & UV \\ VU & V^2 \end{pmatrix} \tag{6.8}$$

The spatial distribution of the dispersion tensor $\overline{\overline{D}}$ depends on the velocity field, in its turn depending on the planimetric structure of the channel network. It is assumed in this model that the velocity field directions remain basically constant during the tidal cycle. As a conseguence the distribution of $\overline{\overline{D}}$ be provided by the velocity field in maximum flood conditions (par. 2.1).

The value of the constant k_e, also adsorbs the frequency distribution of the intensity of tidal currents.

An attempt of the theoretical evaluation in the case of one directional channel has been made (Dal Monte e Di Silvio, 2003). In this work the value of k_e is considered constant ($2.55*10^3$ sec^{-1}) and it corresponds to the maximal value of $D_{xx} \sim 500-1000$ m^2/sec in the inlet area. Similar values have been experimentally found in the lagoon of Venice (Imberger, 1992).

2.4 EQUILIBRIUM CONCENTRATION

The erosion rate E (eq. 6.5) is expressed by the following first-order reaction equation:

$$E = w \cdot \left(C_{eq} - C\right) \tag{6.9}$$

where C is the time-averaged sediment concentration and C_{eq} is the equilibrium concentration of the water column (Chapter 1, par. 4.3). The parameter w is proportional to the fall velocity w_s of the equivalent particle size of the bottom material. The ratio (w/w_s) depends in principle on the vertical profile of the concentration. In the present work w is considered constant an equal to 0.003 m/sec.

The equilibrium concentration in a certain place is the average sediment concentration over the water column which would yield neither erosion or deposition (equilibrium condition). It depends on the grain size diameter of the particles, on the local hydrodynamics (waves and currents) and on the local depth and can assume an expression of the following type (Chapter 1, par. 4.3):

$$C_{eq} = \frac{f_{sea}}{h^m} + a_{tid}\,\frac{q^{n-1}(x,y)}{h^n} + \frac{f_{wind}(x,y)}{h^p} \tag{6.10}$$

where the three terms consider the entrainment effects on the sediments of sea waves, tidal currents and local wind respectively. Note that all the three terms decrease when the local depth increases. Following the transport monomial formula (Engelund-Hansen), the exponents m, n and p are considered, respectively, equal to 3, 5 and 1.

The function f_{sea} is considered increasing parabolically along the distance from the shore, from 0 (in the middle of inlet) to $2.5*10^{-2}$ m^3 and equal to zero in the lagoon basin.

The value of a_{tid}, which depends on the grain size distribution, is also assumed constant ($2.7*10^{-3}$ sec^4/m^3) inside and outside the lagoon basin.

The quantity $q = h\sqrt{U^2 + V^2}$ is provided by the hydrodynamic sub-model (par. 2.1).

The local wind wave function f_{wind} is a function of the local fetch and wind intensity and it may appreciably decrease in presence of sea weeds. In the present simulation it is assumed f_{wind} =$2.5*10^{-5}$ m.

The averaged sediment concentration of the water column C, can be so calculated solving the system (eqs. 6.5-9) expressed in the following symbolic equation (6.11):

$$\nabla \cdot \left(-h \cdot \overline{\overline{D}} \cdot \nabla C\right) + w \cdot C = w \cdot C_{eq} \tag{6.11}$$

3. BOTTOM EVOLUTION

3.1 MARSHES GENERATION

The long-term evolution of the bottom depth, h, is given by adding up the bottom erosion rate E, the eustatism α_e (rise of mean sea level) and the subsidence rate α_s (settlement of ground surface), (eq. 6.12).

$$\frac{\partial h}{\partial t} = E + \alpha_e + \alpha_s \qquad (6.12)$$

A better insight into the physical mechanisms behind this aspect of lagoon morphodynamic is worth pursuing.

Sediment deposition occurs in the shoals when the local concentration C is larger than C_{eq} (eq. 6.9); as the depth progressively decreases, the value C_{eq} increases (eq. 6.10), the settling rate is increasingly compensated by the pick-up rate and the bottom rise slows down. However if sediment deposition proceeds, the bottom will emerge more and more frequently form the water. As soon as the bottom is not submerged for a sufficiently long period of time during the tidal cycle, vegetation takes place, the bottom becomes protected and the pick-up rate vanishes. At this point, all the sediments reaching the marshes are captured and the bottom rapidly rises. Rise, however, is very soon limited by the rapid reduction of water flow when the bottom is above the mean sea level. Above a certain elevation, in fact, only a negligible amount of sediment reaches the marshes to compensate eustatism and subsidence. In the model, the two phenomena are simulated, respectively, considering C_{eq}=0 when $z_b<z_{bv}$ (bottom above the limit of vegetation) and D_{ij} =0 m^2/sec when $z_b<z_{bt}$ (bottom above the limit of the highest tides).

The value of the z_{bv} (limit of vegetation) depends on the local species of halophyte vegetation. In the present simulations it has been assumed z_{bv}=0 m (mean sea level).

The value of z_{bt} (limit of high tides) depends on the significant high waters. In the present simulations it has been assumed z_{bt}=-0.35 m.

3.2 MARSHES DEMOLITION

According to the mechanism described in 3.1, the equilibrium elevation of marshes is to be found between z_{bt} and z_{bv} depending upon the values of α_e and α_s. As matter of fact, the bottom distribution of the marshes in the lagoon of Venice is comprised in quite narrow range. In any case, if the elevation of the marshes is practically constant, their surface may be strongly variable, depending upon the sediment balance in the shoals.

Indeed the collapse of the marsh contour is determined by an excessive depth of the adjacent shoal. The maximum permissible step between marshes and shoals depends basically on the soil characteristics (e.g 0.25 m). This mechanism activated whenever the shoals are subjected to erosion, has not been incorporated in the present simulations.

3.3 EFFECTIVE WATER DEPTH

The average water depth in a certain location of the lagoon is not always given by the value of h, but depends on the local bottom elevation. In fact, if the annual maximum tidal range is a_m, it follows that, during the year, the bottom is permanently submerged only where $z_b > a_m/2$; by contrast the bottom is never submerged where $z_b < -a_m/2$, while we have an intermediate submergence for values in between. if we assume that the frequency distribution of the tidal range is sensibly linear, we may obtain the value of the effective water depth h^* in each location of the lagoon, by multiplying the local value of h by the submergence period of the tide. One find:

$$h^* = h \qquad (\text{if } z_b > a_m/2) \qquad (6.13)$$

$$h^* = \eta_0 \cdot \left(1 - \frac{1}{2} \cdot \left(1 - \frac{h}{\eta_0}\right)\right)^2 \qquad (\text{if } -a_m/2 < z_b < a_m/2) \qquad (6.14)$$

$$h^* = 0 \qquad (\text{if } z_b < -a_m/2) \qquad (6.15)$$

The effective value of h^* should be used instead of h, in every equation of the model.

4. NUMERICAL MODEL

4.1 MODEL DESCRIPTION

The numerical two-dimensional model consists of a number of modules which describe hydrodynamics, sediment transport and bottom evolution respectively. The dynamic interaction of these processes with the bed-topography changes is taken into account in the time-loop.

The following flow-chart describes every step of the simulation (Fig. 6.3). The simulation starts with initial conditions and computes lagoon hydrodynamics and local surface elevation at maximum flood conditions. In a second step, the model calculates the local intertidal dispersion coefficients and equilibrium concentration as a function of hydrodynamic and depth conditions which control sediment transport and the evolution of channels, shoals and marshes. As third step the model computes the local sediment concentration and new

bathymetric depth. An under relaxation procedure is employed for solving the non linear hydrodynamic equations.

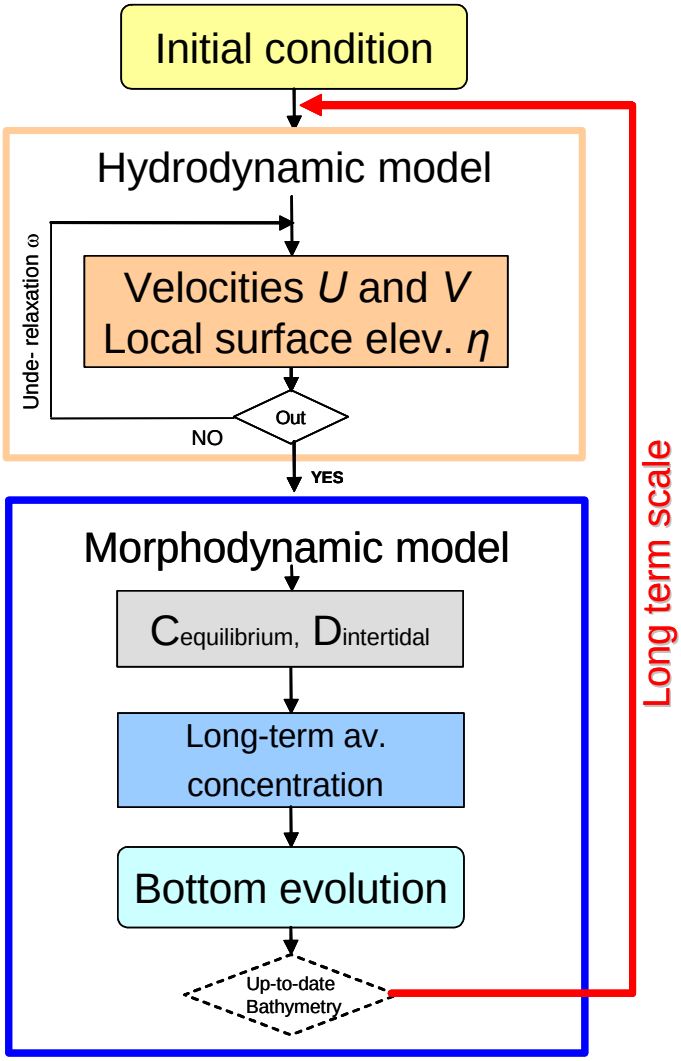

Fig. 6.3 Model flow chart.

4.2 MODEL SETUP

The generation process of the lagoon has been assumed to be initiated by an occasional large breach of the littoral dunes, which will be transformed in the lagoon inlet. Trough the breach water will invade a portion of the coastal alluvial plain behind the dunes which will constitute lagoonal basin.

The model is applied to a schematic representation of the sea (longitudinal direction between 0 km and 3 km, area 42 km^2); breach and inlet area (longitudinal direction between 3 km and 4 km, area 1 km^2); and lagoon basin (longitudinal direction between 4 km and 11 km, area 98

km^2). The schematization makes it possible to investigate the influence of the sea waves on the development of the channel pattern within the lagoon.

As initial configuration, the bottom bathymetry in the sea is considered linearly increasing along the longitudinal direction seaward (from –8 m to -1 m near to the inlet) and constant (–1 m) in the inlet and in the lagoon.

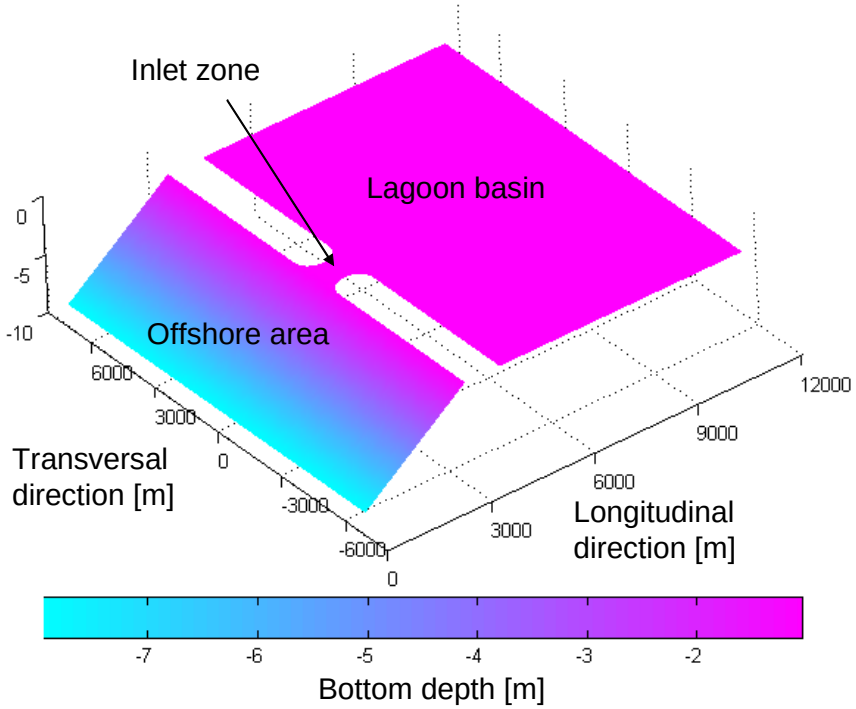

Fig. 6.4 Bottom bathymetry of the flat lagoon conformation (x longitudinal direction, y transversal direction, z bottom bathymetry)

Different triangular model grids are used in the numerical computation but the most of simulations are implemented with a mesh grid of 11’984 triangles of about 200 m sides.

The vertical boundary enclosing the lagoon basin are fixed and impermeable. At the seaward boundary, constant values of tidal range and concentration (equal to the local equilibrium concentration) are imposed.

5. MODEL APPLICATION

The model described in the sections above is still to be subject to appropriate operations of validation, calibration and verification. These operations will be based first of all, to systematic sensitivity analysis with respect to the main parameters of the model: the meteo-marine coefficients f_{sea}, f_{wind} and a_m (eq. 6.10) which control the equilibrium concentration; the coefficient k_e (eq. 6.8) quantifying the tensor of the intertidal dispersion; the coefficient w (eq. 6.9) defining the intensity of sediment exchange between water column and bottom.

The model results, obtained with different parameters, will subsequently be compared with known situations of quasi-equilibrium conditions or morphological evolution at historical scale.

This will be especially done with reference to the lagoon of Venice, but also to other similar environments ("short" tidal lagoons with different tidal range, sea force and local wind), e.g. the Wadden Sea in the Netherlands. It seems likely, in fact, that while the meteo-marine parameters control the quasi-equilibrium morphological configuration of the lagoon, the dispersion tensor and the vertical exchange parameter control the response rapidity of the morphology to natural and anthropogenic changes.

5.1 FIRST RESULTS

The model has been applied to simulate the generation of a tidal basin as the consequence of the sea ingression in a rectangular basin of given surface (7x14 km^2) trough a breach of a given width (1000 m). The maximum annual tidal range has been assumed $a_m/2 = \pm$ 0.35 m and the initial depth in the basin was assumed constant (h=1 m). The provisional values of the model parameters have been assumed as mentioned in the relevant sections. The model results indicate two distinct phases of morphological evolution. During the first phase (lasting a few weeks) the proper ontogenetic process of the channel network occurs: following the breach the depth in the inlet almost immediately increases from 1 m to about 8 m while the scour rapidly propagates towards the sea and (even more) towards the lagoon (Fig. 6.5).

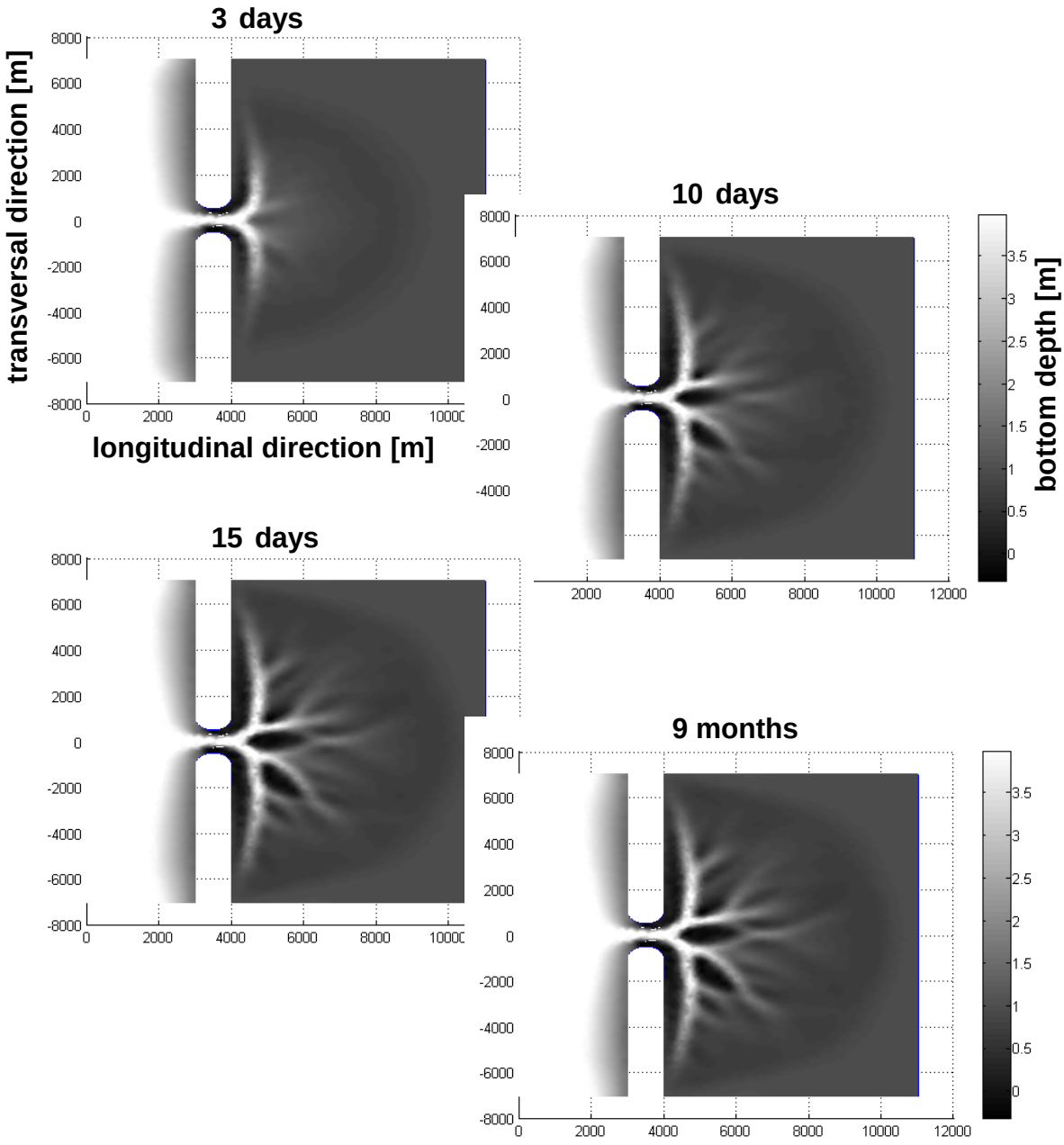

Fig. 6.5 First phase (few weeks) of the ontogenetic process of the channel network.

After a few days the external configuration of the "fuosa" (as it was called in Venice the external delta, now obliterated by the jetties) is practically completed. Within the lagoon, by contrast the tidal network continues to be formed by retrograde erosion of the channels ad simultaneous silting of the adjacent shoals. After about 20 days, the planimetric configuration of the tidal network has reached a quasi-equilibrium configuration, but the bathymetric evolution is still active, with a very slow progressive deepening of the channels and a corresponding rising of the shoals. During this phase some marshes are also formed near the

source of sediment (the inlet), where the bottom elevation reaches the mean sea level and vegetation thrives (Fig.6.6).

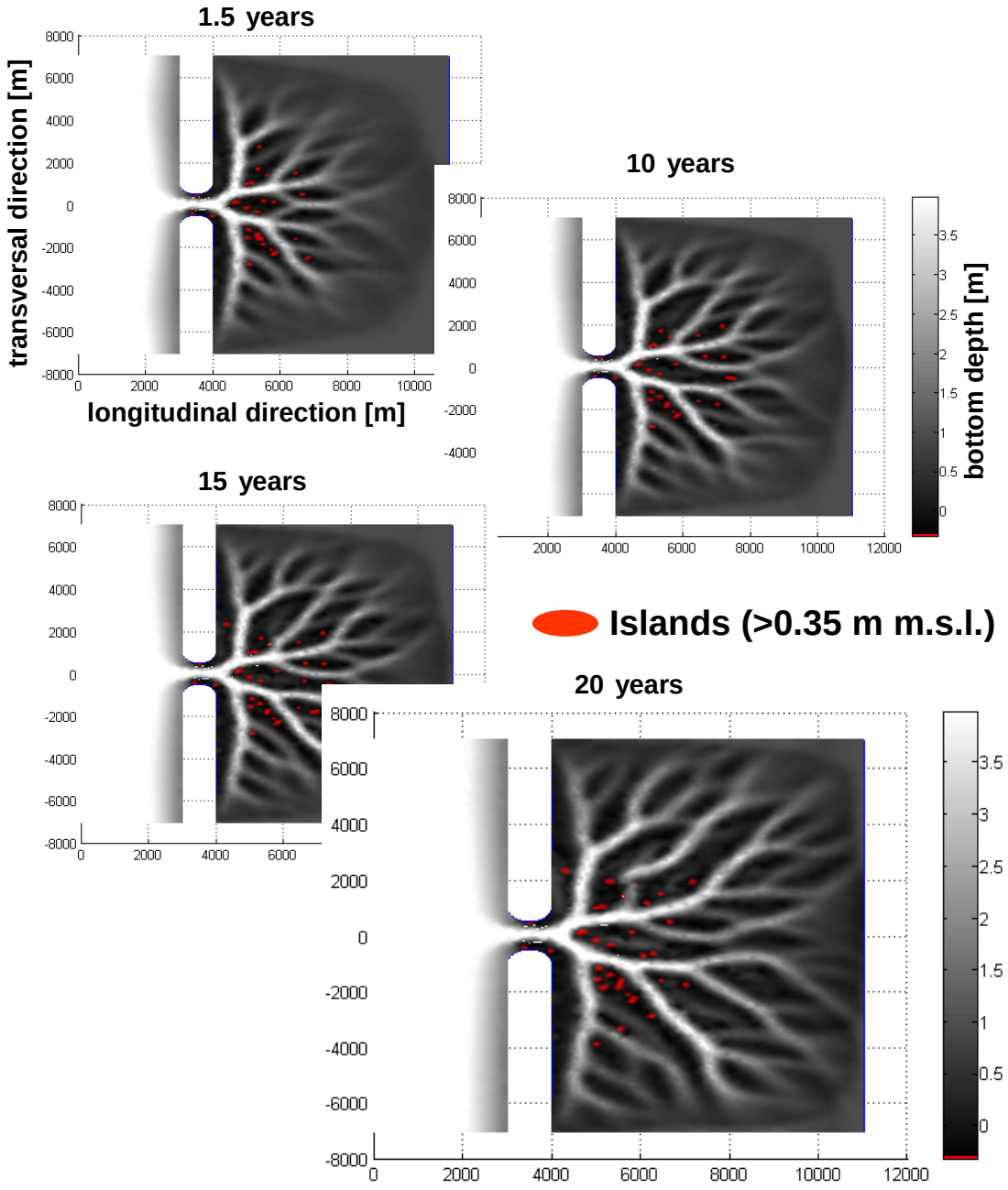

Fig. 6.6 Second phase (several years) of morphological evolution and consequently marshes and islands formation.

The second phase or morphological evolution is much slower than the first one and may last several years. Only bathymetry is involved in the process, while all the quantities basically related to the planimetric configuration (flow field pattern) tend to remain constant. Therefore

the values of the parameters controlled by the flow field pattern (spatial distribution of $q(x,y) = h\sqrt{U^2 + V^2}$ and of the dispersion tensor $\overline{\overline{D}}$, eq. 6.8) do not change in time (Fig.6.7).

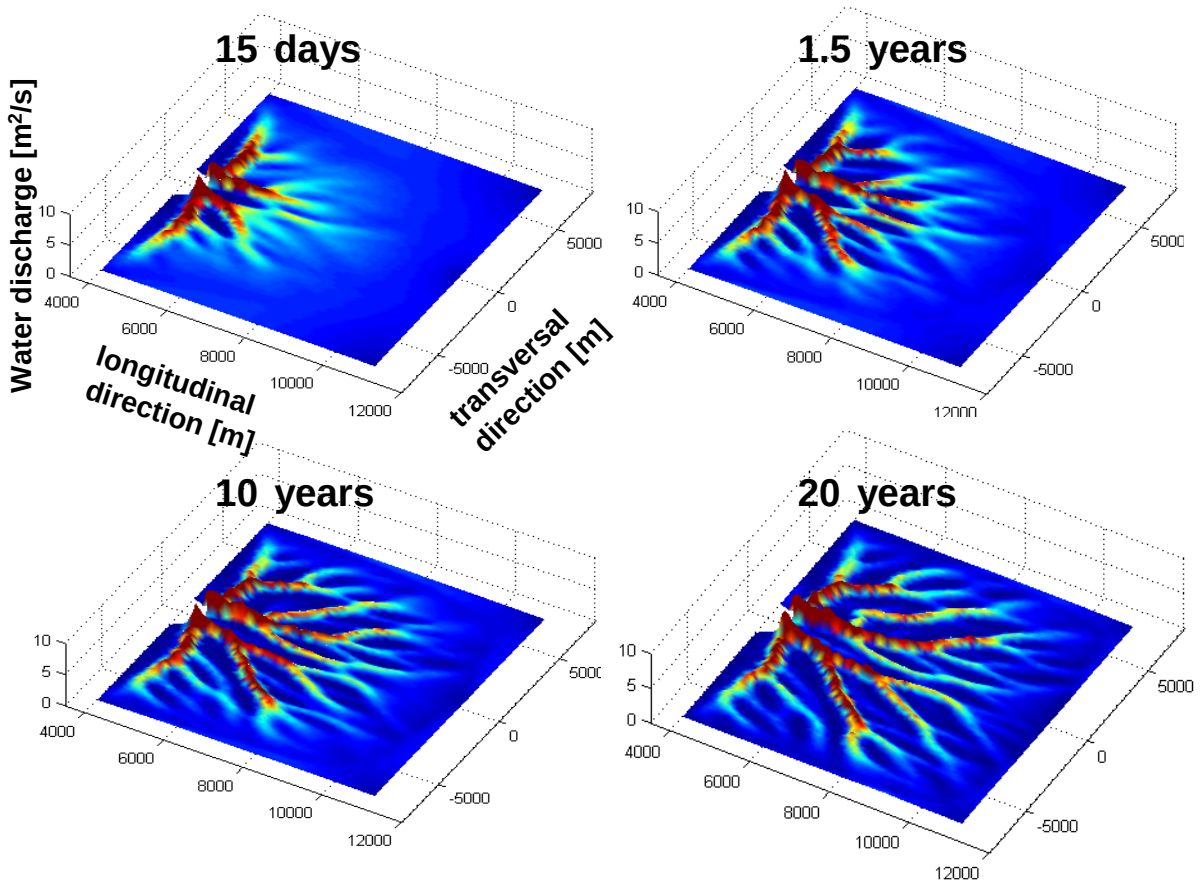

Fig. 6.7 Evolution of the spatial distribution of *q(x,y)* in different time scale (as it is possible to observe, there is a very little changing of *q(x,y)* after 10 years).

This result is extremely important from the practical point of view, as it allows to apply the morphological model to extremely long period of time, for long-term sediment balance, without repeating the computation of the flow field, definitely the model component which is the most time consuming. On the other hand, the immediate planimetric effects produced by new constructions can be simulated by relatively short period of time, even tough the corresponding CPU may be relevant.

5.2 ENERGY EVOLUTION

It may be interesting to observe the time evolution of the total kinetic energy of the lagoon, provided by the following integral:

$$En_{kinetic} = \frac{1}{2} mW^2 = \frac{1}{2} \int_S \rho h^* \left(U^2 + V^2\right) dS \qquad (6.16)$$

where S is the total surface of the lagoon and h* is the “effective” depth.

As it appears from Fig. 6.8 the total energy of the lagoon tends to decrease with time, towards an (equilibrium) value apparently depending on the size of the lagoon and on is meteo-marine parameters.

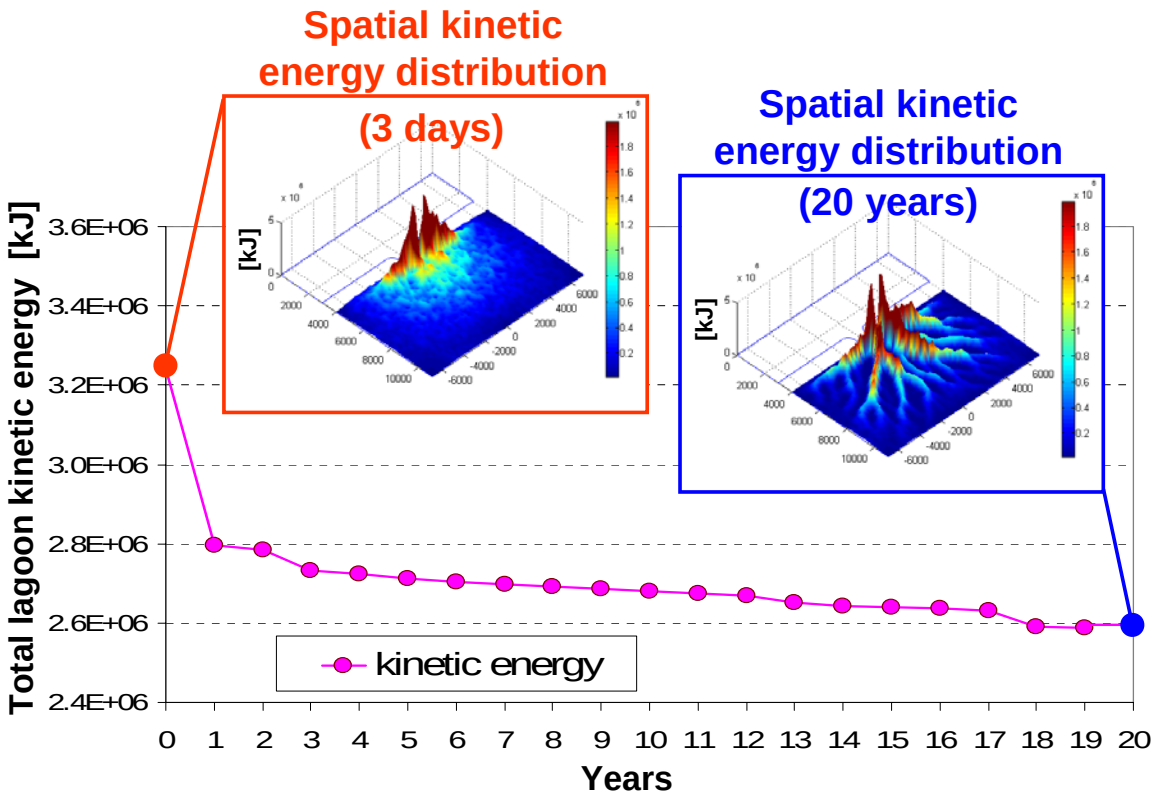

Fig. 6.8 Total lagoon kinetic energy evolution (and its initial and final spatial distribution) during simulation.

6. CONCLUSION

The 2-D “intertidal” morphodynamic model described here is apparently able to reproduce both the “planimetric phase” of the lagoon ontogenesis (with the generation of the planimetric pattern of the tidal network) and the subsequent “bathymetric phase” of the depth adjustment of the channels, shoals and marshes in the lagoon.

Although much more numerical analysis are required for validating, calibrating and verifying the model, the first results indicate that the time scales of the two phases are very different.

During the first phase (lasting a few weeks) the proper ontogenetic process of the channel network occurs: following the breach, the depth in the inlet almost immediately increases while the scour rapidly propagates towards the sea and the lagoon. In this phase the lagoon system seems strongly variable (morphological variations occur rapidly, in few weeks) and kinetic energy of the system is particularly high.

In the second phase, after about 1 month, the planimetric configuration of the tidal network has reached a quasi-equilibrium configuration, but the bathymetric evolution is still active, with a very slow progressive deepening of the channels and a corresponding rising of the shoals and marshes' formation (vegetation thrives). Also the energy system is lower than the beginning and continue, slowly, to decrease during the years.

Discussion and further developments

The simplified morphodynamic models discussed in the present dissertation are all quite promising as far as their application is concerned.

The first one (namely, the one-dimensional model for rivers under the hypothesis of steady-uniform flow) is extremely robust and releasable in a variety of conditions. Although initially this model (STERIMOR) was employed only for mountain rivers (i.e. for quite high values of Froude numbers) (Chapter 5), it was made clear in this thesis that it may be applied also to lowland rivers (quite low values of Froude numbers), provided that appropriate sizes of the morphological box were assumed, depending on the local slope (Chapter 4). This means that no detailed information may be obtained over distances smaller than the box-size (up to tens of kilometers for large plain rivers), but only averaged ones.

On the other hand, averaged information is quite sufficient for problems at the watershed scale and while providing the necessary boundary conditions for detailed investigations (e.g. with a 2D model) (Chapter 1). Simplified models based on the uniform-flow hypothesis, moreover, are the only ones which permit to cope with large unsurveyed watersheds (Ronco et al., 2008a) especially in developing countries.

The second one-dimensional model (namely its more complete form based on the steady waterflow hypothesis, but properly simplified by linearizing the equations) can be analytically solved. The analytical solution permits an extremely useful insight on the relative importance of the boundary conditions and on the river's reaction to the external perturbations (Chapter 3).

Predicting the effects of the external perturbations on the river equilibrium conditions is extremely important from the practical point of view. Evaluating the propagation and attenuation of these perturbations gives us an idea about the possible errors made by neglecting them (as it is usually the case: for example when assuming a unique relationship between water flow and solid discharge).

Further analysis might be conducted in the future by utilizing for these discussions more appropriate physical parameters.

It seems in fact that the new, combiner parameter $\bar{\varepsilon} = \frac{E \cdot Fr^2 \psi \overline{U}}{8\pi\Delta^2 \overline{H}} T_{wave}$ *(Chapter 3) (including the Froude number and the perturbation's wave period) could be more significant than the single parameters utilized up to now.*

The simplified model analyzed in this work for simulating the morphological changes of tidal lagoons (Chapter 6) is also very promising. This morphodynamic models is two dimensional and is based on the concepts of "tide-averaged and storm-averaged concentration" and "intertidal dispersion" of sediments.

Consequently the model does not require a time-consuming simulation of each individual tidal cycle and each individual mind storm, but only of morphological changes on longer time steps.

Although very much simplified from the hydrodynamic point of view, the model incorporates a number of fundamental, complex processes for the lagoonal environments. For example the building and the demolition of the tidal flat, taking into account the role played by the alophile vegetation.

The simplified morphodynamic model of the lagoon indicates that there are two distinct morphological time scales: a shorter one (from weeks to months) for the planimetric initiation and development of the tidal channel network (ontogenesis) and a longer one (from decades to centuries) for the bathymetric evolution of channel cross-sections, shoals and tidal flats.

The model has been applied up to now to a schematized geometrical situation and should be soon applied to more realistic conditions (lagoon of Venice). Moreover besides the intertidal dispersive transport of sediments, a certain amount of convective transport should also be incorporated in the model for simulating one-directional fluvial and littoral currents, as well as the (one-directional) effect of tidal asymmetry.

Finally, all simplified the models analyzed in this dissertation require further verifications against experimental or field measurements and by comparison with non-simplified models.

NOTATION – Chapter 3

Symbol	Definition	Units
A	Wetted cross section	m^2
B	Channel width	m
c_{f_n}	Dimensionles perturbations' celerities (n=1,2,3)	-
C_h	Chézy coefficient	$m^{1/2}/s$
d_k	Representative diameter of k-th cl.	m
$\overline{d}$	Mean diameter.	m
E	Resistance coefficient	-
Fr	Froude number	-
g	Gravity acceleration	m/s^2
H	Average water depth	m
J	Energy slope	-
L_{f_n}	Dimensionles perturbations' attenuation length (n=1,2,3)	-
P_k	Solid discharge of k-th class	m^3/s
Q	Water discharge	m^3/s
s	Hiding-exposure exponent	
t^*	Dimensional time coordinate	s
T_{wave}	Perturbation period	s
U	Flow velocity	m^2/s
x^*	Dimensional space coordinate	m
$\overline{X_n}$	Solution of the characteristic equation (n=1,2,3)	-
Z	Bottom elevation	m
α_c	Transport formula coefficient	-
β_k	Percentage of k-th class	-
β_k^s	Percentage below active-lay	-
δ	Active-layer thickness	m
Δ	Relative mixing layer	-
ζ_k	Hiding-exposure coefficient	-
ψ	Sediment concentration	-

Symbol	Definition or expression
$\overline{A_1}$, $\overline{B_1}$, $\overline{C_1}$	Coefficients for the expression of $\overline{p_{c_1}}$
$c^*_{f_n}$	$= c_{f_n} \cdot \underline{U}$
$\overline{D_1}$, $\overline{E_1}$, $\overline{F_1}$	Coefficients for the expression of $\overline{\beta^0_{1c_1}}$
d	$= d_1 / d_2$
d^*	$= d^{1-s}$
$\overline{h_{c_n}}$	Boundary amplitudes of the water depth waves (n=1,2,3)
$\overline{h_c}$	$= \sum_{n=1}^{3} \overline{h_{c_n}}$
$\overline{k_n}$	$= \left(\overline{X_n}\Delta\omega\right) / \psi$
$L^*_{f_n}$	$= L_{f_n} \cdot \underline{H}$
$\overline{p_{c_n}}$	Boundary amplitudes of the solid transport waves (n=1,2,3)
$\overline{p_c}$	$= \sum_{n=1}^{3} \overline{p_{c_n}}$
S^*	$= 1 - \left(\eta^*\right)^2$
t	$= t^* \underline{U} / \underline{H}$
x	$= x^* / \underline{H}$
$\overline{z_{c_n}}$	Boundary amplitudes of the bottom elevation waves (n=1,2,3)
$\overline{z_c}$	$= \sum_{n=1}^{3} \overline{z_{c_n}}$
α	$= 1 - Fr^2$
$\overline{\alpha}$	$= \alpha / (6\Delta)$
$\overline{\beta^0_{1c_n}}$	Boundary amplitudes of the bottom composition waves (n=1,2,3)
$\overline{\beta^0_{1c}}$	$= \sum_{n=1}^{3} \overline{\beta^0_{1c_n}}$
γ	$= 1 + s\eta\eta^*$
ε	$= (3/2) E \cdot Fr^2$
$\overline{\varepsilon}$	$= \varepsilon\psi / \left(6\Delta^2\omega\right)$
η	$= (1-d) / (1+d)$
η^*	$= \left(1-d^*\right) / \left(1+d^*\right)$
ω	$= 2\pi / T_{wave} \cdot \underline{H} / \underline{U}$

NOTATION – Chapter 4

Symbol	Definition	Expression	Units
$\boldsymbol{Q}$	Water discharge		m^3/s
$\boldsymbol{A}$	Wetted cross section		m^2
$\boldsymbol{B}$	Channel width		m
$\boldsymbol{x^*}$	Dimensional space coordinate		m
$\boldsymbol{t^*}$	Dimensional time coordinate		s
$\boldsymbol{H}$	Local water depth		m
$\boldsymbol{Z}$	Bottom elevation		m
$\boldsymbol{g}$	Gravity acceleration		m/s^2
$\boldsymbol{U}$	Flow velocity	$= \underline{Q}/A$	m/s
$\boldsymbol{j}$	Energy slope		-
$\boldsymbol{B}$	Channel width		m
$\boldsymbol{P_k}$	Solid discharge of k-th class		m^3/s
$\boldsymbol{\delta}$	Active-layer thickness		m
$\boldsymbol{\beta_k}$	Percentage of k-th class		-
$\boldsymbol{\beta_k^s}$	Percentage below active-lay		-
$\boldsymbol{C_h}$	Chézy coefficient		$m^{1/2}/s$
$\boldsymbol{d_k}$	Representative diameter of k-th cl.		m
$\boldsymbol{d}$	Ratio between diameters	$=d_1/d_2$	
$\boldsymbol{\alpha_c}$	Transport formula coefficient		-
$\boldsymbol{\zeta_k}$	Hiding-exposure coefficient		-
$\boldsymbol{\delta}$	Active-layer thickness		m
$\boldsymbol{\underline{H}}$	Reference water depth		m
$\boldsymbol{\underline{B}}$	Reference width length		m
$\boldsymbol{\underline{Z}}$	Reference bottom elevation		m
$\boldsymbol{\underline{P}}$	Reference sediment transport		m^3/s
$\boldsymbol{i_f}$	Bottom slope	$=-\partial \underline{Z}/\partial x^*$	-
$\boldsymbol{i_w}$	Water slope	$=-\partial \underline{y}/\partial x^*$	-
$\boldsymbol{\underline{\beta_k}}$	Averaged percentage of k-th class		-
x	Non-dimensional spatial coordinate	=x*/H	-
$\boldsymbol{t}$	Non-dimensional temporal coordinate	$=t^*\underline{U}/\underline{H}$	-
$\boldsymbol{\alpha}$		$=1-F_r^2$	-
$\boldsymbol{F_r^2}$	Froude number	$=\underline{V}^2/g\underline{H}$	-
$\boldsymbol{E}$	Resistance coefficient	$=2g/\chi^2$	-
$\boldsymbol{\varepsilon}$		$=3/2E\ F_r^2$	-
$\boldsymbol{\eta}$		$=(1-d)/(1+d)$	-
$\boldsymbol{d^*}$		$=d^{1-s}$	-
$\boldsymbol{\eta^*}$		$=(1-d^*)/(1+d^*)$	
$\boldsymbol{S^*}$		$=1-\eta^{*2}$	-
$\boldsymbol{\psi}$	Sediment concentration	$=\underline{P}/\underline{Q}$	-
$\boldsymbol{\Delta}$	Relative mixing layer	$=\delta/\underline{H}$	-
$\boldsymbol{b_c}$	Amplitude of river width perturbation		-
$\boldsymbol{\Omega}$	Frequency of spatial perturbation	$=H/\lambda$	-
$\boldsymbol{\lambda}$	Wavelength of the channel width		m
$\boldsymbol{L}$	Morphological box		m
$\boldsymbol{\omega}$	Angular frequency of temporal perturbation	$=2\pi T_{wave}\cdot\underline{H}/\underline{U}$	
$\boldsymbol{T_{wave}}$	Perturbation wave's period		s
$\boldsymbol{\gamma}$	Irregularity coefficient		s
$\boldsymbol{Q_0}$	Annual flood peak		m^3/s
$\boldsymbol{V_0}$	Annual runoff volume		m^3
$\boldsymbol{V_s}$	Annual sediment runoff		m^3/year
$\boldsymbol{q_c}$	Amplitude of discharge perturbation		-
$\hat{t}$	Non-dimensional (non-equilibrium) time		-

REFERENCES

Abad J. D., Buscaglia G. C., Garcia M. H. (2007).2D stream hydrodynamic, sediment transport and bed morphology model for engineering applications, Hydrological Processes.

Ackers, P. and White, W. R., (1973). Sediment transport: new approach and analysis, Journal of Hydraulic Engineering, 99(11), 2041-2060.

Agarwal K.K. and Idiculla K.C., (2002). Reservoir sedimentation surveys using Global Positioning System, Central Water Commission Ministry of Water Resources New Delhi.

Armanini, A. and Di Silvio, G. (1988). A one-dimensional model for the transport of a sediment mixture in non equilibrium flow conditions. Journal of Hydraulic Res., Vol.26, no.3.

Armanini, A., Fraccarollo, L., Guarino, L., Martino, R., Bin, Y., (2000). Experimentals analysis of the general features of uniform debris-flow over a loose bed. In: Wieczorek, G.F.,Naeser, D., 2000 Eds, Debris-Flow Hazards Mitigation: Mechanics, Prediction and Assessment. A.A. Balkema, Rotterdam.

Basile, P., Peviani, M.A. (1996). Morphodynamic mathematical model for non-uniform grain-size sediment s: an application to the exceptional flood event of 1987 in the Mallero river (Italy). Internal report of FRIMAR Project.

Beasley D B; Huggins L F; Monke E J (1980). ANSWERS: a model for watershed planning. Transaction of the ASAE, 23(4), 938–944

Bonfigli, G., Peviani, M.A., Cadore, A. (1994). Sediment transport studies during artificial floods in the frodolfo river: Objective and Methodologies. Published at the symposium man and mountain ’94, Ponte di Legno., Italy.

Bretschneider, C.L., (1969). Wave forecasting, In: Myers, J.J. (Ed.), Handbook of Ocean and Underwater Engineering. McGraw-Hill Book, New York. Chap. 11.

Brown, C.B. (1950) Sediment transportation (Chapter 12) . In: H. Rouse, Editor, Engineering Hydraulics, John Wiley and Sons, New York (1950), pp. 796–799.

Brunner G.W. and Gibson S. (2005) Sediment Transport Modeling in HEC RAS World Water Congress 2005 173, 442

Cao Z., Rodney D., Shinji E. (2002). “Coupled and decoupled numerical modeling of flow and morphological evolution in alluvial rivers”. Journal of Hydraulic Engineering, Vol. 128., No. 3.

Cea L. et al., (2007) Depth Averaged Modelling of Turbulent Shallow Water Flow with Wet-Dry Fronts Archives of Computational Methods in Engineering 14, 303

Correia, L. R. P., Krishnappan, B. G., and Graf, W. H. (1992). Fully coupled unsteady mobile boundary flow model. J. Hydraul. Engng. Vol. 118., No. 3, 476-494.

Coulthard T.J., Hicks D.M., Van De Wiel M.J. (2007) Cellular modelling of river catchments and reaches: Advantages, limitations and prospects. Geomorphology 90 (2007) 192–207.

Cui, Y., Parker, G., and Paola, C. (1996). Numerical simulation of aggradation and downstream fining. J. Hydraul. Res., 34(2), 195–204.

Cui, Y., Parker, G. (2005). "Numerical model of sediment pulses and sediment –supply disturbances in mountain rivers" . Journal of Hydraulic Engineering, Vol. 131., No. 8, 646-656.

Cunge, J.A., Holly, F.M. ans Verwey, A., (1980). Practical aspects of computational river hydraulics . Pitman publishing, London, England.

Curran, J., Wilcock P. R. (2005). Effect of sand supply on transport rates in a gravel-bed channel. Journal of Hydraulic Engineering, Vol. 131, No. 11.

Defina A., (2003). Numerical experiments on bar growth, Water Resources Research, vol. 39(4), pp. ESG2_1-ESG2_12, ISSN: 0043-1397.

Dal Monte L., Di Silvio G. (2003). Ratio between channel-cross section and tidal prism in short lagoons: validity and limits of the "Law of Jarret", 3rd IAHR Symposium on River, Coastal and Estuarine Morphodynamics, 1-5 Sept., Barcelona, Spain, 2003.

Dal Monte L. and G. Di Silvio (2004). Sediment concentration in tidal lagoons. A contribution to long-term morphological modelling. Journal of Marine Systems, Volume 51, Issues 1-4, November 2004, Pages 243-255

D'Alpaos L. and A. Defina (2007). Mathematical modeling of tidal hydrodynamics in shallow lagoons: A review of open issues and applications to the Venice lagoon. Computers & Geosciences, Volume 33, Issue 4, May 2007, Pages 476-496.

De Vriend H. J., Capobianco M., Chesher T., De Swart H. E., Latteux B., Stive M. J. F. (1993). Approaches to long-term modelling of coastal morphology: a review. Coastal eng. ISSN 0378-3839 , vol. 21, no 1-3 (3 p.1/2), pp. 225-269

De Vriend, H. J. (1996). Mathematical modelling of meso-tidal barrier island coasts. Part I: Empirical and semi-empirical models, P. L.-F. Liu, Advances in coastal and ocean engineering 2115–149.

De Vries, M. (1965). Considerations about non-steady bed-load transport in open channels. Proc., 11th Int. Congress, Int. Association for Hydraulic Research, Delft, The Netherlands, 3.8.1–3.8.11.

De Vries, M. (1973). "River bed variations-aggradation and degradation". Proc., Int. Seminars of Hydraulics of Alluvial Streams, Int. Association for Hydraulic Research, Delft, The Netherlands, 1-10.

Dietrich, W.E., Montgomery, D.R., (1998). Shalstab: a digital terrain model for mapping shallow landslide potential Gradually varied debris flow along a slope. NCASI Technical Report, 29, February.

Dietrich, W.E., Bellugi, D., Real De Asua, (2001). Validation of the shallow landslide model. Shalstab, for forest management. In:Wigmosta, M.S., Burges, S.J., 2001 Eds, Land Use and Watersheds: Human influence on hydrology and geomorphology in urban and forest areas, Amer. Geoph. Union, Water Science and Application, 2,195-227.

Di Silvio, G., (1989). Modelling of the Morphologic Evolution of Tidal Lagoons and Their Equilibrium Configurations. Proceedings of the XXIII IAHR Congress, Ottawa, Canada, pp. C169– C175.

Di Silvio, G. and Peviani, M.A. (1989). Modelling Short- and Long-term evolution of mountain rivers: an application to the torrente Mallero (Italy). Published at International Workshop on fluvial hydraulics of mountains regions. Trent, Italy.

Di Silvio, G., (1991a). Sediment exchange between stream and bottom, a four layer model. Grain Sorting Seminar, Ascona Switzerland, p. 163-191.

Di Silvio, G., (1991b). Averaging operations in sediment transport modelling: short-step versus long-step morphological simulations. The Transport of Suspended Sediments and its Mathematical Modeling, International IAHR/USF Symposium, Florence, Italy, p. 723 (preprint).

Di Silvio, G. and Peviani, M.A. (1991) Modelling short- and long-term evolution of mountain rivers: an application to the torrent Mallero (Italy)". Lecture Notes in Earth Sciences n. 37, Fluvial Hydraulics of Mountain Regions, A. Armanini and G. Di Silvio Eds., Springer Verlag, 1991, pp. 293-292.

Di Silvio, G., Teatini, P., (1992a). Conterminazione Lagunare, Istituto Veneto di Scienza, Lettere ed Arti, VII, Venezia, Italy.

Di Silvio, G., Teatini, P., (1992b). Effects of non-uniform sediment grainsize in the long-term evolution of tidal lagoons. Coast. Eng. Conf. 142, 51– 52.

Di Silvio G., Marin A., (1996). Analythical approach to river morphodynamics: effects of space- and time- irregularities and grainsize non-uniformity. FRIMAR, Technical Rep.no.2 University of Padua.

Di Silvio, G., Gregoretti, C., (1997). Gradually varied debris flow along a slope. Proceedings of First International Conference On Debris Flow: Hazards, Mitigation, ASCE, San Francisco.

Di Silvio, G., Padovan, A., (1998). Interaction between marshes, channels and shoals in a tidal lagoon investigated by a 2-D morphological model. 3rd Int. Conf. on Hydroscience and Engineering. Cottbus, Berlin, German, 3, CD-ROM.

Di Silvio, G., (1999). Interaction between marshes, channels and shoals in a tidal lagoon. IAHR Symposium on River, Coastal and Estuarine Morphodynamics. University of Genoa, Italy, pp. 395–704.

Di Silvio, G., Barusolo, G., Sutto, L., (2001). Competing driving factors in estuarine landscape. Proceedings of the 2nd IAHR Symposium on River, Coastal and Estuarine Morphodynamics, Obihiro, Japan, pp. 455– 462.

Di Silvio, G., Dal Monte, L., (2003). Ratio between channel crosssection and tidal prism in short lagoons: validita` and limits of the ‘‘Law of Jarrett’’. 3rd IAHR Symposium on River. Coastal and Estuarine Morphodynamics, vol. 1. Barcelona, Spain, pp. 52– 533.

Di Silvio, G. (2006). Sediment sources and causes: Approaches to sediment yield evaluation Proceeding of the International Sediment Initiative Conference (ISIC). Khartoum, 2006 November 12-15, Sudan.

Dou, X., Jia, Y., and Wang, S. S. Y. (1998). An alternative methodologyto study local scour at bridge piers. Proc., 1st Fed. Interagency Hydr. Modeling Conf., Subcommitte on Hydrology of the Interagency Advisory Committee on Water Data, Las Vegas, Nev., Vol. 1, 3(1–8).

Dronkers, J., (1978). Longitudinal dispersion in shallow well-mixed estuaries. Coast. Eng. Conf. 3, 169.

DuBoys, M.P. (1879). Etudes du Regime et l’Action Exercée par les Eaux sur un Lit à Fond de Graviers Indefiniment Affouilable, Annales de Ponts et Chaussés, Ser. 5, 18, 1879.

Egiazaroff, I. V. (1965). Calculation of nonuniform sediment concentrations. J. Hydraul. Div., 91, 225–248.

Engelund, F. and Hansen, E. (1967). A monograph on sediment transport in alluvial streams, Teknisk Forlag, Copenhagen, Denmark.

Fagherazzi S., A. Bortoluzzi, W. E. Dietrich, A. Adami, M. Marani, S. Lanzoni, and A. Rinaldo. (1999). Tidal networks: 1. Automatic network extraction and preliminary scaling features from digital terrain maps, Water Resour. Res., 35, 3891– 3904.

Fasolato, G., Di Silvio G. (2004) Evoluzione del fondo di un bacino lagunare simulata con un modello morfodinamico intermareale bidimensionale. Proceeding of XXIX Convegno di idraulica e costruzioni idrauliche. 7-10 settembre 2004. Trento.

Fasolato et al. (2006a). Morphodynamics of mountain rivers following repeated sediment release from reservoirs. Proceeding of International Conference RiverFlow 2006, September 6-8 Lisboa, Portugal.

Fasolato, G., Ronco P., Di Silvio G. (2006b). Simplified models for simulating morphodynamic processes at different space- and time-scales. Proceeding of the 7th Int. Conf. on Hydroscience and Engineering (ICHE-2006), Sep 10 –Sep 13, Philadelphia, USA.

Fasolato, G., Ronco P., Jia Y. (2007). “Studies on sediment transport and morphodynamic evolution of a river due to sediment flushing operations of an alpine reservoir”. Proceeding of the 32nd Int. Congress of IAHR, July 1 –6, Venice, Italy.

Fasolato, G. and Ronco, P. and Di Silvio, G. (2008a). Boundary conditions in river morphodynamics. An analytical solution. Journal of Hydraulic Research (in review).

Fasolato, G. and Ronco, P. and Di Silvio, G. (2008b). Validity of simplified one-dimensional models. Journal of Hydraulic Engineering ASCE (in review).

Fasolato, G., Dall'Angelo C. Di Silvio, G. (2008c) "A long-term model for the generation and evolution of a tidal network" Atti del Corila (in press)

Gallappatti R. and. Vreugdenhil C.B, (1985). A depth-integrated model for suspended sediment transport. Journal of Hydraulic Research **23** pp. 359–377

Hirano, M. (1971). River bed degradation with armouring . Trans. of JSCE. 3(2).

Imberger, J. and Di Silvio, G., (1992). Mixing Processes in a shallow lagoon. In: Edge, B.L., Editor, 1992. Coastal Engineering, ASCE, Venice, Italy, pp. 1867–1868.

Jia, Y., and Wang, S. S. Y. (1996). A modeling approach to predict local scour around spur dike-like structures. Proc., 6th FISC, Subcommittee on Sedimentation Interagency Advisory Committee on Water Data, Las Vegas, Nev., Vol. 1, 90–97.

Jia, Y., and Wang, S. S. Y. (1997). CCHE2D model verification tests documentation. Tech. Rep. No. CCHE-TR-97-4, Ctr. for Computational Hydrosci. and Engrg., University of Mississippi, University, Miss.

Jia, Y., and Wang, S.S.Y., (1999). Numerical model for channel flow and morphological change studies. ASCE, Journal of Hydraulic Engineering, Vol. 125, No. 9, pp 924-9

Jia Y. et al. (2005) Three-Dimensional Numerical Simulation and Analysis of Flows around a Submerged Weir in a Channel Bendway. J. Hydr. Engrg. 131, 682 (12 pages)

Karpik S. R. and Raithby G. D. (1990). Laterally Averaged Hydrodynamics Model for Reservoir Predictions J. Hydr. Engrg., Volume 116, Issue 6, pp. 783-798.

Kassem A.A. and Chaudhry M.H. (2002) Numerical evolution of bed evolution in channel bends, Journal of Hydraulic Engineering, ASCE **128** (5), pp. 507–552.

Kassem, A., Imran, J. and Khan J. A. (2003). Three-Dimensional Modeling of Negatively Buoyant Flow in Diverging Channels J. Hydr. Engrg. 129, 936

Krone, R. B. (1962). Flume studies of the transport of sediment in estuarial shoaling processes.

Lanzoni, S., Seminara, G., (2002). Long-term evolution and morphodynamic equilibrium of tidal channels. J. Geophys. Res. 107, 1 – 13.

Lanzoni S., Siviglia A., Frascati, A., Seminara G. (2006). Long waves in erodible channels and morphodynamic influence. Water Resources Research, Vol. 42, W06D17.

Lee, D.S., R.D. Kingdon, J.M. Pacyna, A.F. Bouwman, and I. Tegen, (1999). Modelling base cations in European sources, transport and deposition of calcium. Atmos. Environ., 33, 224102256, doi:10.1016/S1352-2310(98)00169-1.

Lyn, D. A. (1987). Unsteady sediment-transport modeling. J. Hydraul. Eng., 113(1), 1–15.

Lyn, D. A., Altinakar, M. (2002). St. Venant-Exner equations for near-critical and transcritical flows. J. Hydraul. Eng., 128(6), 579–587.

Madeo E. (2002). Influenza delle condizioni al contorno sul comportamento morfodinamico di un corso d'acqua. Una soluzione analitica. M.Sc.-Thesis (in Italian) University of Padua.

Maner, S.B. (1958) Factors affecting sediment delivery rates in the red hills physiographic area, Transactions of American Geophysics 39, pp. 669–675.

Marciano R. et al. (2005). Modeling of channel patterns in short tidal basins. Journal of Geophysical Research, vol. 110, January, 2005.

Marin A., Di Silvio G. (1996) "Analysis and evaluation of various simplifying hyphotesis in morphological on dimensional models. FRIMAR, Technical Rep.no.1 University of Padua.

Mehta, A. J. and E. Partheniades, (1975). An investigation of the depossitional properties of flocculated fine sediments. J. Hydr. res. ASCE 13: 361–381.

Mehta, A. J., (1986). Characterization of cohesive sediment properties and transport processes in estuaries. In A. J. Mehta (ed.) Estuarine cohesive sediment dynamics. Lecture Notes Coastal Estuarine Studies 14: 290–325.

Meyer-Peter, E., Müller, R., (1948). Formulas for bed-load transport. Proceedings of Second Meeting of the International Association for Hydraulic Research, pp. 39–64.

Miller, J., (1984). Basic concepts of kinematic-wave models. U.S. Geological Survey, Professional Paper N° 1302, Washington, USA.

Morgan, R.P.C. (1995). Soil Erosion and Conservation, 198 pp. Longmans, New York.

Morris, P. H., Williams, D. J. (1996). Relative celerities of mobile bed flows with finite solids concentrations. J. Hydraul. Eng., 122(6) 311–315.

Morris G.L. and Fan J. (1998). Reservoir Sedimentation Handbook. McGraw-Hill., (746 pp.).

Nagata N. et al. (2005). Three-Dimensional Numerical Model for Flow and Bed Deformation around River Hydraulic Structures. J. Hydr. Engrg. 131, 1074 (14 pages)

Nearing, J.R., Simanton, L.D., Norton, S.J., Bulygin, J. (1999). Soil erosion by surface water flow on a stony, semiarid hillslope. Earth Surface Processes and Landforms, Vol: 24 N: 8, Pg: 677-686.

Nicholas A.P. and Walling D.E., (1998). Numerical modelling of floodplain hydraulics and suspended sediment transport and deposition, Hydrological Processes 12 (1998), pp. 1339–1355.

Okubo, A., (1973). Effects of short line irregularities on streamwise dispersion in estuaries and other embayments. Neth. J. Sea Res. 6, 213– 224.

Olsen, N. R. B. (2003). Three dimensional CFD modeling of selfforming meandering channel. J. Hydraul. Eng., 129-10, 366–372.

Ouillon, S., and Dartus, D. (1997). Three-dimensional computation of flow around groyne. J. Hydr. Engrg., ASCE, 123(11), 962–970.

Paola, C. (1988) Subsidence and gravel transport in alluvial basins . In: New Perspectives in Basin Analysis (eds K. L. Kleinspehn and C. Paola) , pp. 231 243. Springer-Verlag, New York.

Paola, C., Heller, P.L., Angevine, C.L. (1992). The large-scale dynamics of grain-size variation in alluvial basins, 1: Theory. Basin Res. , 4, 73 90.

Papanicolaou, A. N., Bdour, A., Wicklein, E. (2004). One-dimensional hydrodynamic/sediment transport model applicable to steep mountain streams. J. Hydraul. Res., 42(4).

Parker, G. P. and Klingeman, P. C. (1982a). On why gravel bed streams are paved. Water Resour. Res., 18-5, 1409–1423.

Parker, G., Klingeman, P. C., and McLean, D. G. (1982b). Bedload and size distribution in paved gravel-bed streams. J. Hydraul. Div., 108, 544–571.

Parker, G. et al. (2000). Probabilistic Exner sediment continuity equation for mixtures with no active layer. Journal of Hydraulic Engineering, Vol. 126, no. 11, November 2000.

Partheniades, E. (1962). A study of erosion and deposition of cohesive soils in salt water, University of California, U.S.A.

Peviani, M.A., Rafaelli, S., Crepaldi L. (1995). Application of trace tecnhique to estimate sediment transport during flood events. Published at the 6th International Symposium on River Sedimentation, New Delhi. India.

Peviani, M. A. (2002). Sviluppo di un modello numerico idrauli-co-morfologico per fiumi a forte pendenza ed analisi dell'evoluzione degli alvei nei tratti pedemontani. Doctoral thesis University of Perugia.

Repetto, R., Tubino (2001). Planimetric instability of channels with variable width. Phys. Chem. Earth (B), vol. 26, pp. 71-76.

Repetto, R., Tubino, M., Paola, C. (2002). "Planimetric instability of channels with variable width". J. Fluid Mech., vol. 457, pp. 79-109.

Ribberink, J. S., Van der Sande, J. T. M. (1985). Aggradation in rivers due to overloading-analytical approaches. J. Hydraul. Res. 23(3), 273–283.

Rinaldo A., S. Fagherazzi, S. Lanzoni, M. Marani, and W. E. Dietrich (1999a), Tidal networks: 2. Watershed delineation and comparative network morphology, Water Resour. Res., 35, 3905– 3917.

Rinaldo, A., S. Fagherazzi, S. Lanzoni, M. Marani, and W. E. Dietrich (1999b), Tidal networks: 3. Landscape-forming discharges and studies in empirical geomorphic relationships, Water Resour. Res., 35, 3919–3929.

Roehl, J.E. (1962). Sediment source areas, and delivery ratios influencing morphological factors, International Association of Hydrological Sciences 59, pp. 202–213.

Ronco, P., Fasolato, G., Di Silvio G. (2006). The Case of the Zambezi River in Mozambique: some investigations on solid transport phenomena downstream Cahora Bassa Dam. Proceeding of International Conference RiverFlow 2006, September 6-8 Lisboa, Portugal.

Ronco P. and Fasolato G. and Di Silvio G. (2007) Simulating the profile evolution of large unsurveyed rivers: the case of Zambezi (Austral Africa). Proceeding of the 32nd Int. Congress of IAHR, July 1 –6, Venice, Italy.

Ronco, P., Fasolato, G., Di Silvio, G. (2008a). "Modelling watershed sediment budget in unsurveyed river". Geomorphology (in review).

Ronco P., Fasolato G., Di Silvio G. (2008b) "Morphological effects on lower Zambezi river of Cahora bassa reservoir" Journal of Hydraulic Engineering - ASCE, (in preparation).

Rosso, R., (2002). Sulla valutazione dei fattori idrologici e geomorfici di innesco delle frane superficiali nei bacini montani. 28° Convegno di Idraulica e Costruzioni Idrauliche, Potenza 16-19 settembre.

Schijf, J.B., Scho¨nfeld, J.C., (1953). Theoretical considerations on the motion of salt and fresh water. Proc. Minnesota Int. Hydr. Cond. (IAHR/ASCE), Minneapolis, MN.

Seminara, G., Tubino, M., (1993). Debris flow: meccanica, controllo e previsione. Monografia del G.N.D.C.I.

Seminara G. (1997). Equilibrio morfodinamico, stabilità ed evoluzione di correnti a fondo mobile. Proceeding (in Italian) of the meeting "Nuovi sviluppi applicative dell'idraulica dei corsi d'acqua". 27-31th January 1997 Bressanone, Italy.

Seminara G. and Tubino M., (1998). On the formation of estuarine free bars. In: J. Dronkers and M. Scheffers, Editors, Physics of estuaries and coastal seas, Balkema, Rotterdam, pp. 345–353.

Sieben, J. (1997). Modeling of hydraulics and morphology in mountain rivers. PhD thesis, also "Communications on hydraulic and geotechnical engineering". Rep. No. 97-3, Delft Univ. of Technology, Delft, The Netherlands.

Stive, M.J.F.,Wang, Z.B., Capobianco, M., Ruol, P., Bujsman, M.C., (1998). Morphodynamics of a tidal lagoon and adjacent coast. In: Dronkers, J., Sheffers, M.B.A.M. (Eds.), Physics of Estuaries and Coastal Seas. Balkema, Rotterdam, pp. 397–407.

Stockstill, R. L., Berger, R. C., and Ronald, E. N. (1997). Two-dimensional flow model for trapezoidal high velocity channels. J. Hydr. Engrg., ASCE, 123(10), 844–852.

Strom K. et al. (2004) Microforms in Gravel Bed Rivers: Formation, Disintegration, and Effects on Bedload Transport, J. Hydr. Engrg. 130, 554 (14 pages).

Strom K. et al. (2007) Flow Heterogeneity over 3D Cluster Microform: Laboratory and Numerical Investigation , J. Hydr. Engrg. 133, 273 (15 pages).

Surian, N. (2002). Downstream variation in grain size along an Alpine river: analysis of controls and processes. Geomorphology, 43. 137-149.

Tubino, M., Lanzoni, S., (1994). Rheology of debris flow: experimental observations and modelling problems. Excerpta, vol.7, CUEN, Napoli, 210-236.

Van Rijn, L. C. (1984) Sediment transport. Part 2: Suspended load transport. Journal of Hydraulic Engineering 110, 1613–1641.

Vreugdenhil, C.B. (1994). Numerical methods for shallow-water flow. Water Science and Techn. Library Vol. 13, Kluwer Academic Publishers Dordrecht, 262 p.

Walling, D E; Webb, B W (1996). Erosion and sediment yield: global and regional perspectives. IAHS Press. Wallingford, U.K., IAHS Publication No.236, 586pp

Williams, J.R. and Berndt H.D., (1972). Sediment Yield Computed with Universal Equation, Journal of the Hydraulics Division, Vol. 98, No. 12, December 1972, pp. 2087-2098.

Wilson, C. A. M. E., Boxall, J. B., Guymer, I., and Olsen, N. R. B. (2003). Validation of a three dimensional numerical code in the simulation of pseudo-natural meandering flows. J. Hydraul. Eng., 129_10_, 758–768.

Winterwerp J. C. (2002). On the flocculation and settling velocity of estuarine mud. Continental Shelf Research, Volume 22, Issue 9, June 2002, Pages 1339-1360

Wishmeyer W.D., Smith D.D. (1978). Predicting rainfall erosion losses, a guide to conservation planning Washington D.C., USDA Agricultural Handbook n. 278

Wright S., Parker G. (2005a) Modeling downstream fining in sand-bed rivers. I: formulation. J. Hydraul. Res., 43(6), 613–620.

Wright S., Parker G. (2005b) Modeling downstream fining in sand-bed rivers. II: application. J. Hydraul. Res., 43(6), 621–631.

Wu, W., Wang, S., Y. and Jia, Y. (2000a). Non uniform sediment transport in alluvial rivers. Journal of Hydraulic Research, Vol. 38, , N. 6.

Wu, W., Rodi, W., and Wenka, T. (2000b). 3D numerical modeling of flow and sediment transport in open channels. J. Hydraul. Eng., 126-1, 4–15.

Wu, W., Vieira D. A, Wang S. S. Y. (2004). One-dimensional numerical model for non-uniform sediment transport under unsteady flows in channel networks. Journal of Hydraulic Engineering, Vol. 130, No. 9.

Ye, J., and McCorquodate, J. A. (1997). ‘‘Depth-averaged hydrodynamic model in curvilinear collocated grid.’’ J. Hydr. Engrg., ASCE, 123(5), 380–388.

Yalin, M.S. (1963). An expression for bed load transportation, Proc. ASCE, Vol. 89, HY3, 1963.

Zedler E. A. and Street R. L. (2006) Sediment Transport over Ripples in Oscillatory Flow. J. Hydr. Engrg. 132, 180 (14 pages).

APPENDIX

Appendix 3.A

For supercritical flow (*Fr*>1) amplitudes $\overline{p_{c_n}}$ results defined as the following expression:

$$\overline{p_{c_x}} = \frac{\left(\eta^* + s\eta\right)\left(\overline{k_w}e^{\overline{k_w}il} - \overline{k_y}e^{\overline{k_y}il}\right)}{\frac{6\psi i}{\omega}\left[\frac{\overline{k_1}^2\left(\overline{k_3}e^{\overline{k_3}il} - \overline{k_2}e^{\overline{k_2}il}\right)}{\varepsilon - \alpha i\overline{k_1}} + \frac{\overline{k_2}^2\left(\overline{k_1}e^{\overline{k_1}il} - \overline{k_3}e^{\overline{k_3}il}\right)}{\varepsilon - \alpha i\overline{k_2}} + \frac{\overline{k_3}^2\left(\overline{k_2}e^{\overline{k_2}il} - \overline{k_1}e^{\overline{k_1}il}\right)}{\varepsilon - \alpha i\overline{k_3}}\right]}\overline{\beta_{1c}^0} +$$

$$+ \frac{\left[\frac{6\psi i\overline{k_w}\,\overline{k_y}}{\omega}\left(\frac{\overline{k_w}}{\varepsilon - \alpha i\overline{k_w}}e^{\overline{k_y}il} - \frac{\overline{k_y}}{\varepsilon - \alpha i\overline{k_y}}e^{\overline{k_w}il}\right) - \left(\overline{k_w}e^{\overline{k_w}il} - \overline{k_y}e^{\overline{k_y}il}\right)\right]}{\frac{6\psi i}{\omega}\left[\frac{\overline{k_1}^2\left(\overline{k_3}e^{\overline{k_3}il} - \overline{k_2}e^{\overline{k_2}il}\right)}{\varepsilon - \alpha i\overline{k_1}} + \frac{\overline{k_2}^2\left(\overline{k_1}e^{\overline{k_1}il} - \overline{k_3}e^{\overline{k_3}il}\right)}{\varepsilon - \alpha i\overline{k_2}} + \frac{\overline{k_3}^2\left(\overline{k_2}e^{\overline{k_2}il} - \overline{k_1}e^{\overline{k_1}il}\right)}{\varepsilon - \alpha i\overline{k_3}}\right]}\left(\overline{p_c} - 2\overline{q_c}\right) +$$

$$- \frac{6i\left(\frac{\overline{k_w}^2}{\varepsilon - \alpha i\overline{k_w}} - \frac{\overline{k_y}^2}{\varepsilon - \alpha i\overline{k_y}}\right)}{\frac{6\psi i}{\omega}\left[\frac{\overline{k_1}^2\left(\overline{k_3}e^{\overline{k_3}il} - \overline{k_2}e^{\overline{k_2}il}\right)}{\varepsilon - \alpha i\overline{k_1}} + \frac{\overline{k_2}^2\left(\overline{k_1}e^{\overline{k_1}il} - \overline{k_3}e^{\overline{k_3}il}\right)}{\varepsilon - \alpha i\overline{k_2}} + \frac{\overline{k_3}^2\left(\overline{k_2}e^{\overline{k_2}il} - \overline{k_1}e^{\overline{k_1}il}\right)}{\varepsilon - \alpha i\overline{k_3}}\right]}\overline{z_c}$$

where subscripts (*x*, *y*, *z*) means a circular permutation of (1, 2, 3), as for instance, (*x*, *y*, *z*)= (1, 2, 3), (2, 3, 1), (3, 1, 2).

Instead, for subcritical flow (*Fr*<1) the expressions of the amplitudes $\overline{p_{c_n}}$ assumes a different form, where subscripts (*x*, *y*, *z*) means a circular permutation of (1, 2, 3) and $\Omega_n = \left(1 + \frac{i\overline{k_n}}{\varepsilon - \alpha i\overline{k_n}}\right)\overline{k_n}e^{\overline{k_n}il}$.

$$\overline{p_{c_x}} = \frac{\left(\eta^* + s\eta\right)}{\dfrac{6\psi i}{\omega\left(\Omega_w - \Omega_y\right)}\left[\dfrac{\overline{k_1}^2\left(\Omega_3 - \Omega_2\right)}{\varepsilon - \alpha i\overline{k_1}} + \dfrac{\overline{k_2}^2\left(\Omega_1 - \Omega_3\right)}{\varepsilon - \alpha i\overline{k_2}} + \dfrac{\overline{k_3}^2\left(\Omega_2 - \Omega_1\right)}{\varepsilon - \alpha i\overline{k_3}}\right]}\overline{\beta_{1c}^0} +$$

$$+ \frac{\left[\dfrac{6\psi i}{\omega\left(\Omega_w - \Omega_y\right)}\left(\dfrac{\overline{k_w}^2}{\varepsilon - \alpha i\overline{k_w}}\Omega_y - \dfrac{\overline{k_y}^2}{\varepsilon - \alpha i\overline{k_y}}\Omega\right) - 1\right]}{\dfrac{6\psi i}{\omega\left(\Omega_w - \Omega_y\right)}\left[\dfrac{\overline{k_1}^2\left(\Omega_3 - \Omega_2\right)}{\varepsilon - \alpha i\overline{k_1}} + \dfrac{\overline{k_2}^2\left(\Omega_1 - \Omega_3\right)}{\varepsilon - \alpha i\overline{k_2}} + \dfrac{\overline{k_3}^2\left(\Omega_2 - \Omega_1\right)}{\varepsilon - \alpha i\overline{k_3}}\right]}\left(\overline{p_c} - 2\overline{q_c}\right) +$$

$$- \frac{\dfrac{6i}{\left(\Omega_w - \Omega_y\right)}\left(\dfrac{\overline{k_w}^2}{\varepsilon - \alpha i\overline{k_w}} - \dfrac{\overline{k_y}^2}{\varepsilon - \alpha i\overline{k_y}}\right)}{\dfrac{6\psi i}{\omega\left(\Omega_w - \Omega_y\right)}\left[\dfrac{\overline{k_1}^2\left(\Omega_3 - \Omega_2\right)}{\varepsilon - \alpha i\overline{k_1}} + \dfrac{\overline{k_2}^2\left(\Omega_1 - \Omega_3\right)}{\varepsilon - \alpha i\overline{k_2}} + \dfrac{\overline{k_3}^2\left(\Omega_2 - \Omega_1\right)}{\varepsilon - \alpha i\overline{k_3}}\right]}\left(\overline{z_c} + \overline{h_c} - \frac{2}{3}\overline{q_c}\right)$$

Appendix 3.B

To annul the determinant of eqs. (3.34), it means to consider:

$$\det\begin{bmatrix} \dfrac{\varepsilon}{6} - \dfrac{\alpha}{6}\overline{k}i & \overline{k}i & \left(\dfrac{\alpha}{6}\overline{k}i - \dfrac{\varepsilon}{6}\right)\left(\eta^* + s\eta\right) \\ \psi\overline{k} & -\omega & 0 \\ \dfrac{\psi}{\Delta}\eta^*\overline{k} & 0 & -\omega + \dfrac{\psi}{\Delta}S^*\overline{k} \end{bmatrix} = 0$$

and after some arithmetic calculations (with $S^* = 1 - \eta^{*2}$ and $\gamma = 1 + s\eta\eta^*$) it can be expressed as:

$$\psi\overline{k}^2 i\left(\frac{\psi}{\Delta}S^*\overline{k} - \omega\right) + \frac{\omega}{6}\left(\varepsilon - \alpha\overline{k}i\right)\left(\frac{\psi}{\Delta}\eta^*\overline{k} - \omega\right) = 0$$

that, with $\overline{\varepsilon} = \dfrac{\varepsilon\psi}{6\Delta^2\omega}$, $\overline{\alpha} = \dfrac{\alpha}{6\Delta}$ and $\overline{X} = \dfrac{\overline{k}\psi}{\Delta\omega}$, results eq. (3.38):

$$i\overline{X}^2\left(\overline{X}S^* - 1\right) + \left(\overline{\varepsilon} - \overline{\alpha}\overline{X}i\right)\left(\gamma\overline{X} - 1\right) = 0 \qquad (3.38)$$

Appendix 3.C

Considering $\bar{\varepsilon} >> \alpha Xi >> 1$ and, as first approximation, $X \sim 1$, eq. (3.38) can be solved with an approximation value of $X_{appr} = 1/\gamma$. For a better solution of the eq. (3.38), it is possible to find a little δ such as $X \cong X_{appr} + \delta$ can be a zero of the eq. (3.38). It's easy to demonstrate that $\delta \cong \frac{\left(\gamma - S^*\right)}{\bar{\varepsilon}\gamma^4} i$ and one zero of eq. (3.38) can be written as: $X_1 \cong \frac{1}{\gamma} + i\frac{\left(\gamma - S^*\right)}{\bar{\varepsilon}\gamma^4}$. To find the other two zeros, it's possible to find an approximation value $X_{appr} \cong \pm\left(\sqrt{\frac{\gamma\bar{\varepsilon}}{2S^*}} + i\sqrt{\frac{\gamma\bar{\varepsilon}}{2S^*}}\right)$, considering $\left(X \sim \sqrt{\varepsilon}\right)$ and to correct this value with $\delta \cong \frac{\bar{\alpha}\gamma}{2S^*}$. So the other two zeros can be written as: $X_{2/3} \cong \frac{\bar{\alpha}\gamma}{2S^*} \pm \left(\sqrt{\frac{\gamma\bar{\varepsilon}}{2S^*}} + i\sqrt{\frac{\gamma\bar{\varepsilon}}{2S^*}}\right)$. Once determined values of X_n the consequent values of $\bar{k}_n$, c_{f_n} and L_{f_n} can be easily expressed with eqs. 3.41-43.

Appendix 3.D

Considering, as first approximation, $\bar{\varepsilon} \cong 0$ and $\bar{\alpha} >> 0$ the zeros of eq. (3.38) can be written as: $X_{1/2} \cong \left(1 + \bar{\alpha}\gamma\right) \Big/ 2S^* \pm \sqrt{\left(1 + \gamma\bar{\alpha}\right)^2 - 4\bar{\alpha}S^*} \Big/ 2S^*$ and $X_3 \cong 0$; if it can be assumed the hypothesis of substantially wide granulometric distribution ($S^* << 1$) and expanding the root of terms with a MacLaurin's series, the first two solutions can be approximated as: $X_{1,appr} \cong \bar{\alpha} \Big/ \left(1 + \bar{\alpha}\gamma\right)$ and $X_{2,appr} \cong \left(1 + \bar{\alpha}\gamma\right) \Big/ S^*$. As for uniform-flow solution (*Appendic 3.C*), these values can be corrected with appropriate $\delta_{1,2,3}$ and with some easy computations the tree solutions become:

$X_1 \cong \bar{\alpha} \Big/ \left(1 + \bar{\alpha}\gamma\right) + i\,\bar{\varepsilon} \Big/ \left[\bar{\alpha}\left(1 + \bar{\alpha}\gamma\right)\right]$, $X_2 = \left(1 + \bar{\alpha}\gamma\right) \Big/ S^* + i\gamma\bar{\varepsilon} \Big/ \left(1 + \bar{\alpha}\gamma\right)$ and $X_3 = \bar{\alpha} \Big/ \left(1 + \bar{\alpha}\gamma\right)$.

Once determined values of X_n the consequent values of $\bar{k}_n$, c_{f_n} and L_{f_n} can be easily expressed with eqs. 3.44-46, with the further approximation of $\bar{\alpha} = f\left(\alpha \cong 1\right)$.

Acknowledgements

This research has been carried on in the framework of research projects by MIUR (Ministry of Research and University) and Autorità di Bacino Alto Adriatico (River Authority of Northern Adriatic Sea).
A special thanks to Prof. Di Silvio for the precious collaboration.